Measurement of local potentials using the scanning electron microscope, and its application in the failure analysis of micro-electronic circuits

MICHAEL WOODWARD

A thesis submitted for the degree of Master of Philosophy of the University of Wales

1992

UNIVERSITY OF WALES

Summary of thesis

Surname: *WOODWARD*

Other names: *MICHAEL*

Candidate for the degree of: *M.PHIL*

Title of thesis: *MEASUREMENT OF LOCAL POTENTIALS USING THE SCANNING ELECTRON MICROSCOPE, AND ITS APPLICATION IN THE ANALYSIS OF MICRO-ELECTRONIC CIRCUITS*

Summary

This thesis describes the development of an electron beam test system based on a conventional scanning electron microscope (SEM), and its application for the determination of voltage and timing information for detailed local study of individual components within micro-electronic circuits.

The project showed how the SEM may be operated at low voltages (less than 5kV), to maximise Secondary Electron (SE) emissions which carry the voltage information and control both the primary electron penetration and energy deposition within a specimen. The conventional SE imaging system was used to display voltage distribution over a relatively large area of any specimen. However, only qualitative measurements are possible, as the detector is not able to discriminate between changes of SE yield and energy distribution, and cannot suppress localised field effects which alter the SE emission's energy profile and angular distribution, causing measurement error.

To achieve quantitative voltage measurements, SE emission was sensed using the Voltage Measurement Electron Controller (VMEC). This additional equipment has several electrodes, each generating electrostatic fields, one of which acts as a SE energy filter detecting changes to their energy distribution as the surface potential alters. The electrostatic field generated by the electrode nearest the specimen increases the collection efficiency of the detector, and suppresses the action of the local fields (which alter the energy and angular distribution of the emitted SE's). These effects were investigated.

Extra equipment was then interfaced to the SEM, including a set of beam blanking plates and their control unit, for the rapid switching of the primary beam, a signal processing unit for noise reduction, image capture and image subtraction, and data analysis.

The analytical capability of this equipment was demonstrated via its ability to display and measure the voltage levels of various local sites across a simple quad NAND *gate device.*

The EBT system which had been developed was used for the analysis of two commercial micro-electronic products, making both voltage and timing measurements from metal conductor tracks with widths as narrow as 1.5 micrometres.

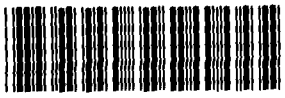

The material contained within this thesis has not already been accepted in substance for any degree, and is not being concurrently submitted in candidature for any degree.

Candidate_____.

Supervisor._____.

The material contained within this thesis represents my own efforts except where references to other works are given.

Candidate_____.

Supervisor_____.

ACKNOWEDGEMENTS

It is with pleasure that I acknowledge the support, encouragement and help of the following people during the work for, and writing up of this thesis.

I am particularly indebted to Professor J.M. Marshall (Joe), of the Materials Engineering Department, University College of Swansea, who as my supervisor, encouraged me to undertake this study, gave guidance during the work and the many helpful comments on the drafts which he changed so that my writing said what I had intended to say.

Others within the Materials Engineering Department who I would like to thank are, Dr. A.R. Hepburn, for writing the ASYST programme and enabling the computer to do that which I hoped it would. Dr C. Pickup for his earlier efforts with programming.

Thank you to Don Ranasinghe at British Telecom. for providing me with the calibration samples, and Mark Kenny of INMOS plc, for wire bonding and packaging these samples.

Other INMOS personnel to whom I am grateful are, David Seal, Mark Chapman and Shane MacCarvill, for providing the transputer and memory devices, and the relevant information required to enable them to work. Richard Clarke for some of the preparation work on the memory devices, and interesting discussions about his experiences in failure analysis.

At Gwent College of Higher Education where I am employed, I would like to thank all my colleagues and friends who have given me encouragement and support during this project. In particular I am indebted to; the college for paying my fees and allowing me to use laboratory equipment and other facilities. To Dr. Ian Bennett, for designing the system and the programming that was required to enable the Transputers to function within the SEM. To the library staff, for providing much of the background information that was required, particularly Ms. Leatherdale, who as a friend was very supportive during the arduous writing up stage. To Alex Wilson the Technical Officer for always being as help as he possibly could, Dr. Clive Day Dean of Faculty, for his memorable comments which finally persuaded me to undertake this work, Dave (mad dog) Willis for printing all the photomicrographs, Peter Watkins for the use of his PC to run the ASYST programme, Geoff Edge for the use of his laser printer, Miss. Speed for reproducing the copies of the thesis and Dave Jones for negotiations with INMOS for the various VLSI devices used, and for the many interesting discussions on micro-electronics. Finally, to the college's Vice Principal, Dr G Williams for his continual enquires as to my progress with this project, I no longer have to avoid him on the stairs.

CONTENTS.

CHAPTER 4.

APPLICATIONS OF ELECTRON BEAM TESTING.

CHAPTER 5.

APPARATUS AND EXPERIMENTAL PROCEDURE.

CHAPTER 6.

RESULTS AND DISCUSSION.

INTRODUCTION

THE OBSERVATION AND MEASUREMENT OF SURFACE ELECTRICAL POTENTIAL USING THE SCANNING ELECTRON MICROSCOPE.

During the mid 1950's, at the Engineering Department of Cambridge University, much of the foundation work for the modern scanning electron microscope was undertaken. This lead to the first commercial microscopes [Stewart 1985]. Today, the use of these instruments has become well established in many scientific/technological fields. Their popularity is due to their spatial resolution, which may be of the order several nanometres, and (because of the small apertures employed) to an excellent depth of field. For example, a typical secondary electron image of a specimen's surface will have a 3 dimensional quality, enabling it to be interpreted easily, and giving the appearance of illumination using a conventional light source [Goldstein 1983]. Such instruments are very versatile, offering a range of imaging and measurement modes. This is due to the variety of quanta emitted as a consequence of the interactions between the electrons of the primary beam and the specimen [Postech 1983]. Each particular type of emission yields its own characteristic information about the specimen.

During these early years at Cambridge, the observation of contrast variations, which appeared to be associated with differences of electrical potential at the specimen's surface, were reported [Smith 1956]. This effect was later investigated

[Everhart 1958]. This work explains the origins of the voltage dependent contrast observed in respect of the secondary electron image.

The potential applications of such an imaging technique were not fully appreciated until Plows [1968] (also at Cambridge), successfully built the first electron beam testing (EBT) system. Such equipment was developed for the extraction of quantitative voltage and timing measurements, from a specimen's surface, using the scanning electron microscope as if it were a sampling oscilloscope. The ability of such equipment to extract such data, whilst utilising the spatial resolution of the electron microscope, encouraged workers to develop this equipment for such applications as design validation and the failure analysis of micro-electronic circuits.

Despite the above advances, it was not until the mid 1970's that the micro-electronics industry became interested in such analysis techniques. By this time, Plows had set up the first commercial company (in 1977) to produce the first add-on unit for existing SEM's, thus enabling them to be used as sampling oscilloscopes. Then, during 1983 he was able to market the first stand alone dedicated electron beam testers [Mulvey 1988].

Demand for such equipment did not begin in earnest until the early 1980's, by which time the micro-electronics industry had continued developing its products, featuring shrinking device geometries and increasing component densities.

The requirements that these new, more complex, devices should be of high quality and reliability has led to the development of more sophisticated testing techniques for functionality assessment and the identification of circuit malfunctions. The classification process for fine circuit defects [Fatini 1984], had become more difficult and time consuming, using the conventional metal probing techniques which are used for functionality testing [Einspruch 1985]. Problems associated with the use of the metallic probe on individual circuit components include capacitive loading, physical damage, and short circuit to neighbouring components due to registration error [Wolfgang 1979].

The above probing problems may be reduced or eliminated using the SEM's electron beam as a probe. The SEM allows large area mapping of voltage distribution across a micro-electronic device. It also facilitates easy and accurate alignment of the electron probe onto individual nodes, with virtually no risk of physical damage and none of the capacitive loading problems inherent in more traditional systems. However, there is a major disadvantage, in that only one node at a time may be probed. It has therefore become practice to employ both metallic and electron beam probing systems; thereby exploiting the advantages of both.

Today, there are many commercial companies marketing dedicated electron beam test systems, requiring considerable capital investment. The present research program was undertaken to determine and evaluate the range and accuracy of information which can be obtained in respect of surface potential and its

variation with time, using the conventional scanning electron microscope (for components of integrated circuits). It was additionally proposed to assess how the range of analysis techniques could be expanded by the inclusion of "add-on" equipment, to allow quantitative measurements of voltage and its time variation for individual components, in a range of integrated circuits.

CHAPTER 1.

FUNDAMENTALS OF SCANNING ELECTRON MICROSCOPY.

(1.1) INTRODUCTION.

The concept of image production using an SEM is relatively simple. A beam of primary electrons is produced from a suitable filament material, usually tungsten or lanthanum hexaboride, by the process of thermionic emission. The electrons liberated from the filament are accelerated through an electrostatic field, the strength of which is selected by the microscopist, toward an anode plate. To increase the fraction of primary electrons having satisfactory trajectories to enter the electron optical column, a negatively biased grid cap or Wehnelt cylinder is used to produce a coarse focusing action. This crossover of electron trajectories is at a point between the source of emission and the anode plate. It is important as it represents the current which would ideally be concentrated into the final probe diameter if there were no lens aberrations.

Beyond the anode, the primary electrons enter the lens system, which consists of electromagnetic condensers and objective lenses. Their purpose is to demagnify and bring to focus the primaries. The interaction between primaries of a given velocity and the magnetic fields of the lenses is described by the vector equation;

$$\vec{F} = -e\ (\vec{v} * \vec{H}) \qquad \ldots\ldots\ldots\ldots\ldots\ldots (1.1).$$

Here, a force F acts on the primary electrons; the action of

this being dependent on the electron velocity $\vec{v}$ and the strength of the magnetic field $\vec{H}$ within each lens (-e being the electronic charge). The resultant force causes the primaries to spiral down around the column's central optical axis, thus packing the electrons closer together and producing a focusing action. Two important factors which are directly related to $\vec{F}$ are:

(1) the current impinging the specimen which is controlled by the action of the condenser lenses, and

(2) the minimum probe diameter, which is influenced by the action of the objective lens.

The primary electrons which exit the microscope's optical train and impinge onto the specimen's surface would ideally be confined to a small circular region, were it not for lens aberrations [Goldstein et.al. 1981]. The electron beam probe is then moved in a rectangular raster pattern over the specimen's surface. At each point of contact between the primary beam and the specimen's surface, a variety of emissions occur. These emissions are a consequence of primaries undergoing a combination of scattering events within the specimen. Secondary electrons (SEs) are just one product of primary electron inelastic scattering events. Within the SEM, a certain fraction of the emitted SEs may then be collected and detected, the magnitude of the detector's output signal being proportional to the SE current. The video output obtained from this signal is used to modulate the brightness of a cathode ray tube (CRT) display, whose electron beam scan is synchronised to that of the primary

beam. The result is an image in which each pixel co-ordinate on the CRT has a corresponding co-ordinate on the specimen's surface. The brightness level of each pixel relates to the SE emission coefficient for that point upon the specimen's surface. The total SE yield (δ) from the surface of the specimen is affected mainly by changes in surface topography, although there will (to a lesser extent) be a contribution due to differences in target material. Thus, image contrast appears similar to that which might be expected if the specimen had been illuminated by a conventional tungsten lamp. The shadowing which occurs is dependent on the position of the detector, rather than the source of illumination. This allows the images of the specimen to be interpreted easily. Coupled with the advantages of greater magnification, spatial resolution and depth of field, the instrument has become increasingly invaluable to scientists and technologists since its introduction in the late 1950's [McMullan 1985].

(1.2) THE EMISSION OF ELECTRONS FROM A SOLID SURFACE IN RESPONSE TO ELECTRON BOMBARDMENT.

Energy analysis of the emitted electrons reveals three distinct categories of such particles; namely backscattered or reflected primary electrons, Auger electrons and SEs. The energies of Auger electrons relate to the band structure of the atomic species [Wallis 1989]. Their numbers constitute only a very small fraction of the total emission current [Menzal and Kubalek 1983] and they are thus not considered in the following description. A typical energy profile for a constant primary beam

displays three distinct regions [figure 1.1]. Region 1 extends to the maximum energy; this being the energy of the primaries electrons striking the target. Such electrons have undergone mainly elastic scattering within the specimen, and on average have lost only a small fraction of their initial energy. The majority of backscattered electrons are found in this region. The electron yield within this region reaches a maximum at about 75% of $E_{p(max)}$. The yield begins to decrease at lower energies, as more electrons lose energy to the target, due to an increased number of inelastic interactions. This gives rise to region 2. If this region of the curve were to be extrapolated back to energy = 0, the yield might be expected to continue to fall. However, as can be seen, at these lower energies there is a sudden increase in yield. Region 3 is generally considered to have a maximum (arbitrary) energy of around 50 eV. The increase of yield in this region is due to the emission of SEs. Such an energy profile enables discrimination between backscattered and SEs, by reference to their energies.

It is important to consider not only electron energies, but to also consider the electron current. The relationship between the different categories of electrons is given in equation (1.2), where I_p is the primary beam current. The emission current is regarded as the sum of I_b (the backscattered electron current) and I_s (the SE current), I_{sc} (the current flowing through the specimen to earth).

$$-I_p + (I_b + I_s) + I_{sc} = 0 \qquad \ldots\ 1.2$$

Figure 1.1

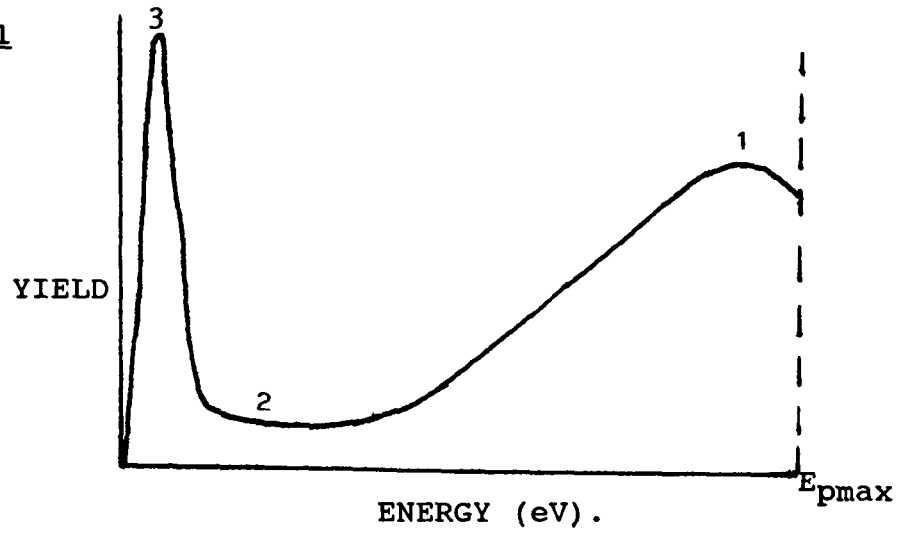

Schematic illustration of the energy distribution of emitted electrons; regions 1 and 2 represents back-scattered electrons and 3 secondary electrons.

The importance of this relationship is that, if it is not satisfied, charge may be either deposited or extracted from the specimen, giving poor quality images and electron beam drifting. For good electrically conducting material, this is not a problem. However, for semi-conductors and insulators, this imbalance can become a problem. In general, the problems of charge imbalance can be overcome by the application of a 'thin' coating of a good conductor material such as gold. However, if the specimen is an active integrated circuit, as is the case for EBT work, such coating is certainly not an option. For EBT, charge balance must thus be maintained by control of I_b and I_{se}, the emission current.

(1.3) THE GENERATION OF SECONDARY ELECTRONS.

When primary electrons impinge on a specimen, they penetrate it, continuing to travel along their initial trajectories until they interact with the specimen's atomic structure (where upon they are scattered). The scattering events are classed as elastic or inelastic interactions. Should the interaction be elastic, the trajectory may be altered significantly (by up to 180 degrees), with little or no energy loss. For inelastic events, only a slight change in pre-event trajectory is likely to occur, i.e. less than 5 degrees. However, there will be a much greater energy loss to the specimen. SE's are generated due to the energy transfer arising from certain inelastic interactions [Mckay 1958]. Such a process allows some of the weakly bound lattice electrons to be excited into higher energy levels. In this excited state, they are able to move freely in a random manner,

with the absence of either electrostatic or magnetic fields. Such electrons will be of low energy, and will have relatively short mean free paths within the specimen. Despite this, certain fractions of the SEs generated close to the specimen's surface may move to the surface and have sufficient energy to overcome the work function and thus escape. These secondaries may be generated either by inelastic scattering of primary electrons as they initially enter the specimen, or by those electrons which have undergone backscattering and are about to re-emerge at or close to the specimen surface.

(1.4) SECONDARY ELECTRON EMISSION.

The phenomenon of secondary electron emission was first reported at the beginning of this century [Austin and Strake in 1902]. Since then, much work has been reported on this phenomenon, with several comprehensive reviews written about this subject [McKay 1958, Dekker 1962]. Although most of the results reported by these authors were for SE generation, using primary electrons of much lower kinetic energies than those generally used within the scanning electron microscope, this early work is very relevant to the study of secondary electron yield, as defined in equation (1.3), within the scanning electron microscope.

$$\delta = \frac{\text{the number of emitted electrons of energy } <50\text{eV.}}{\text{the total number of primaries impinging the surface.}} \quad \ldots(1.3)$$

A typical SE yield distribution for most materials as shown in figure [1.2] is typical.

Figure 1.2

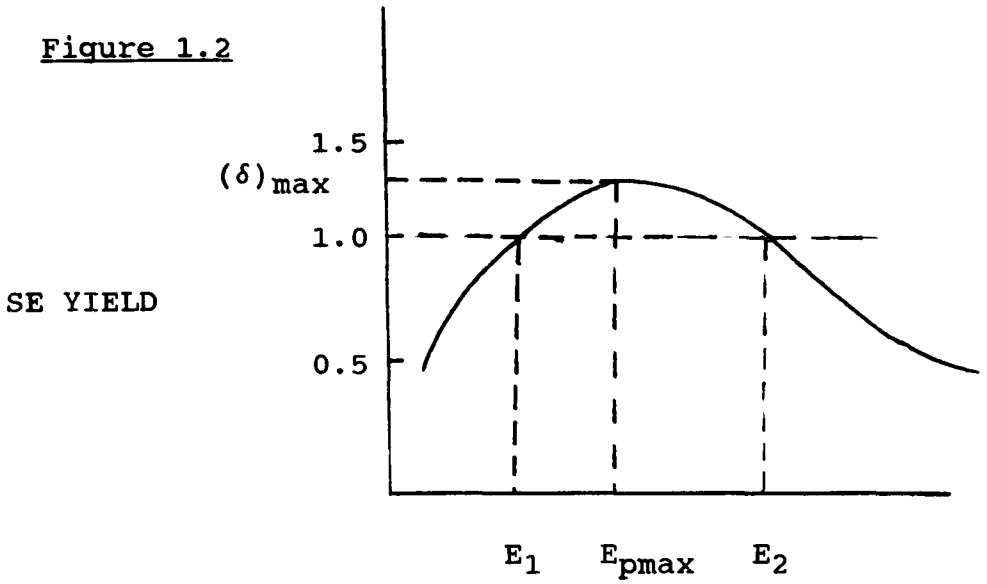

Schematic illustration of the SE yield (δ), from a material bombarded with primary electrons of a range of energies. The maximum yield (δ_{max}) corresponds to a single beam energy E_{pmax}. For energies $<E_1$ and $>E_2$ a net negative charge results. However, for energies between E_1 and E_2 a positive charge results. If, however, the beam energy corresponds to either E_1 or E_2 no net charge results.

The curve shows that at low beam energies, the yield is small. As the energy is increased, the yield begins to rise reaching a maximum (δ_{max}). Beyond this point, the yield begins to fall. This is due to the increased penetration depth of primary electrons and a correspondingly reduced probability that generated SEs will succeed in travelling from their point of generation to the specimen's surface, while still having sufficient kinetic energy to overcome the surface potential barrier (work function). Two important energy values, E_1 and E_2 arise from this consideration, and are indicated in figure (1.2). These relate to the beam energies which give (δ) equal to unity. When primary beam energies are less than E_1 or greater than E_2, then a net negative charge may be deposited on the specimen. This situation is dependent on the electrical conduction I_{sc} of the specimen, and the effect is particularly important if the specimen is an insulator. If, however, the beams energy is between these values, more electrons leave the surface than actually impinge upon it. The result is a net current flow from ground into the specimen. This must be taken into account when analysing active integrated circuits at these low beam energies. If (at energies greater than E_2) negative charge will be deposited into the device, or (between E_1 and E_2) the device may be loaded (positively charged), then in both situations the operation of the device may be adversely affected. Ideally, the energy of the primary electrons should correspond directly to E_2, where a charge balance will be maintained, and the device being tested should function normally.

Analysis of the total SE emission current, for any given beam energy, has been found to have:

(1) an **energy** spread and

(2) two **angular** distribution components [Mckay 1958, Dekker 1962].

The energy component (I_U) has already been indicated in figure (1.2), and may be expressed as

$$I_U = \int_0^{50} n(U)\ dU. \quad \ldots\ldots\ldots\ldots\ldots (1.4)$$

where U is the kinetic energy and 50 eV the arbitrary maximum energy of emitted SEs.

The two angular distributions are dependent on the inclination angle ϕ between the trajectory of the emitted electrons and a normal to the emitting surface (2.6).

$$I\phi = \int_0^{90} n(\phi)\ d\phi \quad \ldots\ldots\ldots\ldots\ldots\ldots (1.5)$$

It has been shown [Jonker 1952] that the maximum SE emission is always normal to the emitting surface, irrespective of the incident angle of the incoming primary electrons. It is further established that their yield decreases with the angle of emergence, this follows a cosine distribution. The second angular distribution is that associated with the Azimuth angle Ω. However

it has been reported that this effect is negligible (Plows 1968). Therefore, the total current (I_e), may be represented by the combination of equations (1.4) and (1.5)

$$I_e = \int_0^{50} \int_0^{90} n\,(U,\phi)\, dU\, d\phi \quad \ldots\ldots\ldots\ldots\ldots\ldots (1.6)$$

CHAPTER 2.

MECHANISM OF SCANNING ELECTRON MICROSCOPE IMAGE FORMATION.

(2.1) INTRODUCTION

The prime objective of the microscope's optics is to demagnify the beam of electrons, which is produced by the electron gun, by up to 10,000 times. The final result should be a finely focused electron beam which impinges upon the specimen. Three important interrelated parameters are:

(1) the **beam current** (i), which is usually in the range 1 pico-amp to 1 micro-amp,

(2) **beam diameter** (d), which ranges from a few nanometres to approximately one micrometre, and

(3) the **beam divergence** (α), 10^{-4} to 10^{-8} steradians.

These determine the beam brightness (β) and are related as follows [Goldstein et.al. 1981].

$$\beta = \frac{4i}{\pi^2 . d^2 . \alpha^2} \quad \ldots\ldots\ldots \quad (2.1).$$

The focused electron beam then leaves the optical column and strikes the specimen. At this location, the primary electrons enter the specimen and undergo elastic and/or inelastic scattering, this is often termed the interaction volume [Goldstein et.al.1981]. The primary electron beam is scanned over the specimen in a raster pattern, being driven by two pairs of

deflection coils. At each point where the primaries make contact with the specimen, a variety of quanta may be emitted. The resulting emissions and their magnitudes are directly related to some specific property of the specimen, each giving its own characteristic information. A variety of detectors are employed to sense the various emissions. The detector output serves to modulate the brightness of a CRT gun. With the scanning action of the primary electron beam synchronised to that of the CRT, a point by point variation or emission profile is built up to form an image.

(2.2) QUANTITATIVE DESCRIPTION OF IMAGE FORMATION.

The image produced on the SEM's CRT is formed due to differences of contrast, which are produced due to variations in pixel brightness [Everhart 1958]. Thus, contrast (C) may be expressed as:

$$C = dB/B \qquad \text{.....(2.2).}$$

Where B is the pixel brightness and dB the difference in brightness from pixel to pixel.

The level of pixel brightness forming the SE image is related to the level of video output from the SE detector. This output is a function of the SE yield from each point on the specimen's surface. It has been shown [Joy 1987], that the prime source of contrast is the variation of angle (θ) between the emitting surface and the angle of incidence of the electron beam. The yield increases rapidly, following a secant

relationship:

$$\delta(\theta) = \delta_0 \sec \theta \quad \ldots\ldots\ldots\ldots\ldots\ldots (2.3).$$

Where δ_0 is the SE coefficient measured at normal incidence to the specimen's surface. However, it has also been demonstrated that, this relationship does not hold true for beam energies below 5.0 KeV [Joy 1987]. At these lower beam energies, morphological contrast arises from the variations of detector collection efficiency with emission angle, which arise from the magnetic and electric field configurations within the specimen chamber.

Equation (1.6) gave a description of the total SE yield. However, resultant emission current will include other quanta such as backscattered electrons. Yet for any primary beam energy, there will be a specific ratio of SEs to backscattered electrons, as considered in figure [1.1]. Therefore, a realistic description of the total electron emission current (I_{eT}) as a function of time (t), must include both categories of electron and relate this to the irradiating beam current I_p.

$$I_{eT}(t) = K_e(x.y) * t * I_p \quad \ldots\ldots\ldots\ldots (2.4).$$

Where K_e is the point emission constant, the value of which is dependent on the SE to backscattered electron ratio, at each specific emission point.

An ideal detector would be able to discriminate between the backscattered electrons and SEs. In practice, however, this is not always possible. Thus, the SE detector is designed such that

it has a metallic ring or cage at its front, which is positively biased up to 200 volts. This increases the fraction of SEs it collects, as the trajectories of the SEs, with their low kinetic energy (less than 50 eV), are deflected towards the detector. The fraction of backscattered electrons collected is reduced by positioning the detector away from the more likely trajectories of these electrons, and because of their higher kinetic energy they are less likely to be attracted onto the SE detector.

Equation (2.4) may be rewritten in a more realistic form, describing the total collected electron emission current (I_c).

$$I_c(t) = K_c(x.y) * t * (I_{eT}) \quad .....(2.5).$$

Where K_c is the collected electron coefficient.

Equation (2.6), expresses the relationship between the video signal (V) and total collected electron emission current.

$$V = K_b * (I_c) * t \quad .....(2.6).$$

where K_b is an amplification coefficient which is the sum of the contributions from components within the detector and its amplification system. The video signal V is used to modulate the CRT grid giving a level of brightness (B);

$$B = K_a * (V*yd) + Bo \quad .....(2.7).$$

where Bo is the black level, and K_a and yd are parameters dependent on the CRT characteristics.

It may now be appreciated that the image observed on the

CRT shows how the output of a specific detector changes as the primary electron beam is moved over the specimen. Reference back to equation (1.6) expresses the components of the SE emission current. A change to any or all of these components results in a variation of contrast at the CRT.

(2.3) VOLTAGE DEPENDENT IMAGE CONTRAST.

The observation that the SE emission current was sensitive to variations in the specimen's surface potential, was reported back in the mid 1950's [Smith 1956]. This effect was investigated later by Oatley and Everhart [1957], who undertook to explain the mechanism behind this contrast formation. They successfully demonstrated its application with the imaging of a germanium-indium alloy p-n junction under reverse bias conditions, producing and recording a distinct voltage-dependent contrast difference between the two sides of the junction. Then later, Plows and Nixon [1968] showed how the with the addition of an electron beam strobing system to an SEM, the voltage contrast technique could be used to observe the time dependent logic states of an MOS transistor ladder operating within the SEM chamber. They were the first to demonstrate that this technique could be used for the analysis of micro-electronic circuits.

The voltage contrast is superimposed on top of the conventional topographic contrast, allowing an easy interpretation of images with good spatial resolution, and showing the voltage distribution over relatively large areas of circuits. Active devices operating within any conventional

commercial SEM could be examined, allowing logic state analysis for prototype evaluation or failure analysis. However, the technique was limited by the fact that the contrast was nondefinite and non-linear [Menzal and Kubalek 1983]. This meant that voltage contrast work could only be used to obtain qualitative information with regard to the relative voltage levels between two nodes. Despite this limitation, a typical voltage contrast image of a digital integrated circuit will show the more positive nodes having a dark contrast, with negative nodes bright and the nodes at ground not showing any additional contrast to that arising from their topographic and material nature.

Consider SEs being generated at a node to which a positive bias has been applied. Immediately above the node, there will be an electric field which acts as a barrier retarding the emission of lower energy SE's [Dinnis 1988]. The barrier height is dependent on the level of bias applied. For example, it has been shown [Everhart and Chung 1974] that, 75% of the SEs emitted from an aluminium target have energies below 5eV, as shown figure 2.1. Thus, for a barrier height of 5volts immediately above the aluminium target, the energy profile would be dramatically altered. The result is a reduction in the level of the detector output, since the SE detector integrates over the energy profile of the emitted SEs. If the emitting node was negatively biased, the SEs would be continuously accelerated toward the detector, due to an increased potential difference between the positively biased detector ring or cage and the emission point. As the detector integrates over the energy spectrum, a much greater output signal

Figure 2.1

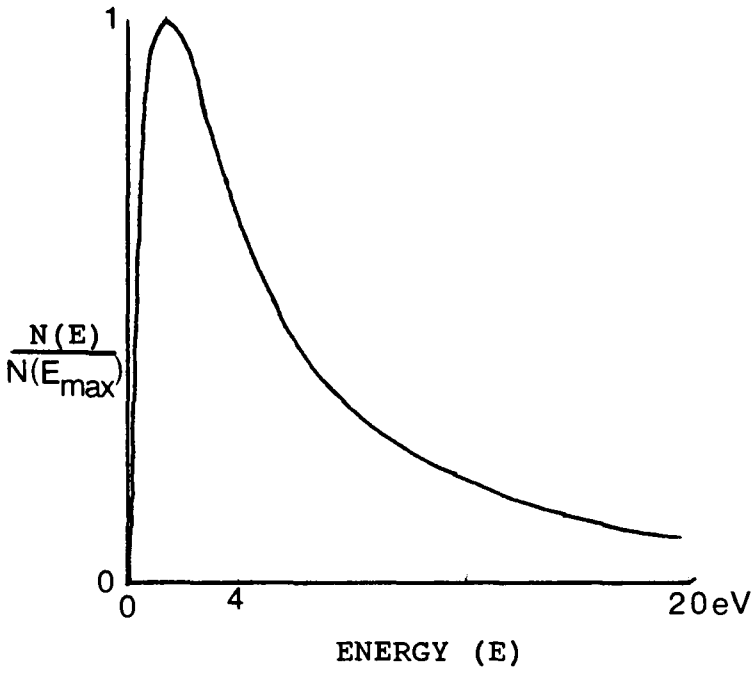

Schematic illustration of the secondary electron emission as a function of kinetic energy for a specific primary electron beam energy.

will occur due to the increased kinetic energies of the electrons.

Quantitative measurements are possible, and many workers have successfully demonstrated such techniques. This has been possible because the energy profiles of both SEs and Auger electrons undergo either an energy gain or loss as a consequence of change in surface potential. It has been shown that there was a linear shift to the 270 eV carbon Auger electron peak when bias was applied to the specimen [McDonald 1970]. There are, however, two major disadvantages to this particular technique for voltage measurement. Firstly, ultra high vacuum conditions are required to minimise surface contamination. Secondly, because the Auger electron yield is relatively low, long exposure times to the primary beam are necessary. This leaves the energy analysis of SEs as the only practical choice for quantitative analysis. There is, however, one important criteria which must be satisfied. The energy profile must remain unaltered, apart from a linear shift which must be proportional to the change of emission point bias. Problems arise because the majority of SEs have such low kinetic energies. This makes their trajectories sensitive to any electrostatic fields between the emission point and the detector. In addition to this, the yield is affected by variations of material composition, work function and topography. All of these factors must be taken into account. The electrostatic fields are most troublesome [Nakamae et.al. 1981], and much effort has been devoted to the suppression of these effects. In particular, the problem of the local retardation field immediately above posi-

tively biased nodes has been explored.

Variation of a conventional SE detector's output with respect to the bias applied to a specimen is shown in figure 2.2. The major disadvantage is the fact that this detector is sensitive not only to the changing secondary electron energy profile (which carries the surface potential information) but also the yield of SEs. It has been shown [Davidson 1988] how, at more positive surface potentials, the detector's output decreases due to the action of the retardation barrier immediately above the emitting surface. He also showed that detector output begins to increase due to the gain of kinetic energy by the SEs as they are accelerated by the increased potential difference between the emitting surface and the front of the detector. It might be assumed that the detector's output would continue to rise as the field strength is increased. However, the detector output is observed not to rise in proportion. This is due to the fact that the detector's collection efficiency falls as the kinetic energy of the SEs increases. Their trajectories are also influenced, to a lesser extent by the collection field of the detector.

Several detectors have been designed specifically for voltage measurement. One of the first of these was the cylindrical mirror analyser [Wells and Bremer 1968]. This detector gives the differential form of the SE energy distribution, but it is now usual to find detectors which give the integral form of the energy distribution [Kursheed 1983]. This is achieved by allowing the collected SEs to pass through a controlled retardation field, enabling the detector to be selective with

Figure 2.2

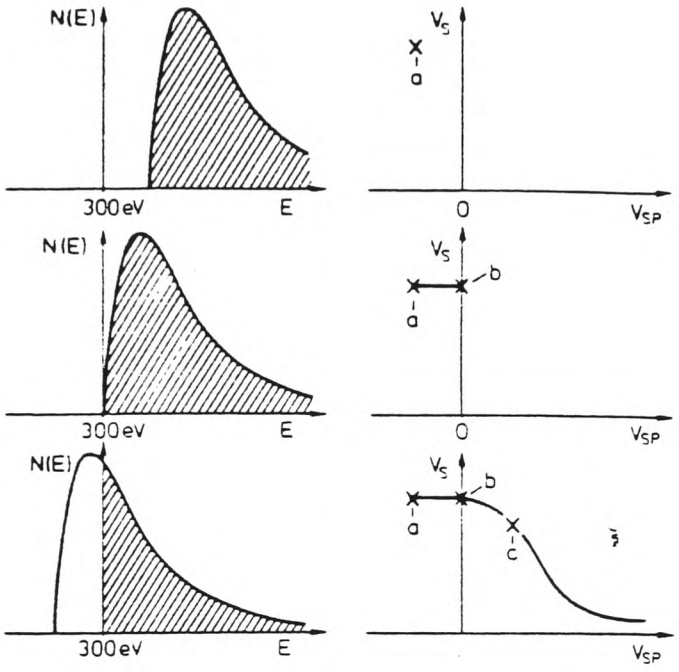

The schematic diagrams show how the SE energy distribution changes as specimen bias (V_{sp}) is altered. SEs are accelerated towards the detector (which integrates over SE distribution), giving a certain level of signal (V_s). When V_{sp} is negative, a typical value of V_s, which is represented by 'a' results. If V_{sp} is then held at ground potential there is little change in V_s, as indicated by 'b', however, when V_{sp} is positive V_s will fall, represented by 'c'. This fall is due to the presence of a retardation field (at the SE emission point), which truncates the SE energy distribution.

respect to energy. This system has been proven to be successful in producing a linear change of detector output current with respect to changing specimen bias.

CHAPTER 3.

QUANTITATIVE VOLTAGE CONTRAST.

(3.1) INTRODUCTION.

Quantitative voltage measurements are achieved by energy analysis of SEs with energies of 20 eV or less [Dinnis 1987]. Therefore, a detector is required which is sensitive to these low energy electrons and to any change in their energy profile, resulting from changes in specimen bias. Such a detector is also required to suppress the two local field effects (LFEs) comprising:

type 1: the truncation of the lower energy end of the SE energy spectrum due to the presence of a retardation barrier at positively biased nodes and,

type 2: the alteration of the SE angular distribution due to the influence of electrostatic fields on adjacent nodes.

As device geometries are reduced with voltage levels remaining similar, elimination of these sources of measurement error becomes increasingly difficult in practice.

(3.2) SURVEY OF QUANTITATIVE VOLTAGE CONTRAST DETECTORS/ SPECTROMETERS.

Surveying the published literature on detector design, it becomes apparent that, since the first published on a cylindrical mirror analyser [Wells and Bremer 1968], many different designs have been considered. The majority of these detectors still use

the scintillator, lightpipe and photomultiplier arrangement first introduced by Everhart and Thornley [1960]. This continued development of detectors has been based upon the improvement of one or more of the following:

(1) the **transport efficiency**, this being defined as a ratio of the numbers of actual to possible detected SEs,

(2) **voltage resolution**, defined as the minimum detectable change of bias applied to a specimen and,

(3) the **linearity**, of detector output with respect to changing specimen bias.

In general these detectors may be divided into two categories:

(1) **Band pass filters**, of which Wells and Bremer's detector is an example. The output of this type of detector has a differential form of the SE energy spectrum, as shown in figure 3.1a and b. Such detectors select a suitably narrow band of the SE energy spectrum and allow only these electrons to pass to the scintillator. Changes in the detector's video output will be due to changes of the SE's kinetic energy as the specimen voltage alters. A major disadvantage of this type of detector is its inherently low signal to noise ratio.

(2) **High-pass filters**, for which the output signal shows an integral form of the SE energy spectrum (usually termed an S-curve) due to the shape shown in figure 3.2a and b. A typical detector will have two electrode plates or grids prior to the

Figure 3.1a

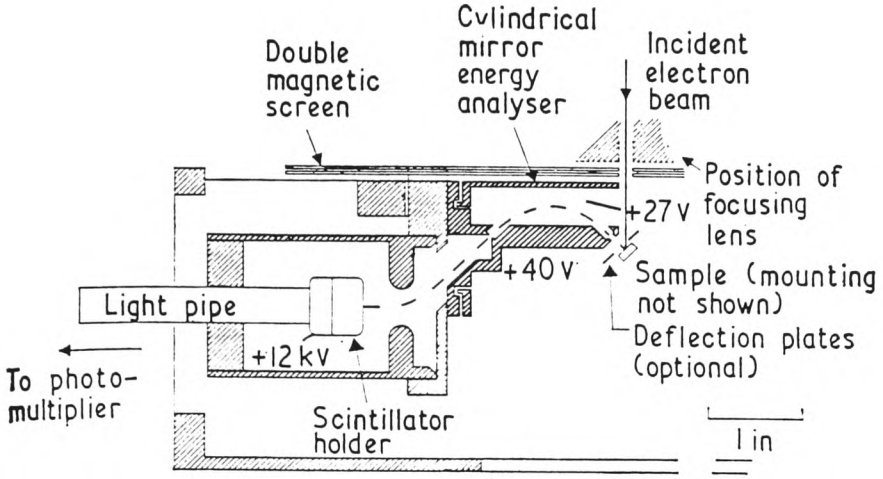

Schematic diagram of the Wells and Bremer detector.

Figure 3.1b

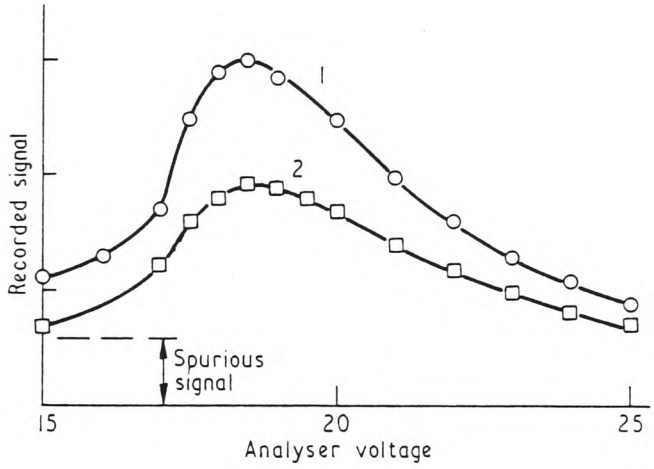

Typical results reported by Wells and Bremer using the above detector. Curve 1 was collected from gold and 2 from silicon targets. The primary beam was accelerated through 5 kV potential with a 30 nanoamps current.

Figure 3.2a

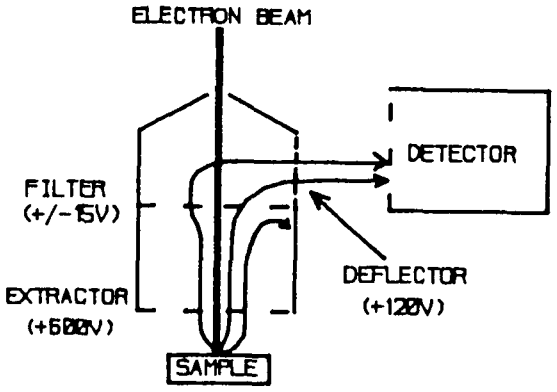

Schematic diagram of the Feuerbum high-pass energy filter secondary electron detector.

Figure 3.2b

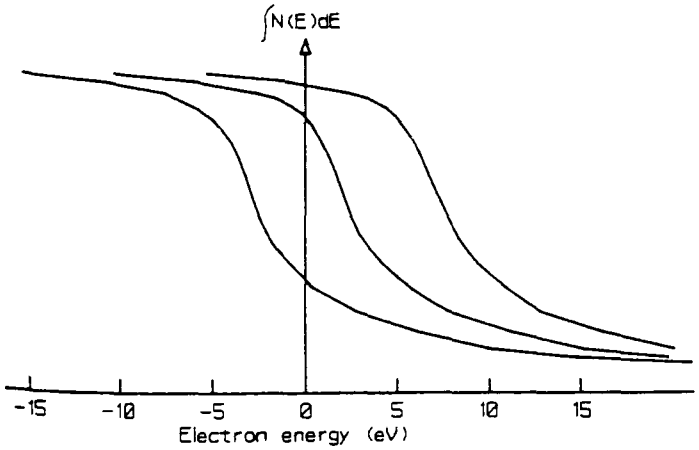

Typical integrated secondary electron energy spectra, from such a high-pass energy filter. The translation along the energy axis of the curves is due to changes of specimen bias.

scintillator. The first acts as an electron extractor, by establishing a positively charged electrostatic field between the entry port of the detector and the emission point at the specimen's surface. This field accelerates SEs into the detector, and also (depending on its strength) suppresses LFE types 1 and 2. The second plate or grid is used to establish a retarding electrostatic field. This acts to either accept or reject SEs, based on their kinetic energies, and so the detector's output reflects changes of the SE energy profile due to changing specimen bias.

This category of detector will have either a planar or hemispherical retardation field as shown in figure 3.3 depending on the shape of the second electrode. The planar field type detectors, however, suffer measurement errors which arise from the fact that only SEs with kinetic energy (E_{se}) components normal to the field are analysed [Menzal and Buchanan 1985]. Those SEs emitted from the specimen's surface at an angle (Ω), will cross the retarding field barrier established by the grid or electrode voltage (V_r) if,

$$E_{se} \cos^2 (\Omega) - eV_{sp} > eV_r \qquad (3.1).$$

with V_{sp} being the specimen's surface potential. This results in a reduced transport efficiency in comparison to hemispherical retardation field detectors.

When the hemispherical type of detector is used, the SE emission point must be kept at the centre or focal point of the hemispherical grid or electrode, so that the energy component E_{se}

Figure 3.3

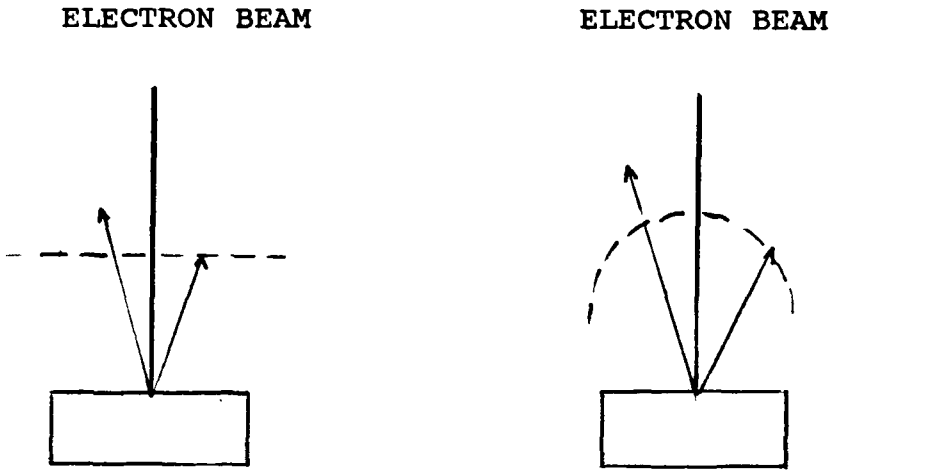

Schematic illustration of the possible configurations of secondary electron energy filters.

is always perpendicular to the equipotential of the retardation field. An improved transport efficiency has been shown [Menzal and Buchanan 1985] with such a detector, compared to that of the planar type. Whilst this type of detector may show an improved energy resolution, there is a major disadvantage in that these detectors are physically large. Since the detector is situated between the final objective lens and the specimen, an increased working distance (i.e. a much longer focal length) is required. Such working distances are often greater than 35 mm and so the spatial resolution is degraded. This compares with working distances of between 12 and 25 mm for planar retardation field type detectors.

A means for resolving the large working distance problem has been demonstrated by Menzal and Buchanan [1985], who mounted a planar detector in the optical column, just above the objective lens. This spectrometer arrangement gave satisfactory voltage measurements, with working distances as short as 3 mm. Another advantage of such a detector arrangement was the increased separation distance (60 mm) between the extraction plate, situated below the objective lens, and the retardation plate above. They showed how energy resolution improved as the separation distance increased. However, it is still not usual for detectors to have a separation distance in excess of 10 mm. One other advantage to this so called in-the-lens detector is that the SEs have to travel back up the objective lens, where they are refocused by it. It has been reported that with such an arrangement the transport efficiency is increased.

The design of electron optics for quantitative voltage detectors was originally based on the application of well understood electron/electrostatic field physics [Kursheed 1983], with some empirical adjustment. Applications of this work also included the description of SE trajectories for specific detector and specimen geometries. These take into account specific electrostatic fields (such as those immediately above positively biased specimen nodes), the fields between their emission point and entry to the detector, and then their trajectories through the detector/analyser system.

This analytical design process has been improved with the application of computer aided techniques, such as the simulation programs designed and developed by Kursheed [1983]. His work includes simulations of two-dimensional rectilinear fields, cylindrically symmetric fields, near surface fields for given nodal dimensions, applied bias levels, and non-symmetric three-dimensional fields. Each specific simulation shows electron trajectories and equipotential field lines, and may be used to calculate important parameters such as transport efficiencies and energy spectra. The main advantage of such programs is that a designer is able to interact with the simulation, observing the effects of changing detector geometries, electrode or grid bias, and surface or surface/detector fields.

(3.3) THE LINTECH INSTRUMENTS VOLTAGE MEASUREMENT ELECTRON COLLECTOR (VMEC).

The first commercially available detector was manufactured

and marketed by Lintech Instruments Ltd., from 1977. This quantitative voltage contrast detector is classified as a high-pass filter utilising a planar retardation field for energy analysis. It may be used in an imaging mode, to produce SE voltage dependent contrast images, showing relatively large qualitative mapping of surface potential distributions. Quantitative measurement of surface potential is achieved by displaying the level of detector output with respect to changing retardation electrode potential (i.e. the so called 'S curves'). If the detector is used in conjunction with a beam blanking system, then time dependent voltage waveforms may be produced. The most successful way of achieving this is to utilise a feedback loop system, of which there are two types:

(1) the **closed feedback loop** [Fleming and Ward 1970], in which a suitable level of detector output is selected and (using a feedback system) maintained. This effect is achieved by altering the level of filter electrode bias to compensate for increases or decreases of detector output which occur as the collected SE emission current alters in response to changes of emission point voltage. The change of filter bias gives an accurate measure of changes to emission point voltage.

(2) The **open loop**, where the change of detector output level is measured directly.

The VMEC's construction is shown in figure 3.4. It was designed to be inserted between the objective lens and the specimen. This has the disadvantage of requiring large working

Figure 3.4

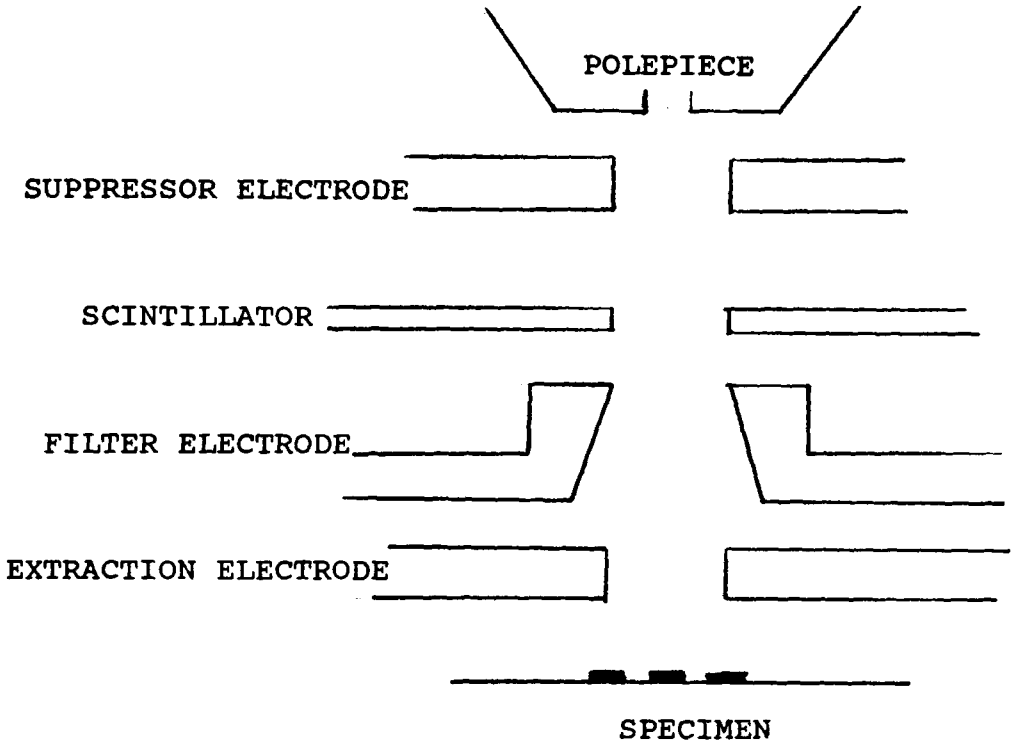

Schematic illustration showing a cross section through the voltage measurement electron collector (VMEC), a high-pass energy filter.

distances and hence reduced spatial resolution. The advantage of such detector is that it is retractable, so that the microscope may be used in any of its other variant modes [Richards and Trigg 1985]. The detector has a radially symmetric geometry, with a series of brass plates. The plate nearest the specimen provides the extraction field, and a static positive bias of up to 5 kilovolts may be applied to it. The extraction field strength is a function of both the plate bias and the separation distance between this plate and the emitting surface.

The second plate is ferrule shaped, and when biased negatively produces the retardation field. The bias applied to this plate varies over the range -25 to +25 volts, and it is the resulting change of field strength which enables the detector to be used as an energy filter, accepting or rejecting secondary electrons based upon their kinetic energy.

Those SEs which cross the retardation field should then be attracted onto an annular scintillator. To improve transport efficiency, a positive 10 kilovolt bias is applied to the scintillator.

The final plate, which is situated above the scintillator, is designed to reduce the possibility of backscattered electrons reaching the scintillator.

(3.4) QUANTITATIVE VOLTAGE/TIME MEASUREMENT.

To achieve functional data extraction from integrated circuits, one requires the SEM to perform as a sampling

oscilloscope [Gopinathan and Gopinath 1978]. The microscope is operated in a spot mode(i.e. the primary electron beam is held in a fixed position on the surface of the specimen). The beam is not allowed to illuminate this spot continuously, but is switched on and off rapidly; the beam switching being synchronised to the changing voltage at the specimen's surface. The beam 'on' pulse is shorter than that of the signal applied to the specimen. It is important, however, that the specimen's signal has a high repetition rate, and that the detector collects and then integrates over all the generated emissions. The application of this technique was first reported in the late 1960's by Plows and Nixon [1968]. They produced voltage contrast images of a metal-oxide-semiconductor (MOS) transistor ladder, to which a high frequency (7MHz; 5 V peak to peak) sinusoidal voltage had been applied. The resulting images appeared to be 'frozen' on the CRT, and by varying the time delay between the trigger pulse and the electron beam pulse 'on', the image's time window could be advanced and the ladder signal observed throughout the device operating cycle.

Electron beam switching is achieved by applying a common trigger pulse to the specimen and to a set of electrostatic blanking plates inserted within the electron optical column. To achieve the off state, a positive voltage of a suitable magnitude is applied to these metal plates. The resultant electrostatic field deflects the electron beam off the microscope's optical axis, and primary electrons no longer reach the specimen. To re-establish the on state, the blanking plates are grounded.

(3.5) SYSTEM RESOLUTION

There are three important interrelated parameters whose resolution limits the accuracy of EBT data[Lischke et al. 1987]:

(1) **Time resolution**, which may be defined as either the accuracy with which a signal delay between any two nodes may be determined, or the accuracy with which a signal change in time can be measured. Alternatively, it may be expressed as the measured increase of risetime, taken directly from the electron beam tester relative to that of the actual signal. Using a conventional sampling oscilloscope, the risetime resolution is limited by the bandwidth of the instrument's electronics. With regard to the electron beam test system, the measurement error (x) of signal risetime (t_s) is directly dependent on the electron beam pulse width (t_p), as illustrated in figure 3.5. The chosen pulse width should be less than the risetime of the signal being sampled (t_s). It may be considered that, as (x) decreases with pulse width, the shortest possible width would be selected. However, as this width is reduced, so the signal to noise level of the detection system is reduced, and the voltage resolution decreases. This is due to the fact that as pulse width is reduced, so the number of primary electrons which impinges upon the specimen is also reduced, for a constant initial primary beam current. To overcome this problem, it might be suggested that the primary beam current be increased. However, as the current is increased so the spatial resolution is decreased. Lischke et.al 1987, suggested that to achieve satisfactory timing measurements, a relative error tolerance should be agreed

Figure 3.5

The increased signal rise time that occurs when using EBT, due to the finite width of the electron beam pulse.

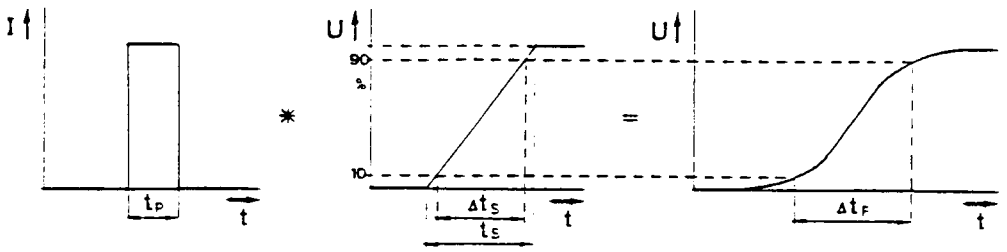

The electron beam pulse width (t_p).

Original signal s(t)

Resulting signal f(t)

t_p :Electron beam pulse width

Δt_s :Signal 10%-90% rise time

t_p :Rise time of voltage pulse

Δt_f :Measured 10%-90% rise time

prior to analysis. Using their graph, which is shown in figure 3.6, it is therefore possible to quote the signal risetime for an agreed error tolerance and electron beam pulse width.

(2) **Voltage resolution** may be defined as the minimum measurable change of specimen voltage. A series of expressions have been derived [Gopinath 1977], which gave the factors that affect the minimum detectable voltage change (dV_{min}), and their relationship to one another. The analysis included both band and high pass type detectors. From this work, it can be concluded that the SE current shot noise has the major effect on dV_{min}. Later workers [Menzal and Buchanan 1985], showed that the noise component must be less than the detector signal induced by the changing SE emission current due to changes of specimen bias. They described dV_{min} for a high-pass, retardation field analyser as:

$$dV_{min} = n.\ C\ (V_g,\ T_o,\ dE/E,\ N(E))\ .\ (dF/I_p)^{0.5} \quad .....(4.2).$$

where n is an acceptable signal to noise ratio, C is the spectrometer constant, E the secondary energies, dF the detection systems bandwidth, I_p the primary electron beam current, V_g the retardation grid or electrode voltage and T_o the transport efficiency.

(3) **Spatial resolution.** To achieve the best values, the electron gun and optics must both function to produce the minimum probe diameter (D_{pmin}), but contain the maximum probe current (I_{pmax}), thus giving the maximum possible probe current density

Figure 3.6

Signal rise time t_s which can be measured within an error limit X using stroboscopical electron beam pulse t_p

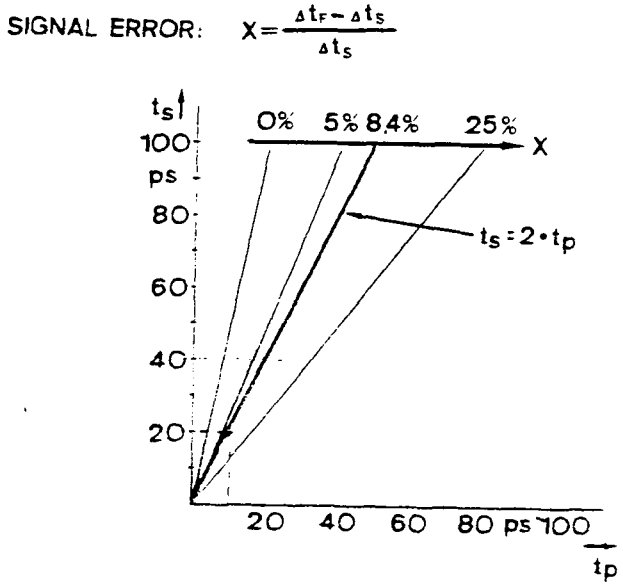

(D_{jc}).

The two major factors which influence (D_{jc}) are the electron gun brightness (B_g) and the lens aberrations of the optics. Gun brightness has a direct effect on I_{pmax}, and is defined as the electron current emitted from the source per unit solid angle. Beam degradation can arise due to lens aberrations, of which there are three types: **spherical** (C_s), **chromatic** (C_c) and **diffraction** of primaries by the defining apertures within the optical column. For primary beam energies above 10 keV, chromatic aberration tends not to be major a problem [Joy 1989]. This is because it arises from the energy spread (dE) of the primary electrons emitted for the electron gun's source material. For thermionic emitters at 30 kilovolts, dE values of greater than 3.0 eV and 1.5 eV, for W and LaB_6 respectively, have been determined. For field emission guns (FEG), values as low as 0.2 eV are typical. In all of these cases the energy distribution may be considered to have a gaussian distribution. However for EBT (which utilise much lower energies), of typically less than 2.5 keV, the energy distribution within the primary beam will be non-gaussian [Joy 1989]. The lower energies are used to minimise electron beam irradiation damage of the devices being tested [Ranasinghe 1987 and Russell et.al. 1989]. At these acceleration energies, dE increases and chromatic aberration further increases the probe diameter. Also, at the specimen's surface, the primary electron-specimen interaction volume changes in comparison to that for much higher electron acceleration energies. The penetration depth is reduced, and the interaction

cross section is increased. SEs are then emitted from an area greater than the diameter of the impinging probe, all serving to reduce the spatial resolution.

CHAPTER 4

THE APPLICATION OF ELECTRON BEAM TESTING.

(4.1) DEVELOPMENT OF EBT EQUIPMENT.

The hardware used for electron beam testing over the past three decades has undergone a considerable amount of development. Initially, EBT work was undertaken on the basic conventional SEM with no additional equipment. However, there were major disadvantages, in that only qualitative voltage measurements and limited timing resolution were possible. These factors encouraged the development of SE energy analysers and electron beam blanking units, to overcome these problems.

The next stage of development was to produce 'add-on' equipment to the SEM, enabling quantitative voltage measurement and the inclusion of electro-static plates within the optical column for rapid switching of the beam, giving considerable improvements to the timing resolution.

At this stage, the commercial market began to open up for EBT manufacturers, due to increased demand for their equipment from the micro-electronics industry. This was at a time when fabrication technology was progressing from LSI to VLSI and the limitations and disadvantages of the mechanical probe for measurements of the internal circuitry of micro-electronic devices became more of a problem. At the same time, the users of EBT equipment required their operation to be less specialised and so the EBT manufacturers began to introduce computer control and

automation.

This was the point at which EBT analysis was first integrated into the fabrication process, particularly at the design evaluation and failure analysis stages. A typical example of how such testing may be introduced is shown in the process layout reproduced in figure 4.1, after [Wolfgang et.al. 1979].

Following the above developments, the next generation of EB testers were 'stand-alone' or dedicated instruments, which included not only SE energy analysers and beam blanking equipment, but electron optics optimised for low voltage operation. The low voltage operation was a prime requirement for those manufacturers using MOS fabrication technology. Their concern was the danger of electrons, either directly or indirectly (by the generation of x-rays) damaging the thin gate dielectrics of their product, and thus causing circuit malfunction. To achieve improved performance of the optics at low voltages (typically less than 2 or 3 kV) the tungsten filament was replaced by the much higher brightness lanthanum hexaboride gun. This had the advantage of a much narrower spread of primary electron energies within the beam, thus reducing chromatic aberration. Moreover, it gave high primary electron beam current densities, improving both spatial and voltage resolution. Such instruments also include computer control of the stage and computer aided signal processing such as image analysis, signal averaging and filtering.

Figure 4.1

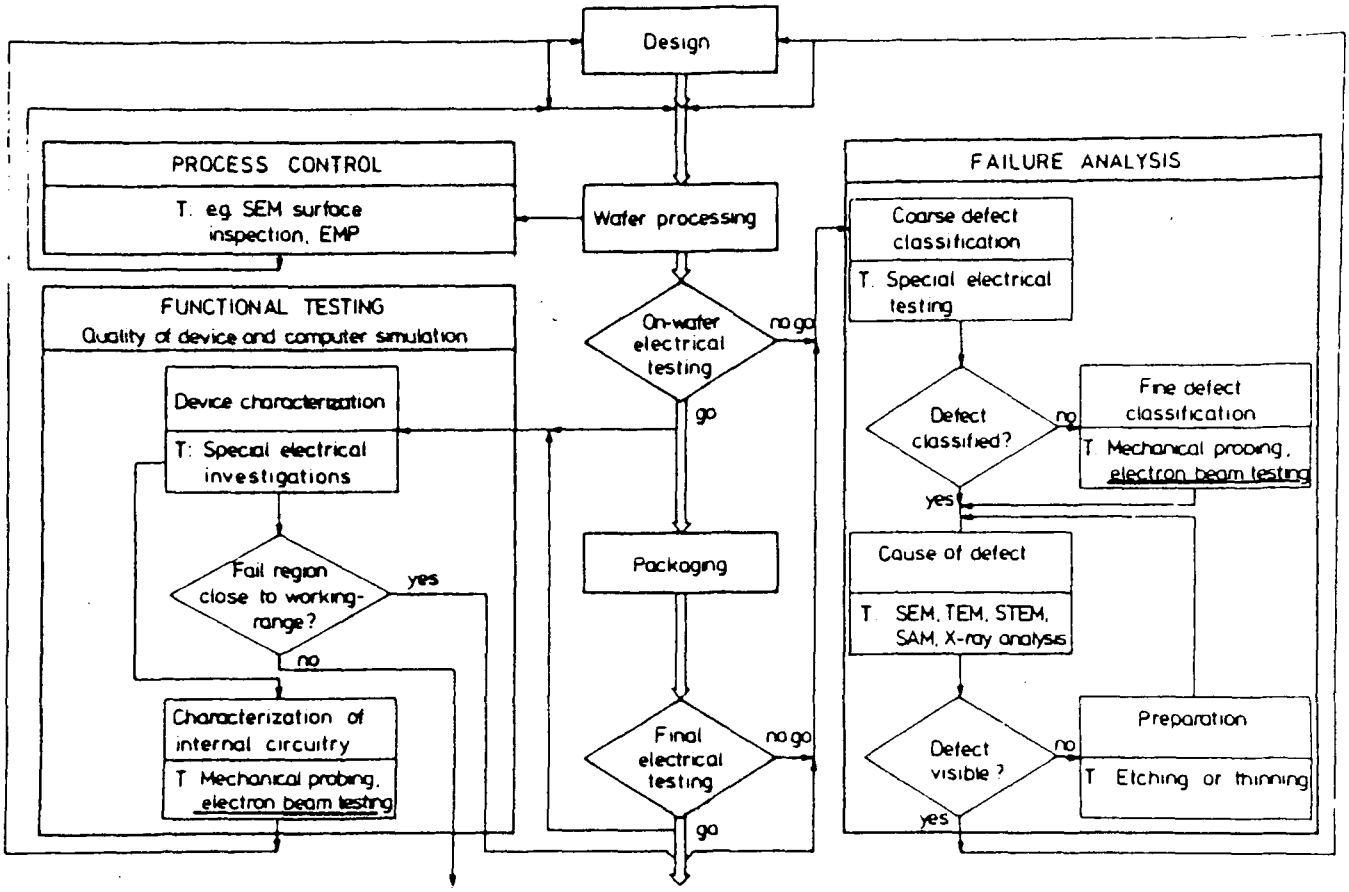

This IC's fabrication flow diagram suggests how EBT may be integrated for process control, failure analysis and functional testing. (T: Techniques indicated are, SEM: scanning electron microscope; EMP: electron microprobe; STEM: scanning transmission electron microscope; SAM:scanning Auger microprobe.)

Semiconductor technology, design, and fabrication continued to develop with single devices containing up to a million internal nodes. Achievement of this degree of integration meant further reduction of internal geometries, and an increase of the internal component to external connection pin ratio. These ULSI devices were also more sophisticated in their operation. Such factors also influenced the development of EB testers, and have led to the present day instruments. These may offer electron beams suitable for sub-micrometre geometry testing and picosecond time resolution. For high speed GaAs devices, the beam switching electronics itself has to be GaAs based [Fujioka and Ura 1981], and the required voltage sensitivity of around 10 millivolts implies the use of a combined lens and energy filter. Such testers are likely to include larger specimen chambers, which accommodate not only single micro-electronic devices but whole wafers. A certain amount of space may be occupied by driver circuitry for the device or wafer to be tested, such components are required to be near the device being tested so as to reduce transmission line interference. Alternative feedthrough cabling may also be required for external equipment used to generated complex functionality test patterns or signals which are designed to exercise internal functions of a device, such as addressing or signal decoding. Interfacing the EB tester to a CAD database system has become a necessary requirement because of increased device complexity. Such a database supports the logical design showing items such as connections between standard cells, and the design layout of the complete device with all interconnections. This may often be supplemented with the original mask designs

being displayed, to help find specific locations on the most complex devices. Computer aided image analysis has been developed so that a specific location may be identified on the original design and the computer will then drive the specimen stage automatically until this location on the specimen is imaged [Fujioka 1987].

(4.2) EBT TECHNIQUES.

Static voltage contrast is the simplest of all the techniques, and is possible using any SEM. The only additional equipment required is a suitable socket holder for the opened package of the device, electrical leads into the vacuum chamber and a d.c. supply. By applying d.c. voltage to any part of a specimen, the resultant image contrast will show those features that are more positively biased as dark, while those which are more negative appear bright.

It has been reported [Wolfgang et.al. 1979], that a voltage sensitivity of the order of 2 volts is the best possible. This does tend to limit the range of semiconductor devices which may be analysed using this technique. For example, ECL devices have voltage or logic swings of only a few hundred millivolts.

Dynamic voltage contrast or voltage coding is similar to static voltage contrast, except that a square or sinusoidal signal is applied to the specimen. The frequency of the applied signal must be an integral multiple of the SEM monitor's line or frame scan frequency.

A typical rapid scan image has a frame frequency of 25 Hz. If a square wave signal is then applied to the specimen at 100 Hz, four sets of alternate light and dark stripes will be seen on the monitor, corresponding to the negative and positive portions of the applied waveform. As the signal frequency is increased, so the widths of the stripes reduce and their numbers increase. The temporal resolution is limited to less than 500 Hz; this being limited by the bandwidth of the SE signal-processing system. This technique has proved itself ideal for circuit tracing, especially where little is known about the internal circuitry of a device with respect to the input/output pins. If a low frequency signal is applied to a specific pin, the characteristic light and dark stripes appear on all the circuitry connected to this specific pin.

The equipment required for this technique is similar to that used for static voltage contrast, but with the addition of a signal generator or a test pattern generator.

Stroboscopic voltage contrast requires a set of electrostatically charged plates which are positively biased; the magnitude of the charge being sufficient to deflect the primary electron beam off the optical axis. The beam blanking drive unit responsible for this action is synchronised to the clocking frequency for the specimen. The unit may be triggered either by the rising or falling edge of the specimen's signal. As the unit is triggered, the blanking plates are charged positive and held at this potential. Then the plates are grounded and the beam returns to the optical axis, irradiating the specimen. The

irradiation time is set to be some fraction of the specimen's clocking frequency. The plates are then charged positive, deflecting the beam off the optical axis once again. Then the unit is triggered again and the process is repeated, as shown in figure 4.2.

The resulting image is formed as the detector integrates over the emissions which occur when the specimen is irradiated. This technique increases the temporal resolution by many orders of magnitude. By increasing or decreasing the delay time between the trigger signal to the blanking drive unit and the grounding of the electrostatically charged plates, a static voltage contrast image of the specimen can be observed at any instant within the specimen clocking cycle.

Several extra items of equipment are required to achieve stroboscopic imaging. These include a picosecond pulse generator, and a system to control the delay between the trigger pulse and the electron beam pulse. A set of electrostatic plates must also be fitted within the optical column of the SEM. Image processor equipment may also be required. As the specimen's clocking frequency increases, so the time window of the primary beam pulse is reduced; the beam spending less and less time irradiating the specimen. Hence, the signal to noise ratio decreases accordingly.

Logic state mapping is a technique which allows realtime observation of the timing relationships between various specimen nodes. Using the stroboscopic equipment, a delay between the

Figure 4.2

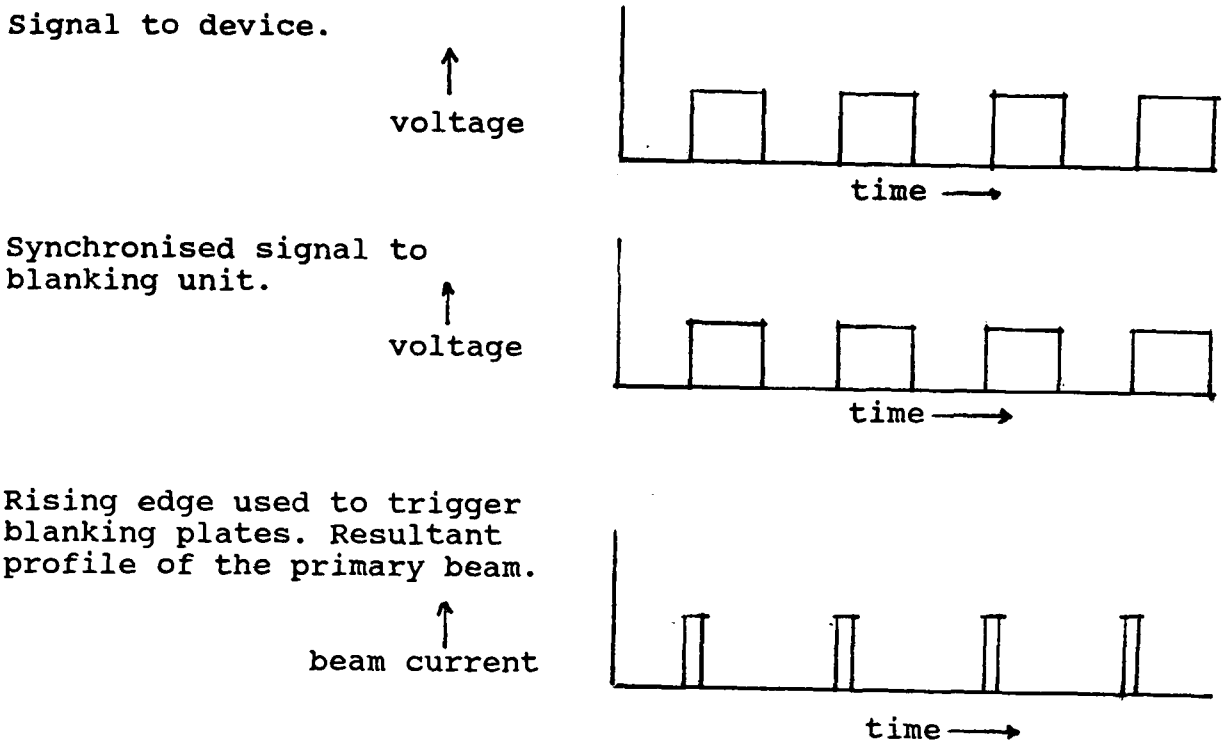

For stroboscopic imaging and voltage measurement the electron beam is pulsed in synchronism to the specimen voltage.

trigger and the beam pulse is synchronised with the SEM frame ramp. The result is a stroboscopic image having a time delay which varies linearly from the top to the bottom.

The technique of **quantitative specimen voltage measurement** has two options. One of these involves collection of an S-curve, while the other utilises a waveform displaying V(t). S-curves are usually collected from nodes biased with a d.c. signal, although they may also be obtained from a node to which a high frequency has been applied, via the stroboscopic system. S-curves are generally used to check the performance of the quantitative voltage measurement detector (for example, the quality of the plastic scintillator) or the electron irradiation parameters, such as the level of beam current irradiating the specimen. As for the waveforms, these may be used to measure V(t), for internal circuit nodes of the specimen. Using the beam blanking system, a delay is automatically introduced between the trigger pulse and the beam 'on' point. A fraction of the emitted SE energies is analysed, for example, using an open or closed loop system. The delay is then increased slightly, and the specimen irradiated once more. This process is repeated each time the delay is increased, until a series of points is produced on a display monitor (each of these representing the results of the SE energy analysis) yielding a V(t) waveform.

CHAPTER 5.

APPARATUS AND EXPERIMENTAL TECHNIQUE.

(5.1) THE SCANNING ELECTRON MICROSCOPE AND ASSOCIATED EQUIPMENT.

The project work was carried out on a JEOL JSM 840 high resolution scanning electron microscope (SEM) [figure 5.1]. This particular microscope was capable of an ultimate lateral resolution of 3.5 nanometers, and possessed a magnification range of X10 to X300,000. Other important operational features included a zoom condenser lens system to minimise incident beam shift, and the JEOL patented mini-objective lens with low aberration coefficients. Fundamental to the project was the requirement that the electron optics perform well at low primary beam acceleration voltages (less than 5.0 kilovolts). As the electron source was a conventional tungsten filament, the beam suffered predominately from chromatic aberration due to energy broadening; that is to a non-Gaussian distribution of electron energies within the beam [Joy 1989].

The 840's specimen chamber was of a suitable size to accommodate the various specimens, mounted in their holders, and still have adequate room to manoeuvre the latter, so that any part of the specimen could be observed. Several of the chamber's side panels could be removed, allowing the Voltage Measurement Electron Collector (VMEC) to be inserted, for quantitative voltage measurement. The chamber's back panel was replaced with one in which a 100 way feedthrough system had been fitted [figure 5.2]. This was used for connecting the various devices

Figure 5.1.

GENERAL VIEW OF THE SEM LABORATORY.

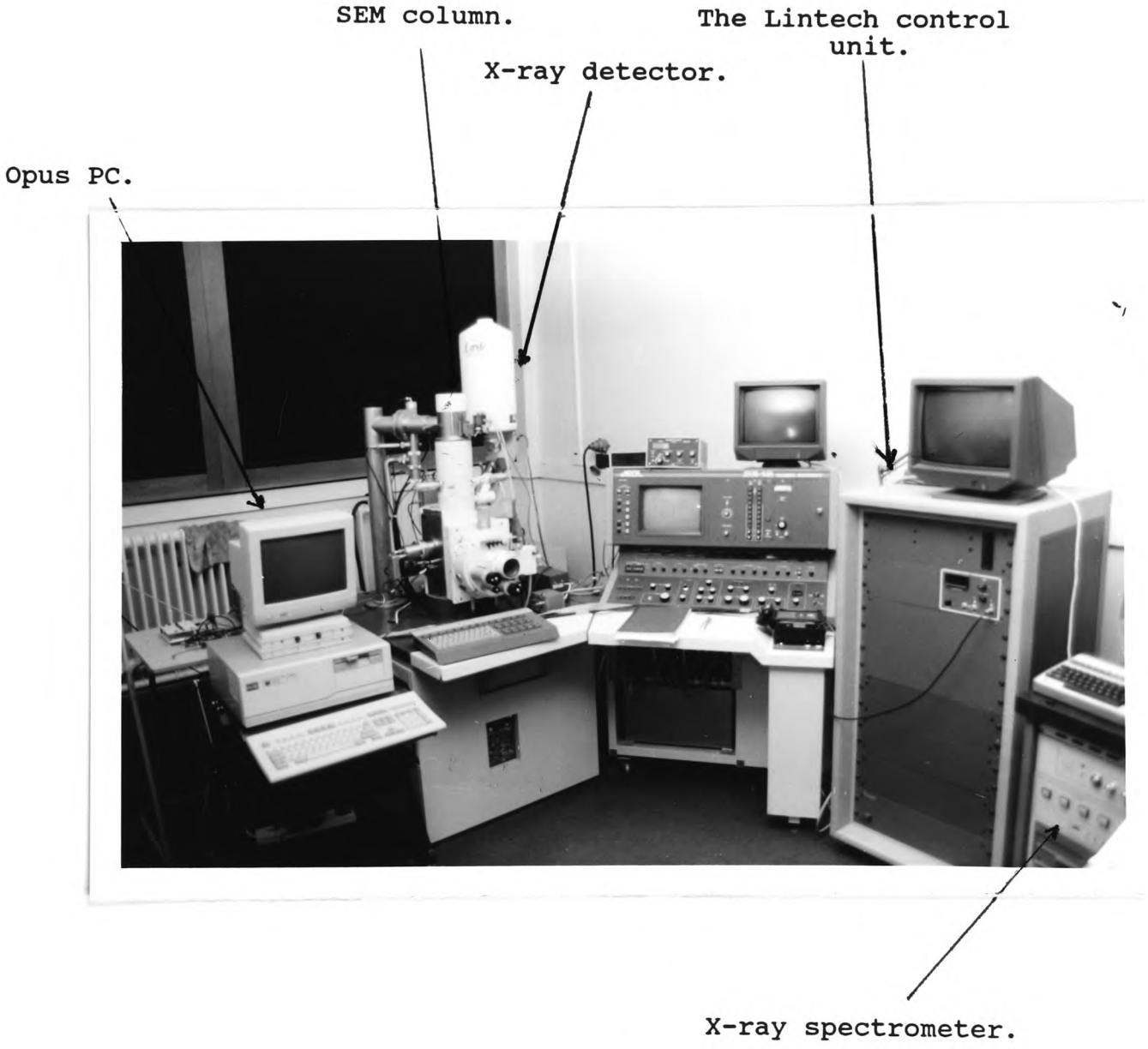

Figure 5.2

SEM viewed from the back, showing the vacuum feed through system via which electrical connections to the sample are made.

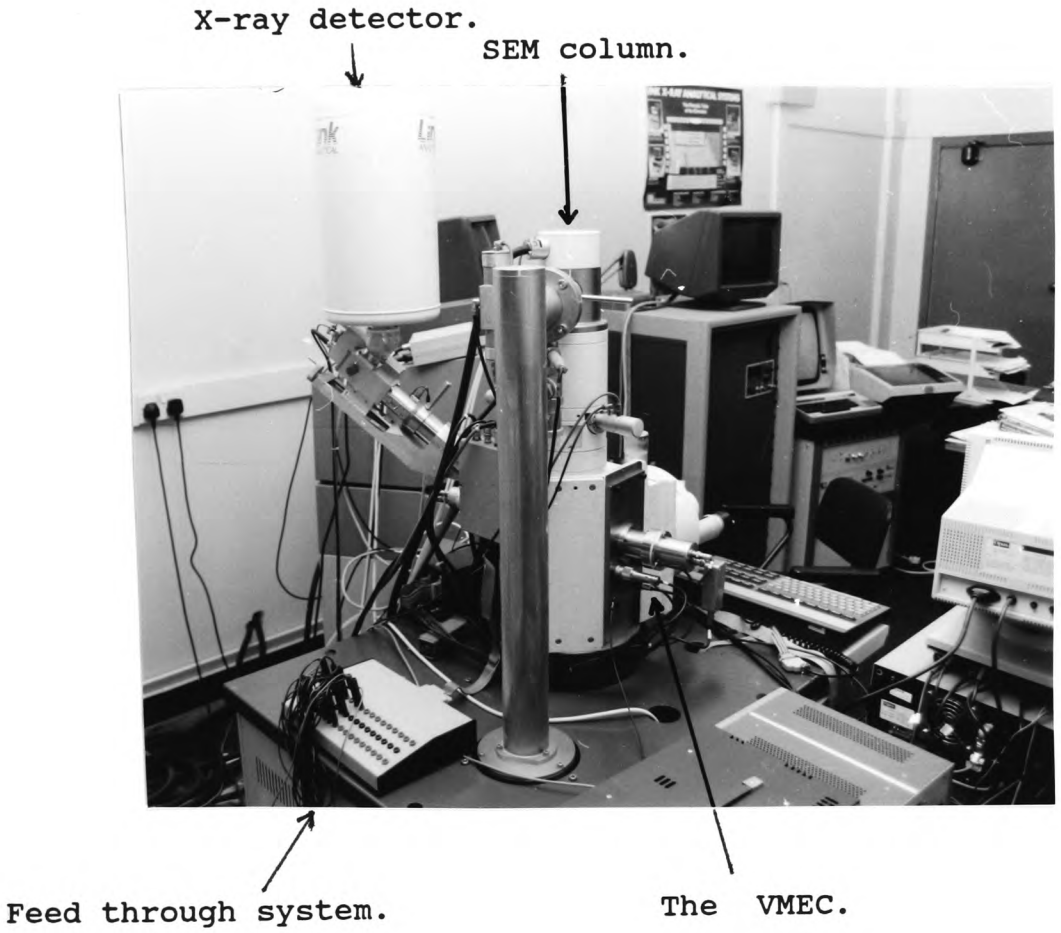

under test to the required power supply and signal generators.

Detection of SEs was via a conventional Everhart-Thornley type detector; the front being biased continually at 200 volts positive, to increase the collection efficiency. For the initial research, the microscope was operated with only the standard equipment.

To achieve quantitative measurement of both surface potential and it's change with time, additional equipment was supplied by Lintech Instruments Limited. This equipment was interfaced to the conventional SEM, although there was a certain degree of incompatibility of the electron beam scan drive of the SEM with the output of the Lintech system. This gave some image distortion at rapid scan rates. It was necessary to periodically insert and remove the VMEC, as its physical size and position hindered backscattered electron image and X-ray microanalysis. A beam blanking system was inserted temporarily in the optical column, between the anode plate and the first condenser lens. When not required, the plates would be retracted away from the optical axis, using a pneumatically controlled system. Included in the Lintech system was an image/signal processing unit. This was required because of the inherently poor signal to noise ratios which are a consequence of the stroboscopic work. Additional image analysis hardware and software were supplied by Brian Reece Scientific. This enabled image capture and subtraction to be performed.

Data analysis was introduced into the project using Procomm ver 2.1, and a data link between the Lintech and an Opus PC 3. This enabled waveforms and S-curve data to be transferred and converted into ASCII code files. These were subsequently analysed using the Keithley ASYST software.

(5.2) SPECIMENS.

Six different specimens were employed throughout the project. These were:

(a) A polished **aluminium SEM stub**, normally used as a mounting for SEM specimens. This specimen was prepared by conventional metallographic polishing and lapping techniques, to a finish of +/-0.25 micrometres, using diamond paste. This was done to reduce the effects of angular distribution on SE yield, due to surface morphology.

(b) A metallographically polished section of an **aluminium silicon alloy**. This was used to show the differences of detected SE energy spectrum, from pure silicon precipitates and the aluminium 0.05% silicon matrix. The matrix was of a similar composition to that of aluminium conductor tracks used on integrated circuits.

(c) **A calibration specimen**, designed especially for assessment of localised electrostatic fields on the SE energy profile (fabricated at British Telecom Martlsham Heath Ipswich). The device was mounted in a conventional 22-pin dual-in-line ceramic package, without its metal lid. The specimen was fabricated on a silicon substrate, onto which a micrometre of silicon dioxide had been grown. On top of this layer, aluminium lines had been patterned, giving a range of line widths and interline spacings. As with conventional integrated circuits, a micrometre of silicon dioxide had been deposited onto the device as a protection layer. This was removed using a standard

etchant, of the type that is usually used to etch p-type silicon.

(d) A commercially produced simple **7400 quad nand gate** device. Two of these devices were used, the first was mounted in a ceramic package with a metal lid. This was carefully removed using a scalpel blade, and the chip inside was found to have a protective silicon dioxide layer which was removed using the p-type etchant. As this circuit was damaged part way through the analysis, a second device was employed. This, however, was encapsulated in plastic rather than ceramic. Exposing the chip required the plastic immediately above it to be removed. A micro-milling machine was used to remove approximately 1 to 20 millimetres of plastic, before immersing the specimen in boiling sulphuric acid. Care was taken to allow the acid to remove just enough plastic to completely expose the device.

(e) A commercially produced **64k static random access memory**; this being the 1600L device manufactured by INMOS Ltd. This device was fabricated using complementary metal oxide silicon (CMOS) technology with 2 micrometre minimum design rules. It was a TTL standard device, packaged in a 22 pin dual-in-line ceramic package with metal lid, which was removed with the scalpel blade. The protective passivation layer used was silicon nitride, which was removed by plasma etching at INMOS plc.

(f) A commercially produced 32bit microprocessor, the **T414 transputer** manufactured by INMOS plc. This is sold as a 32-bit microcomputer with 2 kilobytes of on chip random access memory plus read only memory from which the device may boot up

and a configurable memory interface of four standard (INMOS) communication links. It has a maximum running speed of 20 MHz. The device package was ceramic, with a metal lid having 84-pins set in a grid array. The lid was removed prior to analysis, along with the silicon dioxide passivation layer, using the techniques already mentioned.

(5.3) EXPERIMENTAL PROCEDURE.

(5.3.1) DETERMINATION OF OPTIMUM SEM LOW VOLTAGE OPERATING CONDITIONS FOR VOLTAGE MEASUREMENT.

Voltage measurement using the SEM usually requires the microscope to be operated at relatively low primary beam energies, (less than 5keV compared to the more usual 20 to 30 keV). At these lower beam energies, the yield of SE's is maximised, but spatial resolution is compromised, due to lens aberrations. In particular, chromatic aberration occurs, due to an increase of the energy distribution of the primary electrons [Joy, private communication].

The initial project work was to determine several important parameters associated with this low energy operation. The first of these was the yield of SEs as a function of the primary beam energy. The specimen used for this work was the aluminium stub, which was held permanently at ground potential during the electron beam irradiation at various low energies. Other microscope parameters such as the beam current, magnification, irradiation time and separation distance between the specimen and the VMEC were kept constant. The SE yield was indicated by measurement of the area under the differentiated SE energy profile curve between two chosen boundary values.

The actual energy of the beam was then measured by collection of the x-rays emitted from the specimen in response to primary beam irradiation. For this work, the x-ray detector was

operated with only a thin formvar plastic window isolating the detector's silicon crystal from the SEM chamber. This enabled x-rays with energies as low as 200 eV to be detected. The beam energy was determined as that energy at which the x-ray continuum cut off occurred.

The SEM may be used as a tool for the voltage measurement of narrow metal conductor tracks on ICs. However, the track must be wider than the electron probe. If the probe's diameter is greater than the track width, then SEs will be generated from the surrounding material, and this may result in measurement error [Menzal and Kubalek 1983]. Therefore, the electron probe diameter was measured under typical low energy operating conditions using the technique recommend by Goldstein et.al. [1981]. This required the beam to be scanned in a single line across a 'sharp' object and the edge of a freshly cleaved silicon (100) wafer was used for this purpose. The profile of SE detector signal with respect to beam position across the wafer was displayed, and the beam diameter was determined as the distance between the 10% and 90% signal levels. However, it should be noted that there will be some measurement error, as the energy profile of the beam is assumed to be Gaussian, which is not the case at these lower beam energies, particularly as a tungsten filament was the electron source [Jansen 1985]

Using the electron beam at various energies means that energy will be deposited at the surface of the specimen and at various depths [Everhart and Hoff 1971]. The deposition of energy into ICs has important implications, as certain devices have

structures which are sensitive to irradiation damage, For example, the thin (less than 50 nanometres thick) gate oxide of MOS devices is particularly vulnerable. Results have been reported [Reiners et.al. 1985] showing a definite shift in the threshold voltage of MOS transistors under prolonged electron beam irradiation.

To understand where within a specimen energy deposition occurs, computer simulations have been developed [Joy 1988 and Napchan 1987]. These simulations use Monte Carlo random number generation routines to simulate electron scattering events within a material. The results display possible electron trajectories and calculates the maximum path length of primaries within specimens. This work showed that energy deposition from primaries is unlikely to cause the devices under test to malfunction. However, the x-rays generated due to electron specimen interactions can penetrate the gate oxide [Miyoshi et.al.1982], depositing energy which may generate electron-hole pairs. Holes may then become trapped at the silicon-silicon dioxide interface, resulting in a shift of threshold voltage of MOS devices.

(5.3.2) QUANTITATIVE MEASUREMENT USING THE CONVENTIONAL SE DETECTOR.

The project work described above has enabled the selection of optimum settings of low primary electron beam energies and currents for EBT work. Next, measurements of specimen voltage were made. As the voltage information is carried by SEs, the

effect upon the detector's output signal of changing the bias applied to an aluminium stub from +25 through to -25 volts was recorded.

This work has shown the inability of the conventional SE detector to accurately sense the changing energy profile of the emitted SEs, and the VMEC was therefore inserted into the SEM as shown in figure 5.3, and figure 5.4 showing a sample in its holder positioned close to the VMEC.

(5.3.3) CHARACTERISATION OF THE VMEC.

This high pass energy filter was more complicated to operate than the conventional detector, so a characterisation exercise was undertaken. An operational procedure was first derived, and this was subsequently adhered to in obtaining an image using the VMEC.

With the low energy primary electron beam irradiating the specimen with the required acceleration voltage and beam current, the VMEC was operated as follows. The extraction electrode was biased up to 2kV, in steps of 20V. The maximum possible bias which may be applied to this electrode is 5kV. This produced an electrostatic extraction field of sufficient strength to give the detector satisfactory collection efficiency. However, it was not intended at this stage that the field be used to suppress effects of any localised fields which may exist at the specimen surface.

Figure 5.3.

POSITION OF VMEC IN THE SEM CHAMBER.

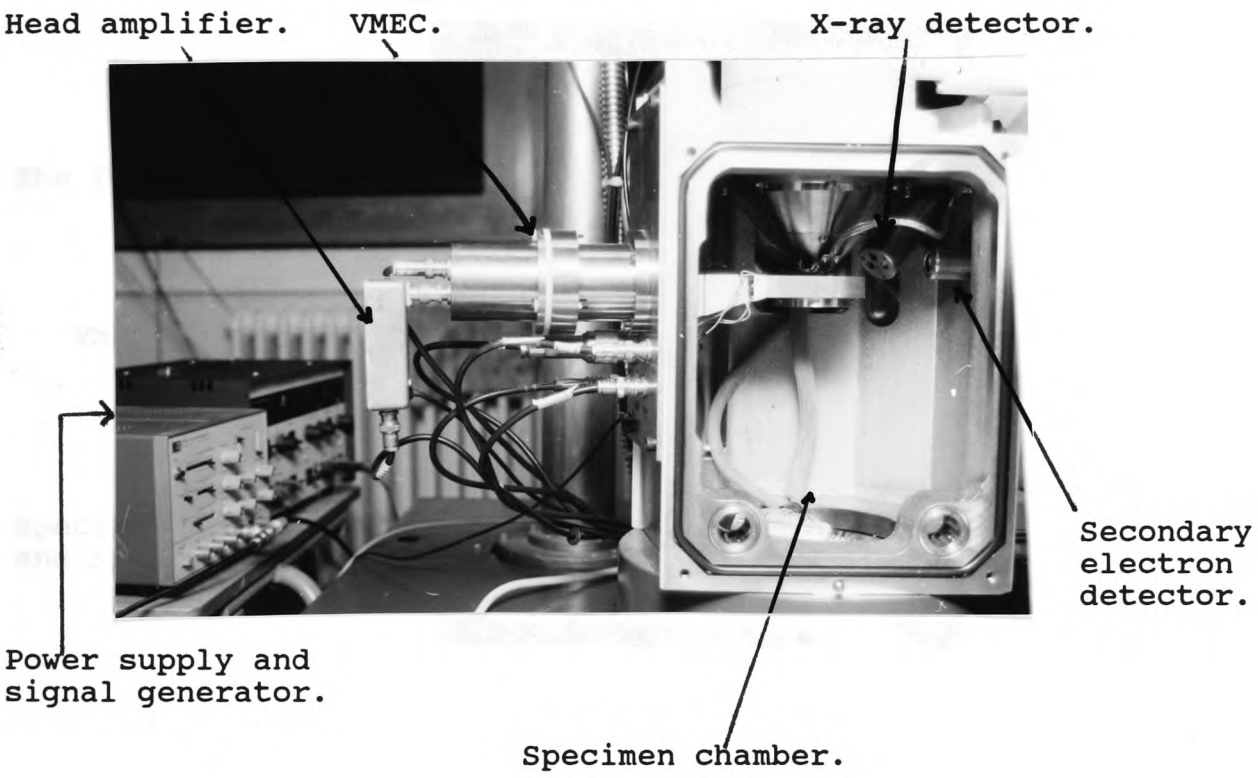

Figure 5.4

THE POSITIONING OF THE VMEC, SPECIMEN AND THE SEM's POLEPIECE.

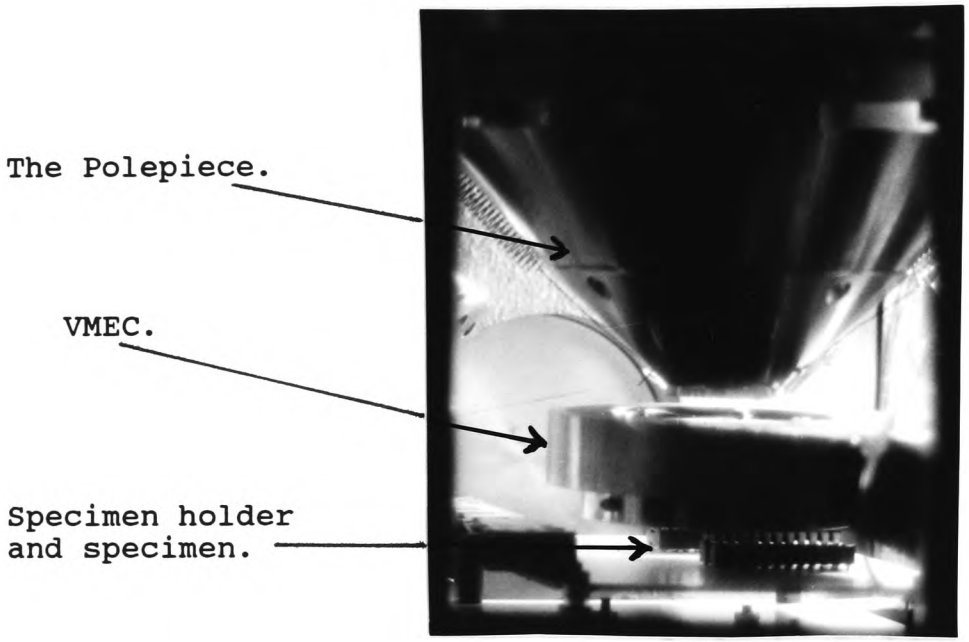

The offset or video level was then set. This could be adjusted between + to - 32 volts, in steps of 0.2 volt, and was made positive until the screen on the monitor began to brighten.

Next, the photomultiplier tube voltage was steadily increased from zero, in steps of 5 volts; the maximum possible bias being 2.19 kV. As the tube voltage was increased, so an image of the specimen was formed on the monitor. The level of the tube voltage controlled the image's contrast. Minor adjustments were made to avoid extremes of light and dark.

Finally the filter electrode bias was set. This electrode's electrostatic field acted to either accept or reject SEs on the basis of their energy, its bias being set between + and -25 volts. By observing the image on the monitor, the filter electrode bias was increased from zero, causing those nodes on the sample which are positively biased to darken progressively.

For quantitative measurements, a similar set up procedure was followed, with the electron beam being held static on a selected node. The filter electrode bias was automatically ramped continuously over the full range of electrode bias. By observing the graphic display monitor of the Lintech system, the photomultiplier voltage was adjusted to give an 'S-curve' with the steepest slope. A final adjustment to the position of the curve on the monitor was made using the offset bias.

To evaluate the data produced from the signal output of the VMEC, a data transmission and analysis system was developed, as described in section 5.1.

A simple program was written in ASYST (appendix 2), which allowed the collected data to be analysed. For example, this permitted the translation of an 'S-curve' along the filter electrode voltage axis. This procedure was used to determine the specimen's voltage shift. A series of 'S-curves' was analysed to determine the value of detector output to be used for the optimal measurement of voltage change. This was found to be between 0.5 and 0.75 of the maximum level of detector output. Another sub-routine of the ASYST program was used to measure the area under any selected portion of the differentiated curves. This allowed determination of changes of the SE yield.

Detector characterisation was then undertaken, first considering the effect of extraction electrode bias upon detector efficiency. The aluminium stub used was held permanently at ground potential, and all beam conditions were kept constant as a series of 'S-curves' was collected. The extraction field strength was varied for each curve. Each 'S-curve' was later differentiated, and the area under the resulting curve between two chosen boundaries was determined, and used to measure the relative SE yield.

The above work was repeated with the aluminium stub bias being varied from zero to +5 volts; 'S-curves' being collected at one volt intervals. This work showed how the localised potential barrier (LFE 1) can affect the shape of an S-curve and the SE energy distribution.

From the previous results, it was possible to select the optimum level of extraction electrode voltage. This was done and the stub then biased from ground to +15volts, with S-curves being collected at 5 volt intervals. The next stage was to make measurements on the narrower aluminium strips of the specimen supplied by British Telecom, the geometries of which are similar to those of commercial ICs. This work was necessary as, at the much smaller geometries of actual devices, local field effects are more of a problem and can lead to increased measurement error.

(5.3.4) ASSESSMENT OF THE LOCAL FIELD EFFECTS, OF TYPES 1 AND 2, AS SOURCES OF MEASUREMENT ERROR.

Here, a standard separation distance of 6 millimetres was used between the detector and the specimen. All SEM operating conditions were standardised, being typical of those used during EBT. The power and the signals applied to the devices were also typical of those normally used for TTL devices; ground and +5 volts, being the low and high reference voltages respectively. The signal applied was a 500kHz square wave with a 50% duty cycle and a voltage amplitude of 5 volts.

A series of S-curves was collected for metal lines of widths 20 and 5 micrometres to which d.c. bias values of ground and then +5 volts were applied, using a range of extraction electrode voltages from 1 to 4 kV. The curves were then differentiated, and the area under the same portion of each curve was determined.

The previous work had concentrated on assessment of localised field effect (LFE) type 1, the action of a retardation barrier at the emitting node. The next stage was to measure, using the British Telecom device, the combined action of LFE 1 and 2. For this work, bias values from ground to 5.5 volts were applied to a metal line. S-curves were collected from the various levels of applied bias, at the narrowest portion of the metal line (8 micrometres as indicated in appendix 1). Several sets of curves were collected as before, but with d.c. bias of either ground or +5 volts being applied to the adjacent metal lines. The combined effects of LFE 1 and 2 and the application of the extraction field suppress these effects.

From all the previous data, the relationship between measurement error and the area under a chosen part of the SE energy distribution curve was found. This was used to predict the voltage measurement accuracy of any curve.

The final assessment of the LFEs was to measure, using the VMEC in a closed-loop measurement mode, the V(t) of a high frequency signal applied to the device. Again, from the narrowest line with a +5 volt d.c. potential applied to the adjacent lines, the measurement error was determined.

The 'set up' procedures both for qualitative and quantitative analysis were then evaluated by EBT of a simple 7400 TTL quad nand gate device as described in section 6.10.1.

CHAPTER 6.

RESULT AND DISCUSSION

(6.1) DETERMINATION OF THE OPTIMUM PRIMARY ELECTRON BEAM ACCELERATION VOLTAGE.

As quantitative voltage measurements within the SEM are based solely on changes of the SE energy profile in response to changing specimen voltages, it is important to generate the maximum possible SE yield; as voltage resolution is known to be dependent upon the signal to noise ratio [Gopinath 1977].

The yield of SEs is a function of primary beam acceleration voltage [McKay 1948]. Figure 6.1 shows the SE electron yield from the polished aluminium stub, as a function of primary electron beam energy for a constant beam current. This yield distribution is typical of any solid material irradiated by accelerated electrons. At lower beam energies, the SE yield is correspondingly low. As the energy increases, so does the SE yield. With more SEs being generated, more energy is deposited into the target. Eventually, the yield reaches a maximum, and figure 6.1 shows this to be at a beam energy of about 0.7kV. This value is significantly higher than the 0.3 kV reported by other workers [McKay 1948 and Dekker 1962]. This 'false' maximum is due to an inability of the present tungsten electron gun to maintain a constant beam current when very low acceleration voltages are used, due to electron-electron interactions, resulting in a final electron probe with a lower current density [Jansen 1985]. Whilst these results do not give an accurate

Figure 6.1

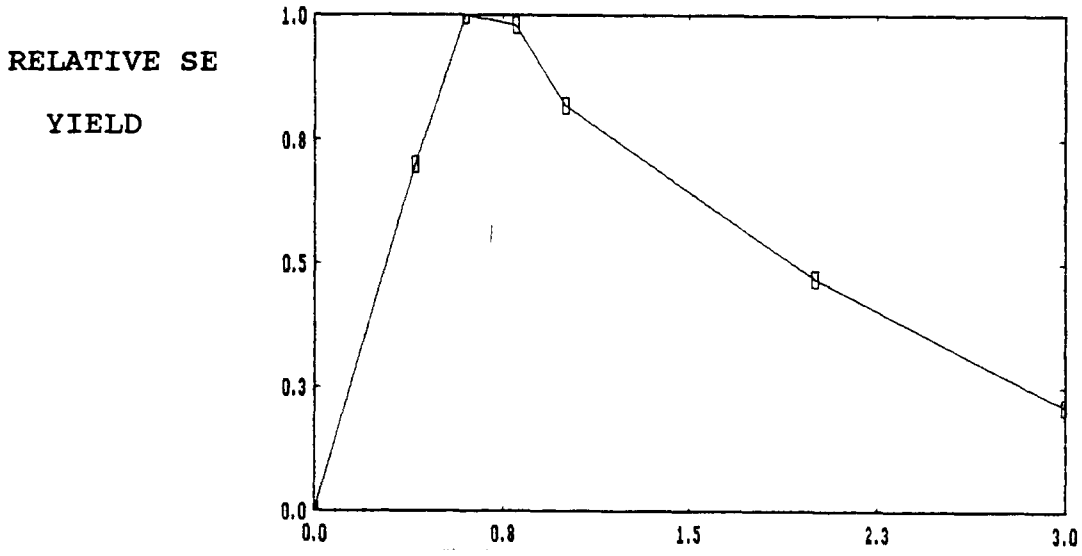

SE emission as a function of primary electron beam acceleration voltage.

profile of the 'true' SE yield, they never the less show which primary beam energy gives the maximum SE yield within this specific SEM. If the beam energy is increased above 0.7kV, the SE yield begins to fall, as also shown by other workers. The reason for the reduced yield is that at these higher energies, primary electrons are able to penetrate deeper into the specimen, so generating more SEs at greater depths. Because of their characteristic low energy, SEs are unable to reach the surface and escape from the specimen.

Figure 6.2 shows two x-ray spectra which were collected to check the accuracy of the selected values of acceleration voltage. The actual energy of the primary electron beam as it impinges onto the specimen is taken to be equal to the maximum energy of the x-ray continuum. Two characteristic x-ray peaks can also be seen for carbon and oxygen; these being likely to originate from contamination on the specimen surface.

From figure 6.1, it can be concluded that the VMEC is sensitive to changes of the SE yield. The maximum yield occurs at around 0.7kV, and it might be assumed that this is the optimum value of acceleration voltage. However, this does not take into account other primary electron beam parameters (and in particular the diameter of the beam) and its effect upon spatial resolution, as considered below.

(6.2) DETERMINATION OF THE PRIMARY BEAM DIAMETER AS A FUNCTION OF ACCELERATION VOLTAGE FOR SELECTED BEAM CURRENTS.

Based on the previous results showing the SE yield with

Figure 6.2

Typical examples of x-ray spectra, used to measure the maximum energy deposited into the specimen by the primary electron beam.

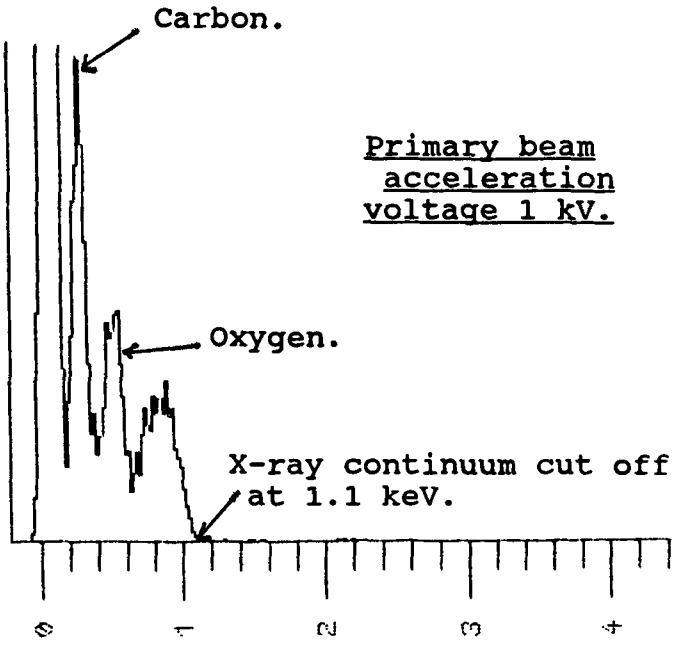

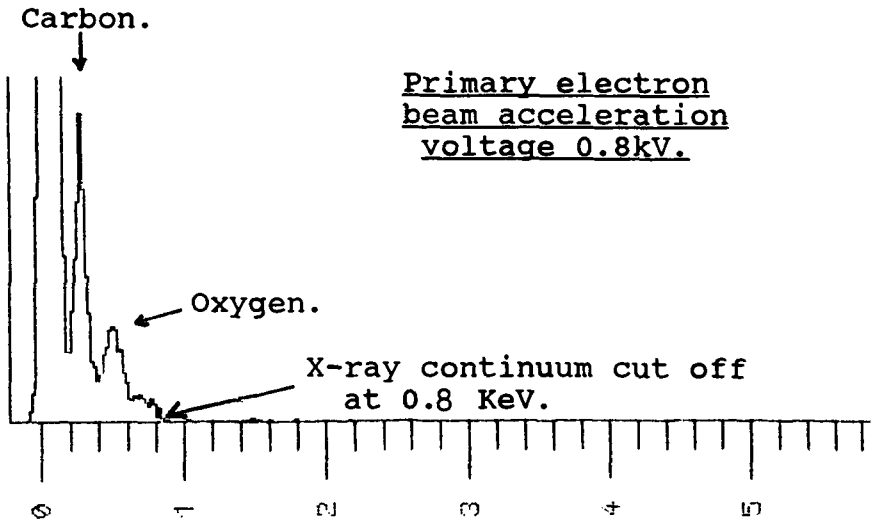

respect to acceleration voltage, it was necessary to determine the electron beam diameter for various beam currents. This measurement was undertaken using the technique described in section 5.3.1. A typical example of the SE detector's output as the primary electron beam is scanned across the freshly cleaved edge of a silicon wafer is shown in figure 6.3.

The probe diameter was then measured, for a fixed objective lens aperture of 1 millimetre, at beam acceleration voltages of 2, 1, and 0.8 kV and beam currents of 3, 1.5, 0.75, and 0.3 nanoamps. These parameters were chosen to be typical of the values used during electron beam testing. Attempts were made to make measurements at lower acceleration voltages, but the quality of the line profile was too poor and the diameter was not measurable. The final results are shown in figure 6.4.

Figure 6.4 shows how the probe diameter diminishes as lower values of probe current are selected. Therefore, to improve spatial resolution lower beam currents are preferred. However, the level of interactions between the primary electrons and the specimen will also fall, causing less quanta to be emitted. The figure also shows that for any given value of beam current, the measured probe diameter increases as the acceleration voltage is decreased. This will give a corresponding reduction in spatial resolution.

During EBT work, it is important to consider the size of the electron probe diameter relative to the size of the node being probed. The probe diameter must be smaller, to allow visual

Figure 6.3

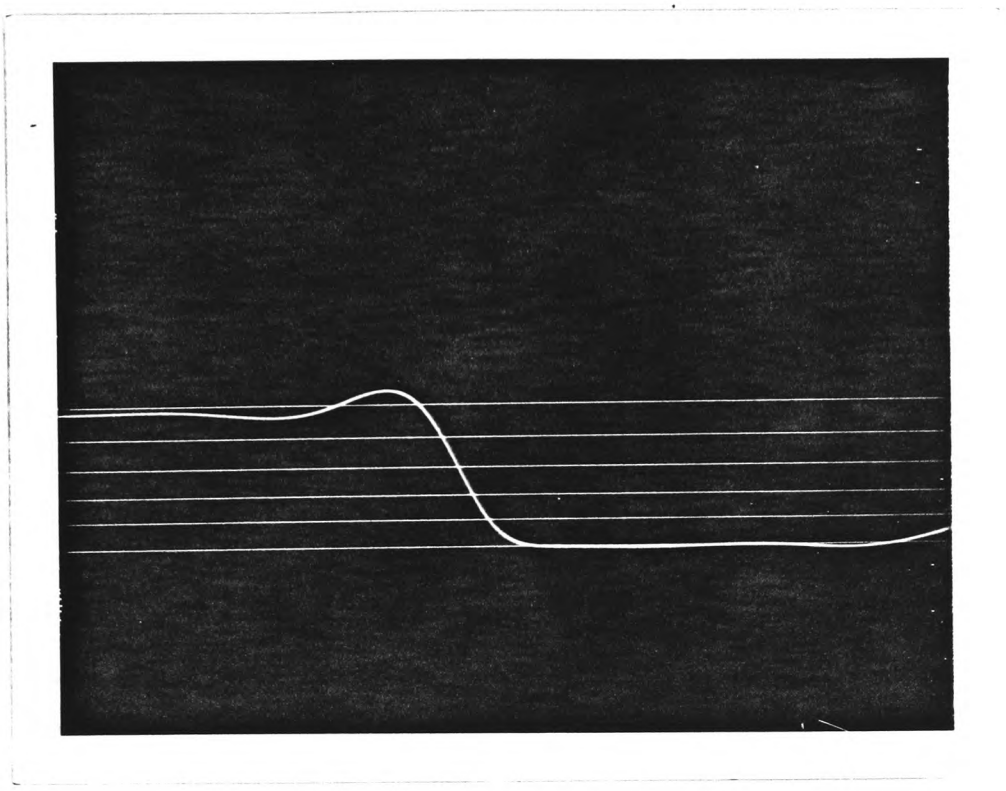

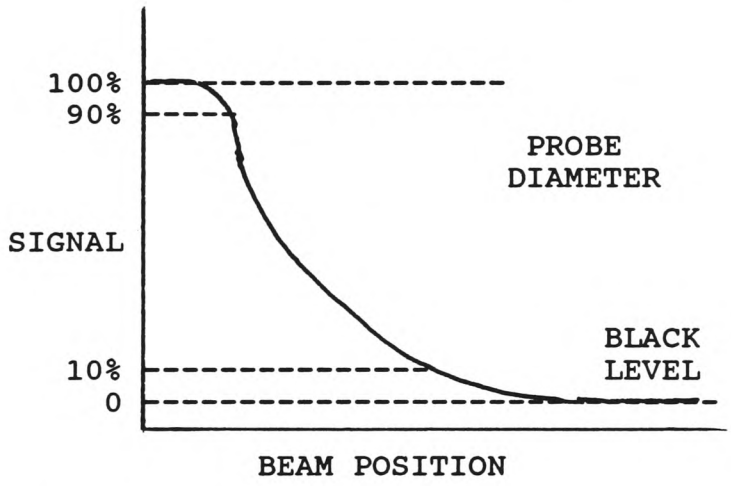

The figures show the SE detector's output, as the primary electron beam is scanned in a single line across the freshly fractured face of the silicon wafer. This information is used to measure the primary electron beam diameter, as indicated in the schematic illustration.

Figure 6.4

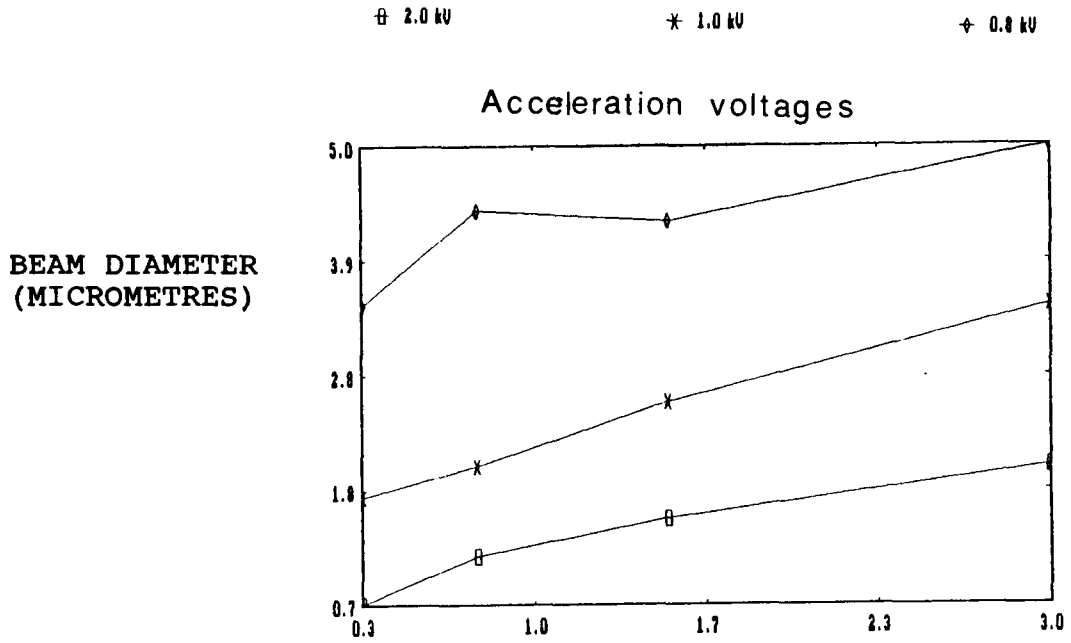

The effect on primary electron beam diameter of acceleration voltage and beam current

resolution of the node and to avoid the generation of SEs from the surrounding material. As will be shown later, there is some variation in the SE emission profile from different materials, and this may give rise to voltage measurement error.

(6.3) PENETRATION OF THE PRIMARY BEAM ELECTRONS.

Monte Carlo simulations as shown in figures 6.5 a and b show, for typical EBT beam acceleration voltages, the deposition of energy within aluminium. They indicate the maximum penetration of electrons to be approximately 30 nanometres. With the thickness of the aluminium conductors on most VLSI devices being of the order of 1 micrometre, there is little chance of these electrons reaching any of the sensitive device structures. However, little can be done to minimise the secondary process of x-ray generation that may cause damage. Figure 6.6 states the values of energies required to generated x-rays from the materials the primary electrons are likely to encounter.

When EBT work is carried out on MOS technology devices, it is common practice to use primary beam acceleration voltages of 1 kV or less, thus avoiding the generation of the relatively high intensity K series characteristic x-rays within aluminium or silicon. However, background x-radiation with energies equivalent to that of the electron beam energy will be generated, and thus the possibility of shifting the threshold voltage exists.

At the final stage of micro-electronic circuit fabrication, it is usual to form a protective or passivation layer over the devices. This typically involves the formation of a silicon

Figure 6.5a **TYPICAL EXAMPLES OF MONTE CARLO SIMULATIONS OF ELECTRON TRAJECTORIES IN ALUMINIUM FOR TWO DIFFERENT ACCELERATION VOLTAGES.**

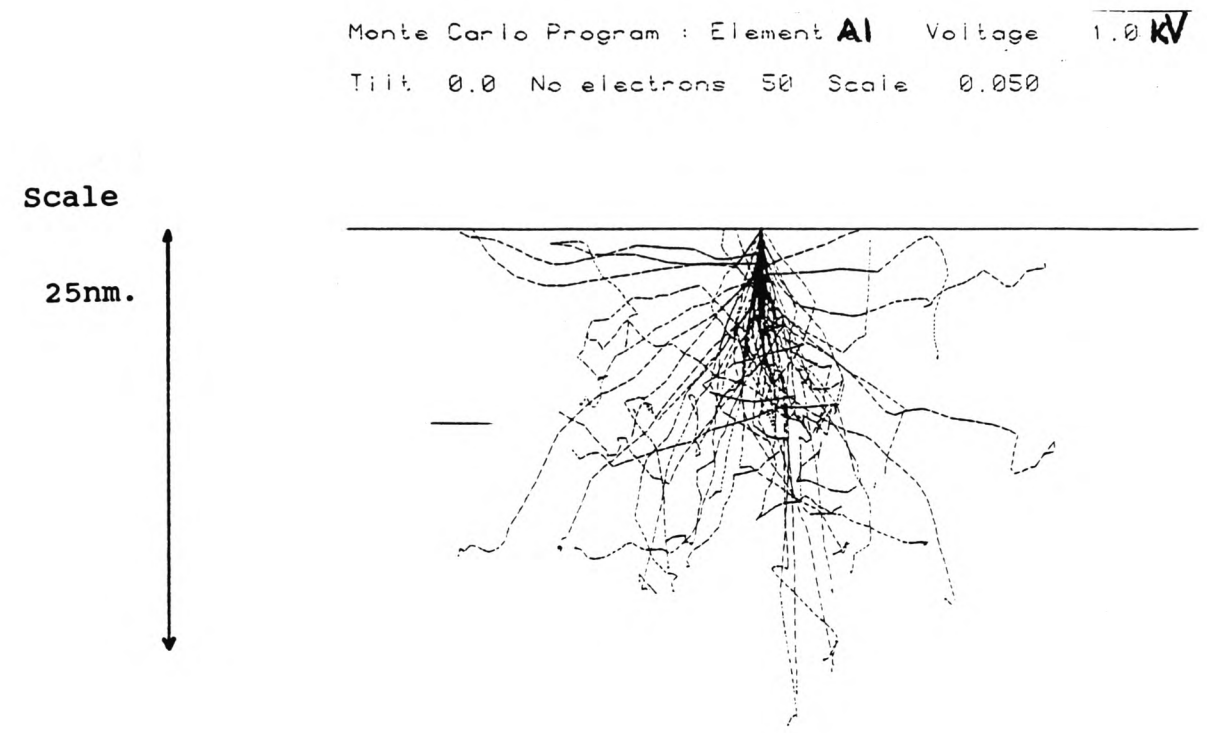

Figure 6.5b.

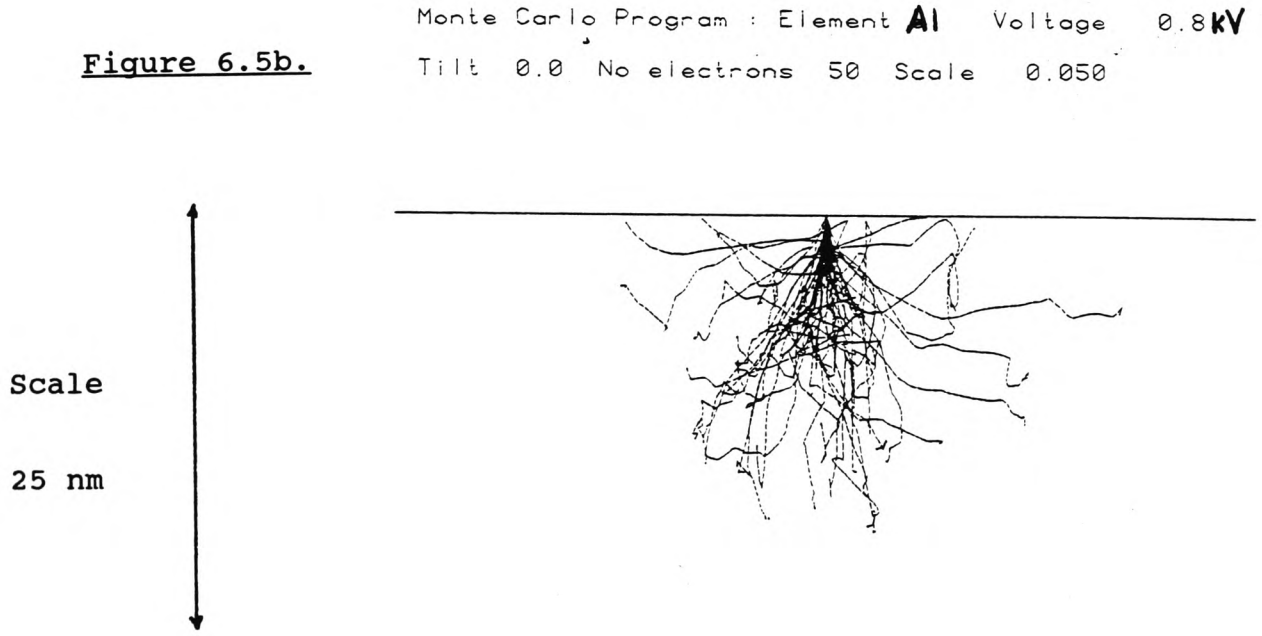

Figure 6.5c. MONTE CARLO SIMULATION OF ELECTRON TRAJECTORIES IN SILICON DIOXIDE, FOR THE SAME ACCELERATION VOLTAGE AS USED IN FIGURE 6.5b.

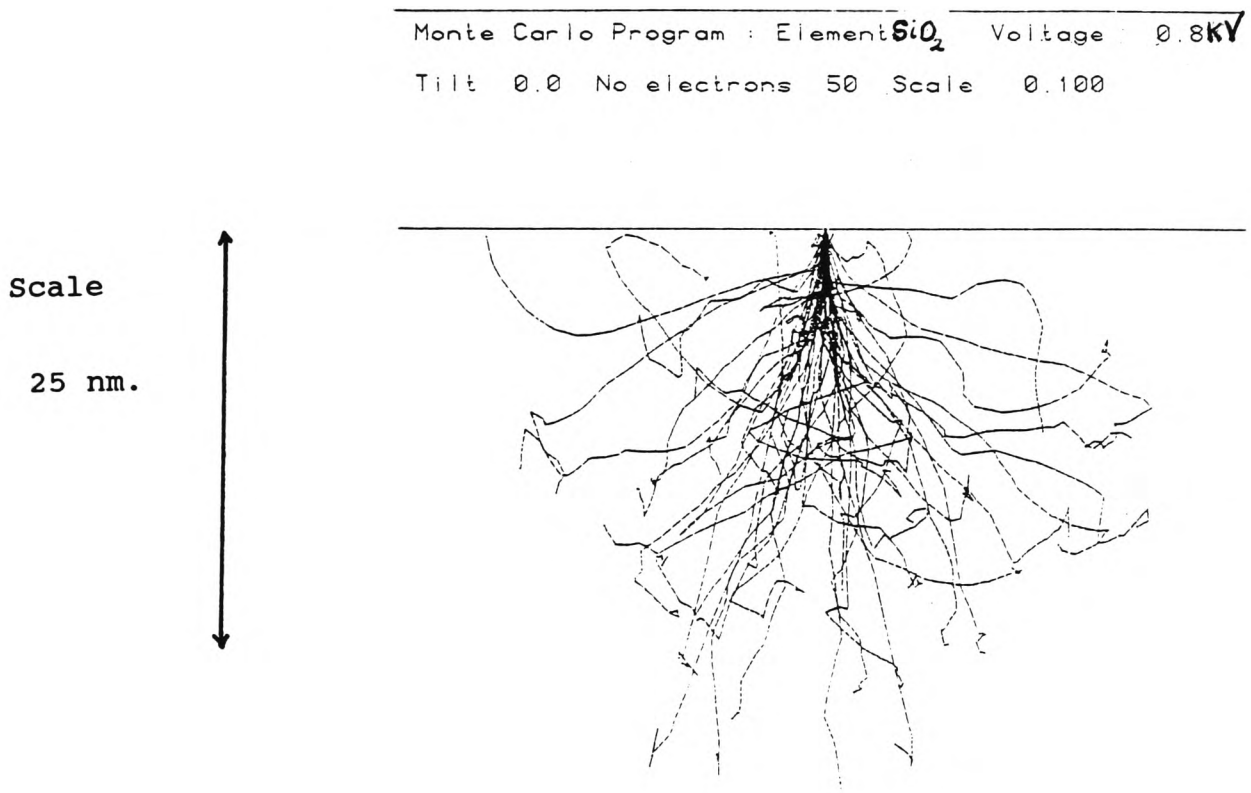

Figure 6.6

POSSIBLE SOURCES OF CHARACTERISTIC X-RAYS.

ELEMENT.		EXCITATION ENERGY (keV)
Boron	(from boron-phosphate-silicate-glass (BPSG)).	0.185
Nitrogen	(from silicon nitride).	0.393
Oxygen	(from silicon dioxide and BPSG).	0.525
Aluminium.		1.486
Silicon.		1.739

X-ray energies for nondiffractive analysis ASTM data series DS 46.

nitride or oxide layer. When such passivation layers are irradiated by the primary electron beam, oxygen or nitrogen x-rays will be generated, and these are a possible source of damage. Removal of the passivation layer eliminates this problem. Another possible x-ray source is the dielectric material that lies between the device metallisation features. This may be silicon dioxide and/or boron-phosphate-silicate-glass from which oxygen x-rays may be generated.

These potential x-ray energy sources cannot be avoided, and operation of the electron-optics at energies low enough to eliminate all possible characteristic x-rays is not possible. It is therefore important to try and minimise their generation. For example, when observing the general area of a device, the microscope magnification should be kept as low as possible, minimising the energy deposited by the primary beam per unit area and so reducing the intensity of the x-rays produced.

(6.4) SECONDARY ELECTRON DETECTOR OUTPUT AS A FUNCTION OF SPECIMEN VOLTAGE.

This series of measurements was made using the polished aluminium stub specimen. Bias was applied to the stub within the SEM, via the specimen ground connection. The applied voltage was measured using a digital voltmeter connected between the power supply to the specimen and the microscope's chamber walls, which were used as a reference for ground. The amplitude of the video output from the conventional Everhart-Thornley SE detector was measured by connecting a second digital voltmeter, via a standard

'T'shaped BNC connector, directly onto the detector.

The detector's output was then measured as a function of applied specimen bias over the range -20 to +20 volts. Figure 6.7, shows the effect of specimen bias on detector output. The detector output changes as specimen bias alters, as this type of electron detector integrates over the combined angular and energy distributions, but cannot discriminate between the two. Consider the effect of applying positive bias. As the specimen becomes more positive, so the amplitude of the detector signal is reduced. This decrease is attributed to a reduction of the electrostatic field between the emission point (at the specimen surface) and the front of the detector, with the collector bias remaining constant. SEs therefore arrive at the detector with less kinetic energy, and so produce a smaller photon yield at the scintillator, thus giving a corresponding reduction in detector output.

If this reduced field was the only effect, it might be reasonable to expect the detector output to fall in a linear manner as the specimen is more positively biased. However, as can be seen from the figure, this does not happen. This is because of the action of the retarding barrier, which acts to return lower energy secondaries to the emitting surface. At around +10 volts, the detector output begins to stop decreasing, as the majority of SEs are unable to escape from the specimen. For maximum energy of emitted SEs of 50 eV, if 50 volts were applied to the specimen, no SEs would escape and the video signal would consist of detected backscattered electrons and electronic

Figure 6.7

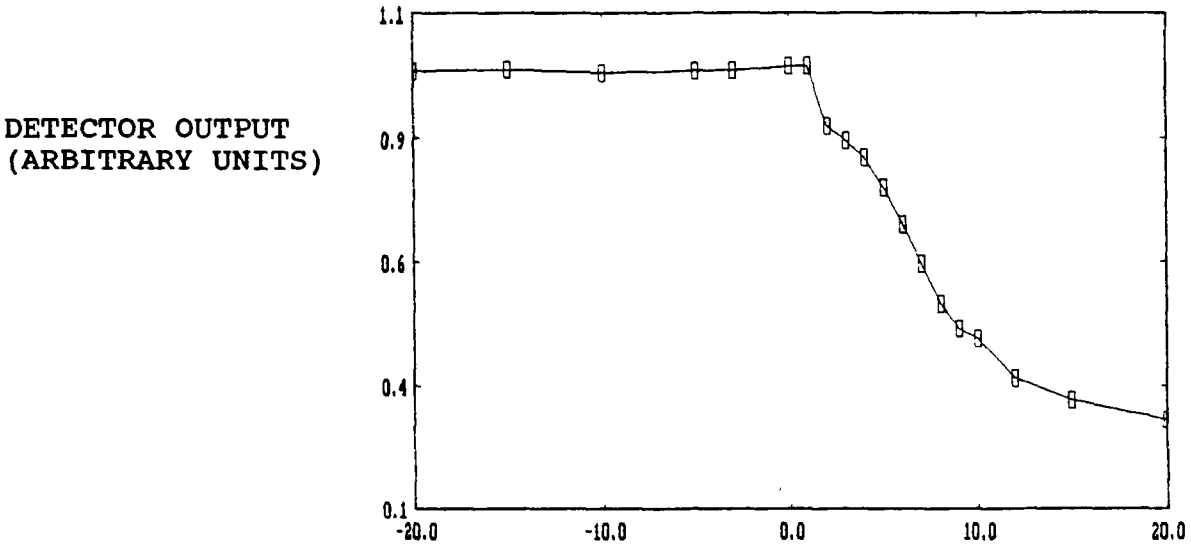

The output signal from the conventional SE detector as a function of specimen (aluminium stub) bias.

noise.

Next consider the effect of biasing the specimen negative. The field intensity between the specimen and the detector will now increase. As a result, emitted SEs will gain kinetic energy. As these SEs impact upon the detector, there will be a corresponding increase of scintillation, and the detector output will increase proportionally. However, figure 6.7 shows no such increase. In fact, very little change to the detector's output is observed at any point, and at around -10 volts it begins to decrease. These unexpected results occur because when SEs emerge from the specimen's surface, they will continue travelling in their original direction if no force acts on them. If however, a force does act, then they will be deviated to an extent depending on the magnitude of the force experienced and their initial kinetic energy. Those SEs having trajectories almost normal to the emitting surface tend to have the largest kinetic energy. An explanation has been proposed [Dekker 1968], along the lines that such SEs are likely to have taken the shortest distance from the point of generation to the specimen/vacuum interface, and therefore tend to have lost least energy. Thus, the standard level of collector bias may be insufficient to alter these SEs initial trajectory sufficiently to cause them to impact onto the detector's scintillator. As the specimen bias becomes more negative, so the kinetic energy of emitted SEs increases, and the effective collection efficiency of the detector decreases.

The above results show that the level of detector video output alters as a function of specimen bias, and that while the

standard Everhart-Thornley SE detector may be used to produce images showing contrast due to variation of voltage distribution, it is not suitable for quantitative measurements.

(6.5) CHARACTERISATION OF THE VMEC.

The VMEC detector is a high-pass energy filter, the output of which may be used to form an image of the specimen, or to make quantitative measurements with regard to changes of the SE emission current. For quantitative measurements, the VMEC output varies in response to changes in filter electrode bias. A typical result is shown in figure 6.8; which shows the numbers of SEs emitted with energies greater than E, as a function of E. On an ideal curve, that portion having the steepest slope will correspond to the energy value at which the SE yield is at a maximum. These data in figure 6.8 were collected from the polished aluminium stub, held constantly at ground potential. Very few SEs are detected when the filter electrode is biased at -25volts. As the bias is made more positive, so more of the collected SEs have sufficient kinetic energy to cross the retardation barrier and are detected. Once the filter electrode is positively biased, the curve begins to rise rapidly to the maximum value of detector output. The ideal curve should then show a plateau. However, this ideal is not achieved and the level of detector output begins to fall. This is likely to be due to the detector design. Computer simulations by Khursheed [1983], show the trajectories of SEs through the VMEC. He demonstrated that, as the filter electrode becomes more positively biased, so the SEs with lower kinetic energy are

Figure 6.8

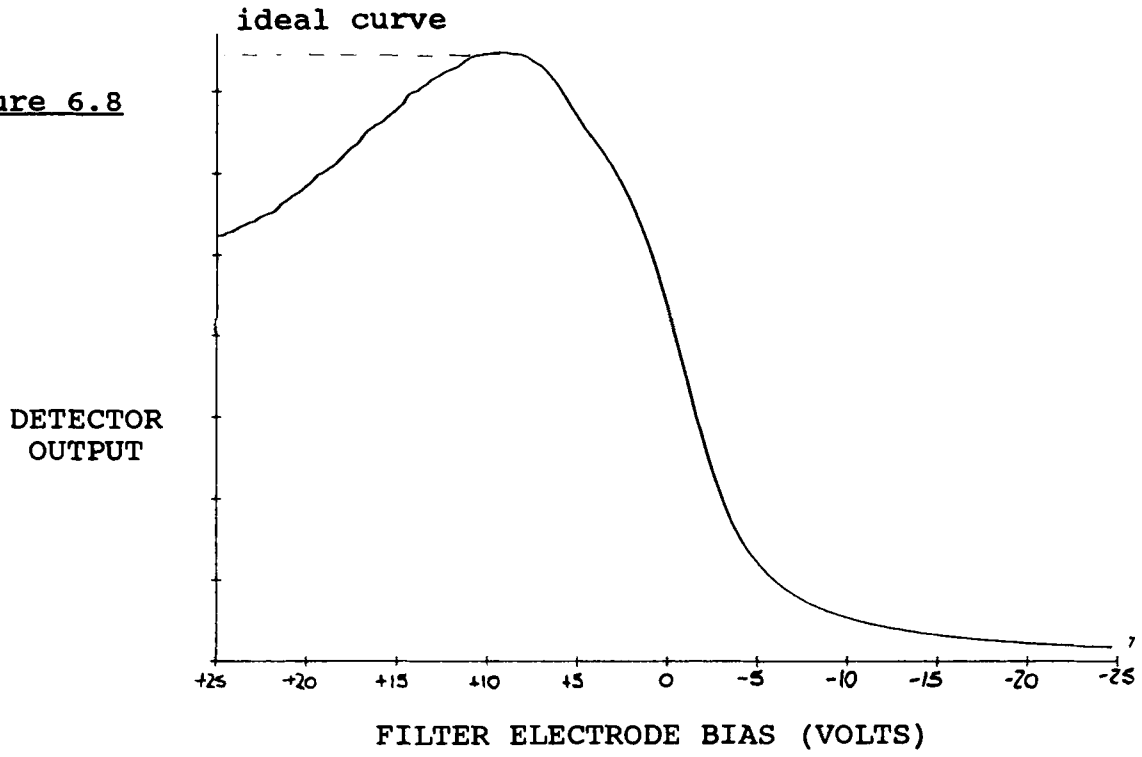

Typical 'S'-curve from the VMEC, showing how this detector's output changes as a function of filter electrode bias. The specimen used was an aluminium stub held at ground potential. The 'broken' line indicates the ideal detector output. As can be seen, the actual detector output falls as the filter electrode becomes more positively biased.

attracted onto the electrode and not detected. This problem was realised early in the present project and appropriate allowances were made when quantitative measurements were undertaken (either using 'S' curves (see below) or the closed feedback loop system, (which is a standard feature of the Lintech instruments equipment).

Use of the 'S' curves for quantitative measurements required them to be differentiated, in order to optimise for measurement accuracy. Changes to the energy profile were assessed by measuring the values of filter electrode bias corresponding to certain pre-determined values of detector output. For any series of measurements, a reference curve was used, from which the levels of detector output at 50 and 75% of the maximum energy were measured. These values were always taken from the higher energy side of the curve's maximum to minimise measurement errors, as the greater the kinetic energy of the emitted SEs the less likely they are to be influenced by local fields at the specimen's surface or between their emission point and the detector. Measurements were then made as follows. If, for example, the bias to the specimen was changed, the collected curve would shift along the filter electrode bias axis in response. To measure how much shift had occurred, two lines were drawn from the points on the curve which corresponded to the two pre-determined values of detector's output. From each of the points, lines were dropped which crossed the filter electrode bias axis, these values were recorded. The difference in value between these points and those measured from the original

reference curve was taken to be the measure of the curve's shift.

(6.5.1) SELECTION OF THE OPTIMUM EXTRACTION ELECTRODE BIAS FOR QUANTITATIVE MEASUREMENT.

The extraction electrode is nearest to the specimen, although there is a metal safety cap at ground which surrounds this electrode, preventing actual contact with the specimen. The electrode's primary function is to establish an electro-static field between the detector and the specimen, with the level of bias being adjustable between ground and 5 kilovolts in steps of 20 volts. The resulting field is intended to:

(1) increase the detector's **collection efficiency**, thus improving its signal to noise ratio,

(2) suppress **localised retardation barriers** immediately above any positively biased nodes (local field effect type 1) and,

(3) influence the **electro-static fields** generated by nodes adjacent to the SE emission point (local field effect type 2).

Initially, the detector's collection efficiency was investigated as a function of extraction electrode bias. The specimen used was the aluminium stub, which was held at ground potential. The separation distance, between the specimen and the detector was set using a 4 millimetre plastic spacer. The results are shown in figure 6.9. This shows the relative detector efficiency, measured as the area under the differentiated secondary electron energy profile, between two

Figure 6.9

RELATIVE SE YIELD

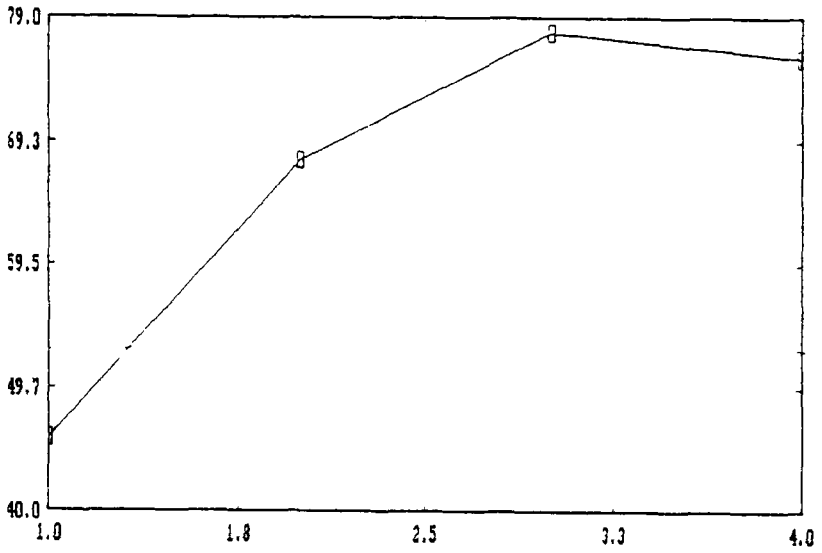

EXTRACTION ELECTRON VOLTAGE (kV).

The VMEC's SE collection efficiency as a function of extraction electrode bias.

limits which corresponded to a specific level of detector output. The figure demonstrates that the detector efficiency increases as the extraction field strength is increased up to a value of 3 kilovolts per millimetre. Above this, the efficiency begins to fall, and at 4 kilovolts there has been a 2.3% reduction. This effect may again be explained by reference to the previously mentioned computer simulation work, which showed that the VMEC acts like a lens, double focusing the collected SEs. By changing the extraction field strength, the focal length of the detector is changed. An adverse effect is that a certain fraction of the SEs are brought to focus on the filter electrode, and do not reach the scintillator.

(6.6) ASSESSMENT OF THE ABILITY OF THE EXTRACTION ELECTRODE TO SUPPRESS :

1. THE RETARDATION BARRIER (Local Field Effect type 1).

2. CROSSTALK (Local Field Effect type 2).

Again, the aluminium stub was used, with the separation distance between the detector and the stub set at a constant 6 millimetres (the width of the plastic spacer plus a further 2 millimetres representing the distance which the extraction electrode is set behind the safety cap). For this work, the stub, its holder and the stage were connected to a D.C. power supply (via the SEM stage's ground connection), and shared a common ground with the microscope's outer casing. Via this low resistance connection, bias could be easily applied to the specimen.

S-curves were then collected from 0 to 5 volts (in one volt steps), for extraction electrode potentials 1, 2, 3, and 4 kilovolts. This work was repeated several times, with data being stored and later transferred to the PC for analysis.

The shift of each S-curve, in response to changes of applied specimen bias, was then measured. The measurements being made using the method described earlier (points taken on each of the curves that correspond to the pre-determined 50 and 75% of detector's maximum output). However, even at these optimum values, some large errors occurred. In the worst case, the measured voltages differed from the actual values by as much as 38%. Some of these errors, however, could be attributed to the detector suddenly emitting a high level of video signal, due to an intermittent fault in the detector which could not be traced. This made it necessary to always make several measurements and report the average result.

The work continued determining how the voltage measurement error is affected by changing the extraction field strength. The results are shown in figure 6.10, which displays the percentage measurement error, with 5 volts applied to the stub. An extraction electrode potential of 1.5 kilovolts resulted in a measurement error of 16.4%, with this error falling as the extraction electrode bias was increased. At an electrode bias of 3 kilovolts, the measurement error fell to its minimum of 3.1%. Increasing the extraction voltage further does not reduce the measurement inaccuracy, but slightly increases it. This is due not to the action of the retardation barrier, as the barrier

Figure 6.10

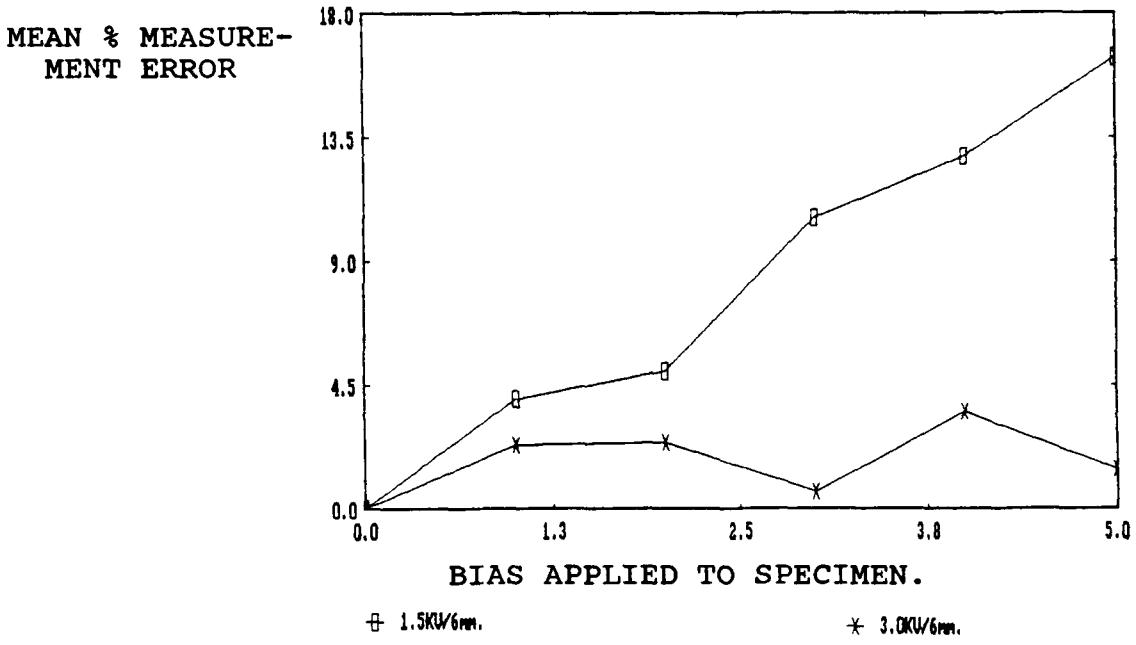

The effect of extraction field strength on voltage measurement error when the specimen is biased at various voltages.

will have been suppressed, but to the reduced collection efficiency of the detector.

With the extraction electrode held at a constant 3 kilovolts, the aluminium stud was biased between 0 and 15 volts (at 5 volt intervals) and S-curves collected. The results and their differentiated counterparts are shown in figure 6.11 a and b. For the differentiated curves, their displacement along the energy axis at the chosen values of detector output, was measured with results as shown in figure 6.12. The voltage measurement error was found to increase as the area under the differentiated curves decreased, as the specimen was more positively biased.

(6.6.1) THE ACTION OF LOCAL FIELD EFFECTS (LFEs) 1 AND 2 FOR NARROW CLOSELY SPACED METAL LINES.

The specimen supplied by British Telecom was used to assess the effects of LFE types 1 (the localised barrier above positively biased nodes which influences the SE energy spectrum by not allowing the lower energy SEs to escape), and LFE 2 (which is due to bias on adjacent nodes influencing the angular distribution of emitted SEs). For all of the measurements, the primary electron beam was kept at a constant acceleration voltage of 1 kilovolt, and the beam current held at 1 nanoamp.

It has previously been shown that the application of a positive bias results in a barrier which retards the emission of certain lower energy electrons. The retardation barrier height has been described as increasing in proportion to the level of applied positive bias. However, it is also a function of the

Figure 6.11a

THE SHIFT OF POSITION OF 'S'-CURVES WHEN SPECIMEN POSITIVELY BIASED.

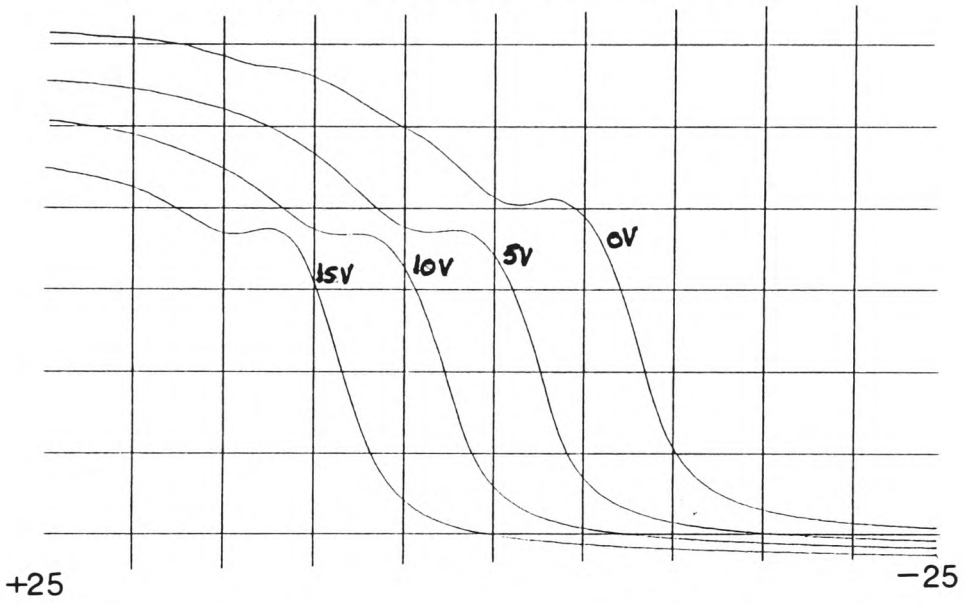

FILTER ELECTRODE BIAS (VOLTS)

The 'S'-curves are translated along the filter electrode bias axis as the aluminium stub is biased from 0 to 15 volts.

FIGURE 6.11B

'S'-CURVES DIFFERENTIATED WITH RESPECT TO FILTER ELECTRODE VOLTAGE. THESE CURVES SHOW THE SE ENERGY DISTRIBUTION AND HOW IT TRANSLATES ALONG THE FILTER ELECTRODE BIAS AXIS IN RESPONSE TO CHANGE OF SPECIMEN BIAS.

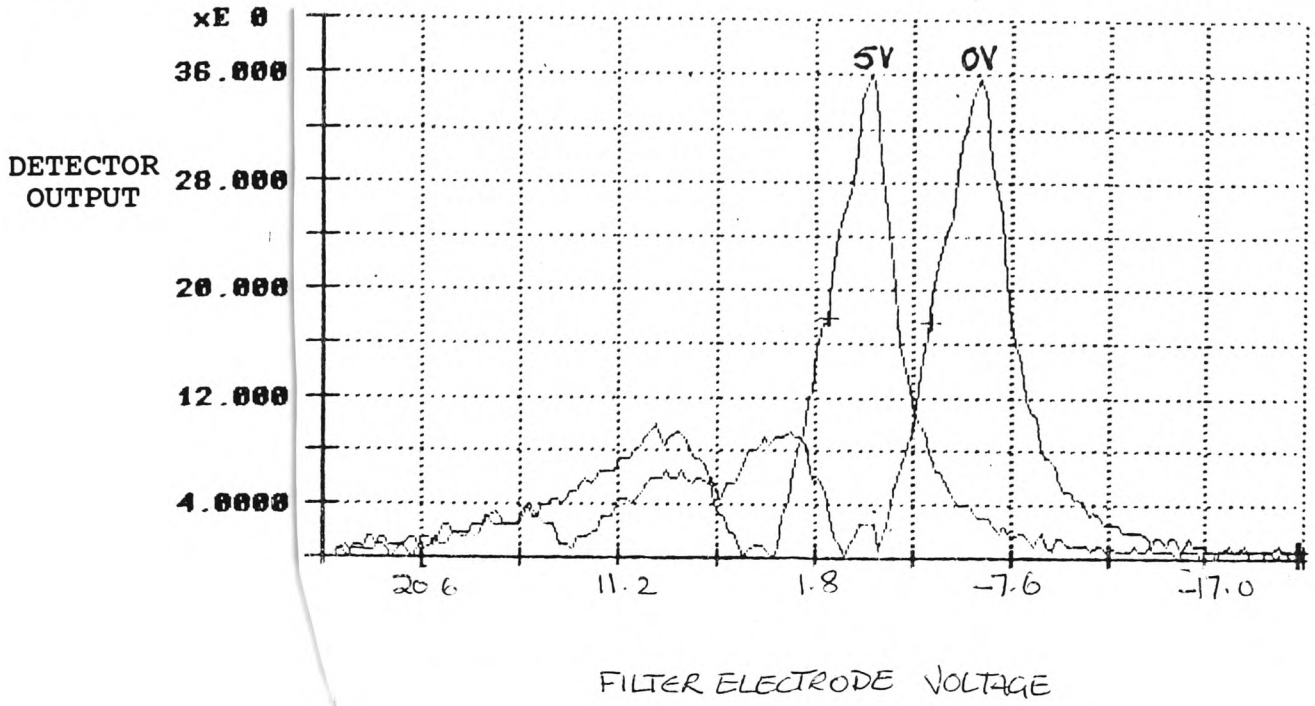

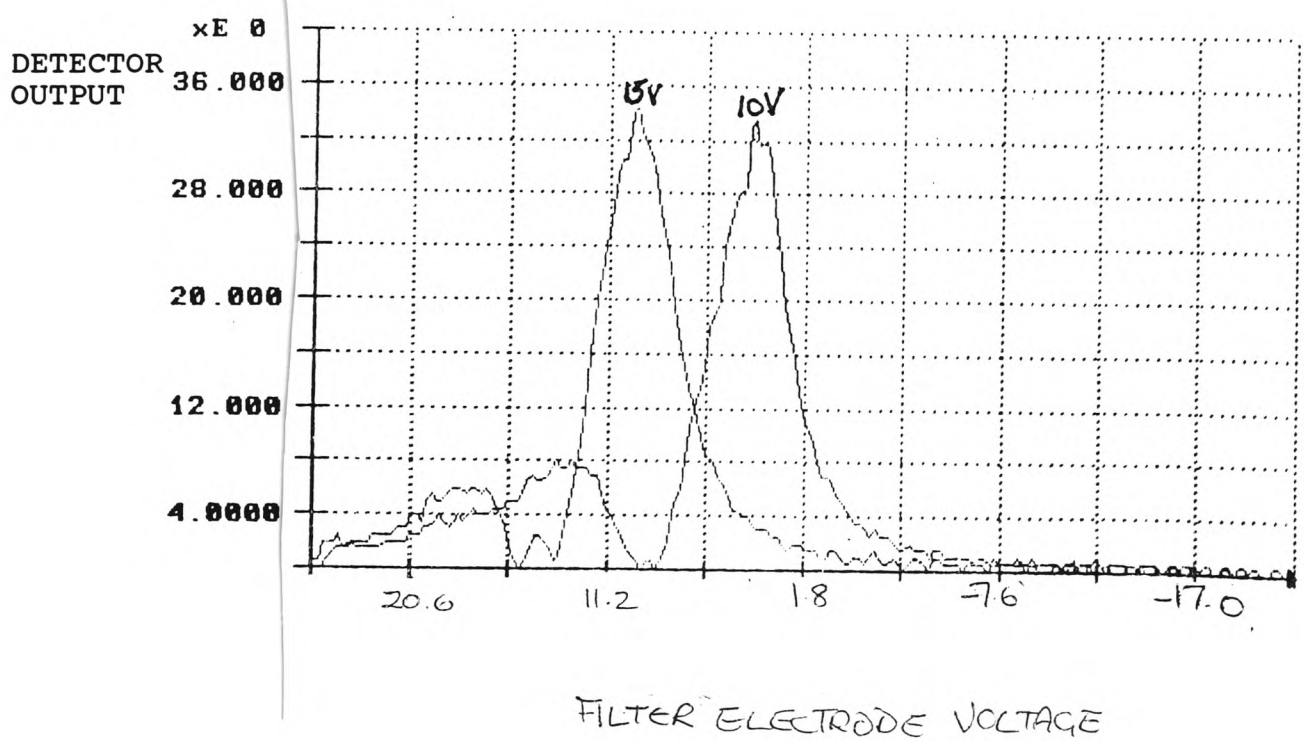

Figure 6.12

MEAN AREA UNDER SELECTED DIFFERENTIATED S-CURVES.

SPECIMEN BIAS.	MEAN VALUE OF MEASURED BIAS FROM CURVE SHIFT.	% ERROR	AREA UNDER CURVES.
0	-	-	542
5	5.25	4.6	539
10	10.54	5.3	520
15	15.95	6.1	512

specimen's dimensions. This is important, as the dimensions of metal conductors on ICs are progressively being reduced, while their operating voltages remain at the same level.

To explore the situation, a series of S-curves was collected over a range of extraction electrode bias. With the metal lines all held at ground potential, S-curves were collected from lines having widths of 20 and of 8 micrometers. This was then repeated with each line biased +5 volts. Data were then analysed (using ASYST) to determine the area under a suitable portion of the SE energy distribution. Figures 6.13 a and c show how insufficient extraction field reduces the 'S'-curves, due to incomplete detection of SEs, as their energy profile becomes truncated. Figure 6.14 shows the previously explained phenomenon that, as the extraction electrode bias is increased, the area under the SE distribution curve increases up to a maximum value, and then begins to decline.

The effect of decreasing line width was to reduce the area under the curve. This was felt likely to be due to reduced accuracy of positioning the electron beam centrally on the metal line. If the beam contacts the edge of the metal track, there will be a sudden change in the angular distribution of the emitted SEs, resulting in a reduced collection efficiency of the detector. This surface topographic related phenomenon is therefore another possible source of measurement error.

When +5 volts is applied to the metal line, the figure 6.14 shows a reduced area under the SE curves. This effect is most

noticeable for the 8 micrometre line. Curves were collected from the 20 micrometre line for extraction electrode voltages of 3 and 3.5 kilovolts. They show only small variations of SE area, indicating reasonable suppression of the retardation barrier. At an extraction electrode voltage of 4 kilovolts however, there is a much greater difference between the two curves, implying a greater degree of measurement error.

For bias values of 5 volts and extraction electrode voltages of 1 kilovolt and below, curves were collected from the 8 micrometre line. These were of sufficiently poor quality that no measurement of area under the SE curve could be made. It was not until the extraction voltage had been increased to 1.5 kilovolts that such measurements became possible. Even at this value the area being assessed was very small. From such data, it was concluded that an extraction voltage of at least 2.5 kilovolts would be advisable. If the metal line width was less than 8 micrometres, the extraction field would need to be increased still further, probably to 1000volts/millimetre. However, at these higher intensity extraction fields, the detector's efficiency would fall. This effect limits the accuracy of measurement for narrower conductor tracks.

Next, crosstalk (or local field effect type 2) was investigated. This phenomenon concerns the influence which the electrostatic fields on adjacent nodes have upon the trajectories of the emitted SEs, and the ability of the electrostatic field between the detector and the specimen to suppress this effect. The British Telecom specimen was used for this work, with one of

the 8 micrometre lines being biased between 0 and 5 volts in one volt steps, while the metal lines on either side of it were held at a constant 5 volts. Two sets of S-curves were collected, one with an extraction field of 333 volts/millimetre and the other 666 volts/millimetre, between the detector and the specimen's surface. The results are shown in figure 6.15. It can be seen that there is a steady increase of measurement error as the line becomes more positively biased. A maximum error value 16.8% was reached at 5 volts.

(6.7) MEASUREMENT ERROR AND AREA UNDER THE SE ENERGY PROFILE.

Using the data presented above, it was possible to plot percentage measurement error as a function of the area under the appropriate SE curves. It was found that the percentage voltage measurement error (as determined by shift of the S-curves), decreased logarithmically with increasing area under the differentiated curves, as shown in figure 6.16. The voltage measurement accuracy was proportional to the detected SE current [Gopinath 1968].

(6.8) THE EFFECT OF MATERIALS DIFFERENCES AS A SOURCE OF VOLTAGE MEASUREMENT ERROR.

Previously published data [Mckay 1948 and Dekker 1962], has shown that, the emitted SEs from any solid material, when irradiated by primary electrons over a range of energies, gives SE yield curves (as a function of primary electron energy) all with the same characteristic shape, a typical example is shown in figure 1.2. However, the energy required to generate the maximum

Figure 6.13a

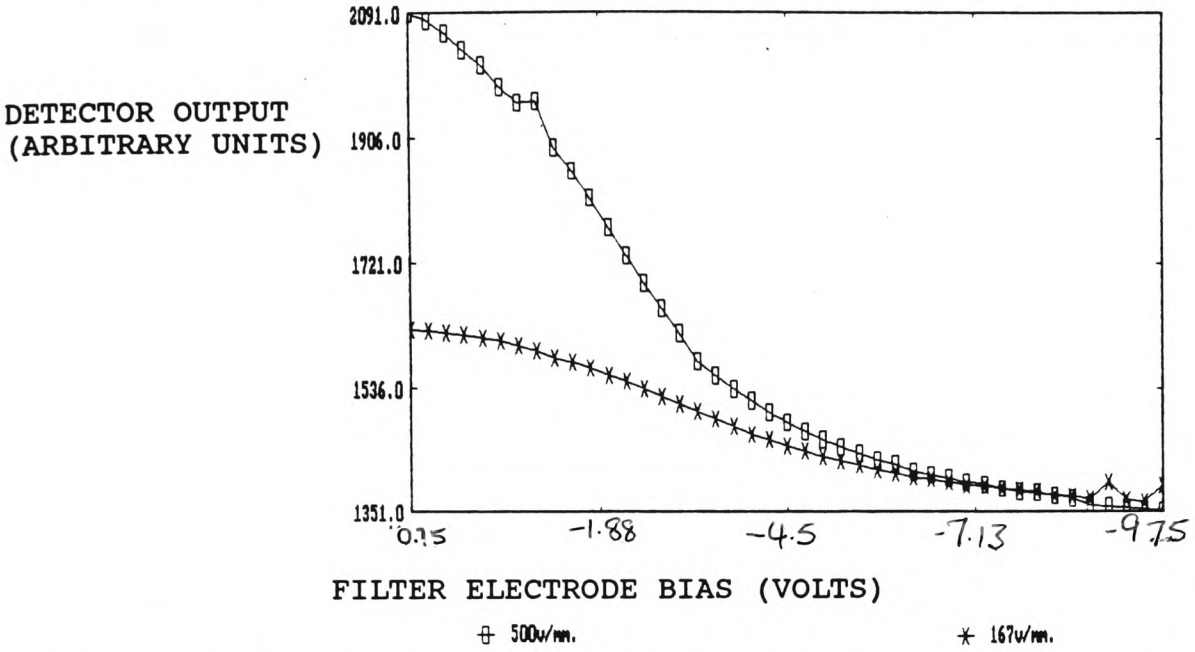

The above 'S'-curves show the effect of decreasing extraction field strength on the slope of the curves. Since the slope of the 'S'-curve is decreased, voltage measurement is made more difficult, leading to an increase in measurement error.

Figure 6.13b

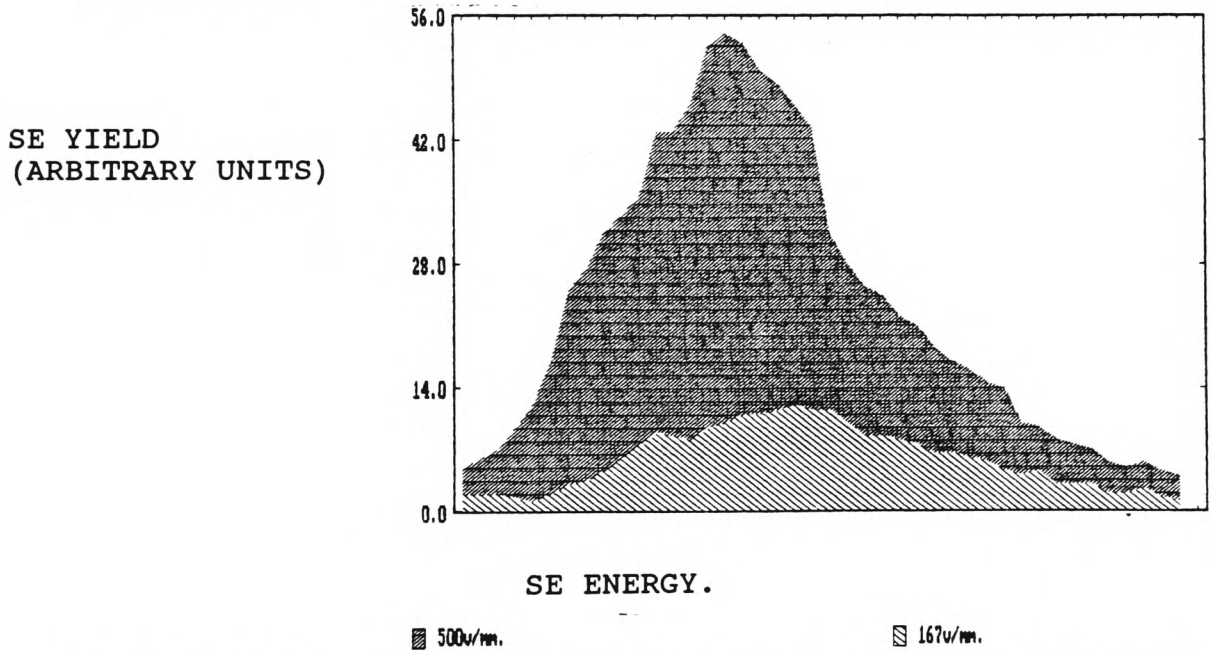

By differentiating the 'S'-curves, the actual detected SE energy profile can be seen to be truncated (due to the presence of LFEs), thus reducing the level of SE yield.

Figure 6.14

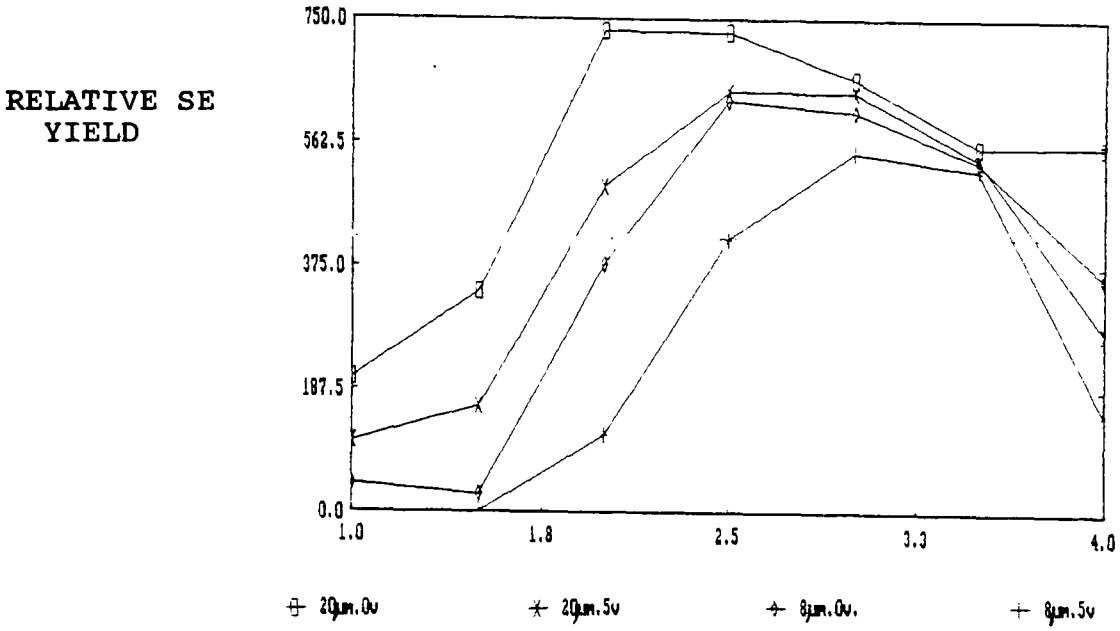

The effect on the detected SE emission of metal line widths and specimen bias.

Figure 6.15

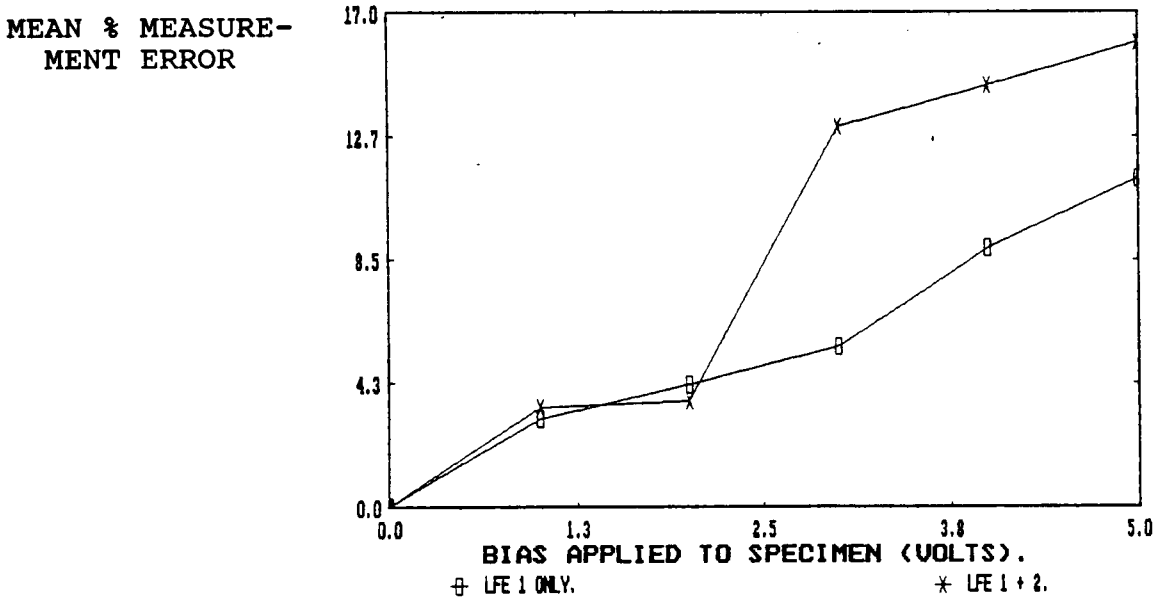

Assessment of LFE 1 and 2 on voltage measurement error.

Figure 6.16

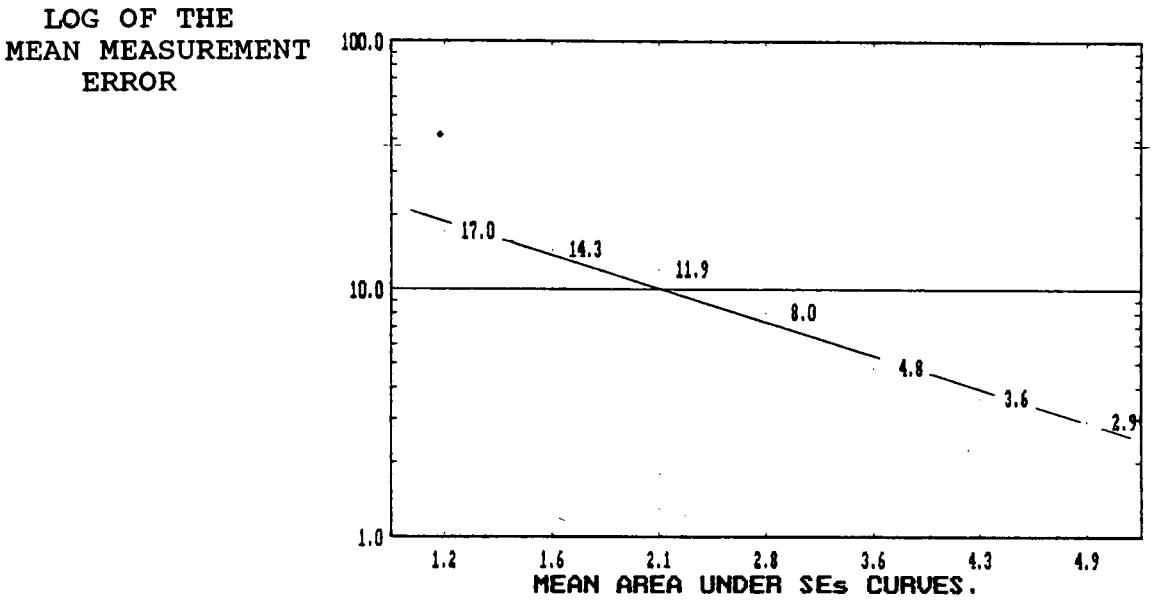

The relationship between voltage measurement error and the area under various differentiated curves.

SE yield (E_{Pmax}) varies for each material. In many cases, the energy differences between E_{Pmax} for different materials are only a few electron volts. If however, the materials are categorised as electrical conductors, semi-conductors or insulators, the average values of E_{Pmax} have, in general, greater energy differences. If a specimen such as an IC (which is constructed with materials which are in all three categories of electrical properties), is irradiated by a beam of primary electrons of any given energy, the yield of SEs will be different for each category of material. An error in voltage measurement will arise if a node of one material is compared with another, irrespective of their bias.

To assess the possibility of error due to material differences, using materials likely to occur in ICs, a standard metallurgical alloy of 10% silicon in aluminium was used. Careful preparation had removed much of the surface topography, the result of cutting the specimen. 'S' curves were collected from several primary silicon crystallites, and from the aluminium rich matrix. The results were compared for identical electron beam irradiation conditions. It was found that when a 1 kilovolt acceleration of the electron beam was used, the SE yield from silicon was less than that from aluminium. This was to be expected, as the SE image showed silicon to be darker than the matrix. The reduced yield in itself was likely to give increased measurement error. The other difference between the curves was a displacement along the filter electrode axis. This second type of measurement error was found to average a value of 0.55 volts.

(6.9) WAVEFORM MEASUREMENT.

In the treatments above, all of the measurements have been used to determine static voltage levels. Whilst this is useful, many applications of EBT analysis of ICs require the determination of dynamic voltage levels. This is also possible with the Lintech system, but requires improved time resolution. Thus, a beam blanking unit must be used. The signal which controls this unit must be synchronised to that of the signal driving the device or specific node being tested. For such voltage measurements, S-curves are not used. Rather, a feedback loop system is employed [Davidson 1989].

The British Telecom calibration sample was used to demonstrate the equipment's ability to produce waveforms from which the voltages on the lines could be measured. The waveforms were collected from line 8, within the region 'D', as shown in appendix 1. Waveforms were collected under two different conditions; the first having lines 7 and 9 at ground, and the second with both of these lines at 5 volts. Again, a range of extraction electrode voltages was used. The signal to the devices was a square wave, with an amplitude of 5.5 volts and a frequency of 180 kilohertz.

The results of this examination are shown in figure 6.17, which displays the mean measured voltage as a function of the extraction electrode bias. The figure also shows that the measurement accuracy decreases with decreasing extraction electrode voltage. Measurement errors may be attributed to the

Figure 6.17

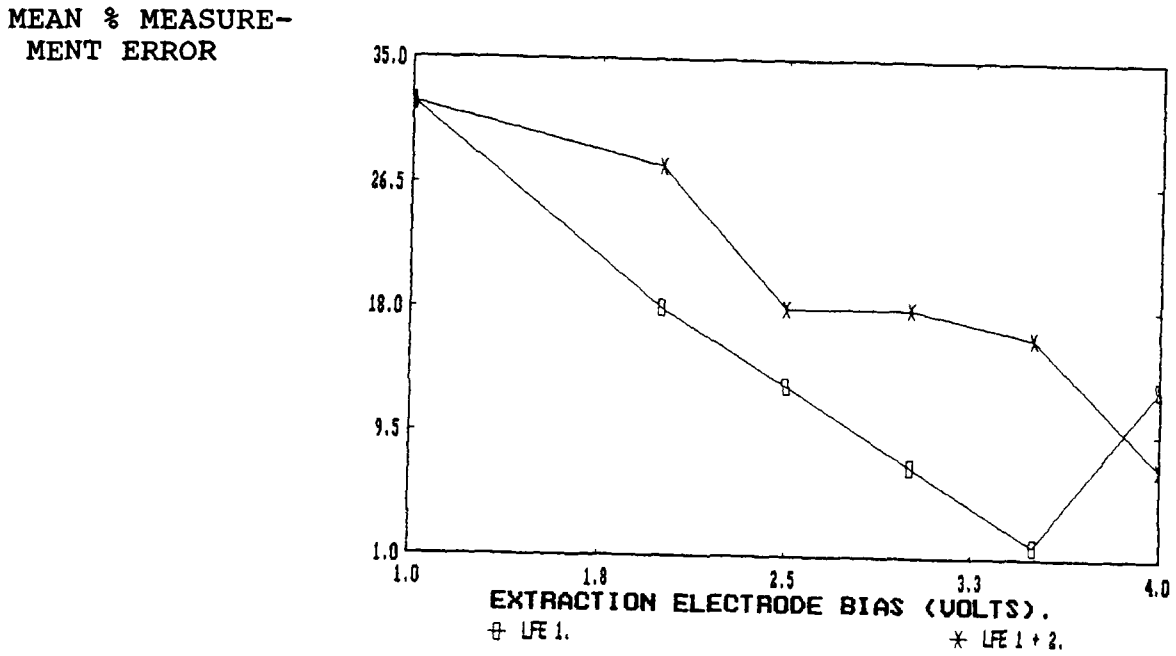

Measurement error due to LFE 1 and 2. The signal applied to the specimen being a square wave with a voltage amplitude of 5.5 volts and frequency of 180 kHz.

adverse action of local field effects. From measurements made with lines 7 and 9 at ground potential, it may be concluded that error will be mainly due to the retardation barrier immediately above the positively biased line. Even with the extraction electrode at 4 kilovolts, the extraction field is not sufficient to suppress this barrier. At this value, there is an increased measurement error compared to the results obtained at 3.5 kilovolts. This may well be due to a change of the detector's focal length, as described in section 6.5.1.

When lines 7 and 9 are held at a constant 5 volts, the measurement error is increased due to the influence of the electrostatic fields of the adjacent lines. These act to defocus the emitted SEs, increasing their angular distribution. However, with the VMEC's extraction electrode at 4 kilovolts, the action of the extraction field is to reduce the defocusing effect and so to reduced the final measurement error.

CHAPTER 7.

APPLICATION OF ELECTRON BEAM TESTING TECHNIQUES.

(7.1) ELECTRON BEAM TESTING (EBT) OF A 7400 QUAD NAND GATE DEVICE.

A simple 7400 quad nand gate device was used to demonstrate the full range of information which could be extracted using the electron beam tester.

The ceramic package's lid and silicon dioxide passivation layer were removed, and the device was mounted in a 14 pin dual-in-line holder within the chamber of the SEM. It was decided to exercise only one of the device nand gate structures.

Using the feedthrough system at the back of the SEM's vacuum chamber, the following electrical connections were made to the device:

Pins V_{cc} and V_{dd} were connected to a standard d.c. power supply. The appropriate pins were then connected to a signal generator, which was set to produce a square wave with an amplitude of 5 volts and a period of 2000 nanoseconds.

The SEM was operated through the Lintech system, using the VMEC, with a beam acceleration voltage of 0.8 kilovolts and a beam current of 1 nanoamp. The device was positioned just below the safety cap of the VMEC, with the plastic spacer not being used. It was estimated that the separation distance was approximately 2 millimetres, but the actual distance between the

device and the detector was about 1.5millimetres greater, as the device was recessed in its package.

Figure 7.1 shows the area of the device to be investigated. This is a conventional secondary electron image, with the power and signal to the device switched off. Therefore no voltage contrast, only topographic and material contrast, is observed. The micrograph shows the bond wires connected to their pads, where (A) is the input pin connected to the signal generator, (B) is the output, (C) is held permanently at +5 volt as was (D) which is V_{CC}. The aluminium conductor tracks can clearly be seen.

Figure 7.2 was recorded once 'static' voltages had been applied. Voltage dependent contrast can be seen superimposed on the topographic and material contrast. The bond pads and their wires (A and D) plus the internal circuitry are now biased to +5 volts and so appear much darker in contrast than do B and C, which are at ground.

Figure 7.3 was recorded at increased magnification compared to figures 7.1 and 7.2. It shows a combination of both 'static' and 'dynamic' voltage contrast. Bond pad C is still held static at +5volts, whilst a low frequency 13.9 Hz signal is applied to A. An interference effect is seen to occur for this pad and its internal circuitry, determined by the scan frequency of the electron beam. The alternating light and dark stripes are a direct visual representation of the response of the pad and its related circuitry to the low frequency signal being applied. When

THE FOLLOWING ARE THE RESULTS OBTAINED FOR THE EBT OF THE 7400 QUAD NAND GATE DEVICE.

Figure 7.1

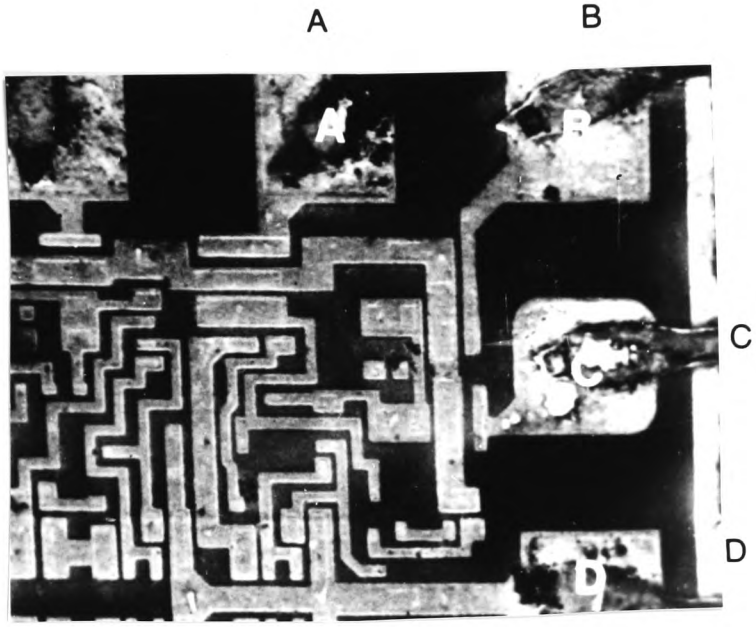

Horizontal field of view = 580 micrometres.

The above is a conventional SE image, of one of the four nand gate structures.

Figure 7.2

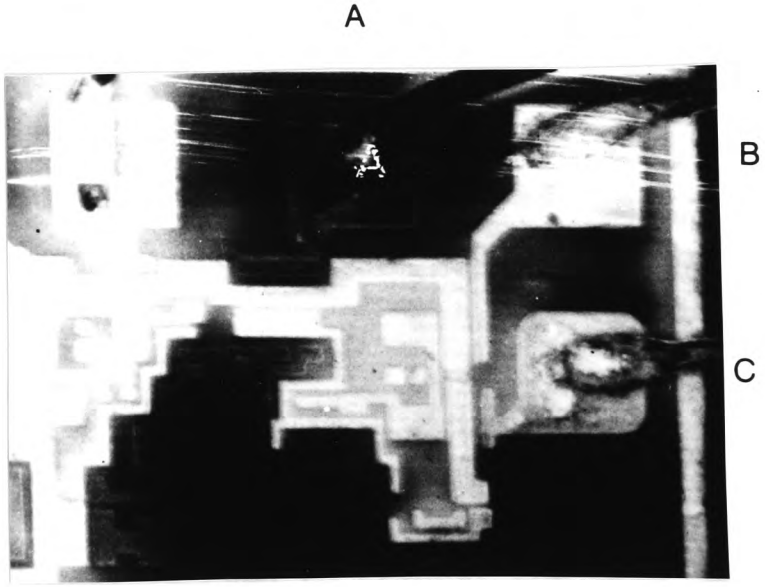

Horizontal field of view = 580 micrometres.

Static voltage contrast image; more positively biased areas appear dark.

the stripe is dark, the circuitry is at +5 volts, and when it is light, it is at ground. Comparing these stripes to those superimposed on pad (B), it can be seen that they are 180 degrees out of phase. Thus, the device has successfully inverted the input signal.

Figure 7.4 is very similar to figure 7.3, except that the applied signal frequency has been slightly increased to 22.7 Hz, while the scan of the electron beam has been kept constant. The effect is to reduce the width of the stripes and increase their numbers.

Figure 7.5 was taken with the input signal frequency increased to 550 KHz, and the stripes are not resolved. At such a frequency, the image appears to display 'static' voltage contrast. However, if compared to figure 7.1, there are three levels of contrast observed, rather than two. The two extremes of dark and light correspond to the +5 volts of V_{cc} and ground of V_{dd} respectively. The third intermediate level of grey corresponds to the active circuitry, and is the average signal level between the two extremes.

To achieve the timing resolution necessary to image the device at any time during the input signal cycle, the electron beam is strobed, that is, switched on and off rapidly whilst being synchronised to the device's input signal. The rising voltage of the input signal is used to trigger the beam blanking unit, which pulses the blanking plate to a d.c. level of +3 to +4 volts; this being sufficient to push the beam across the spray

Figure 7.4

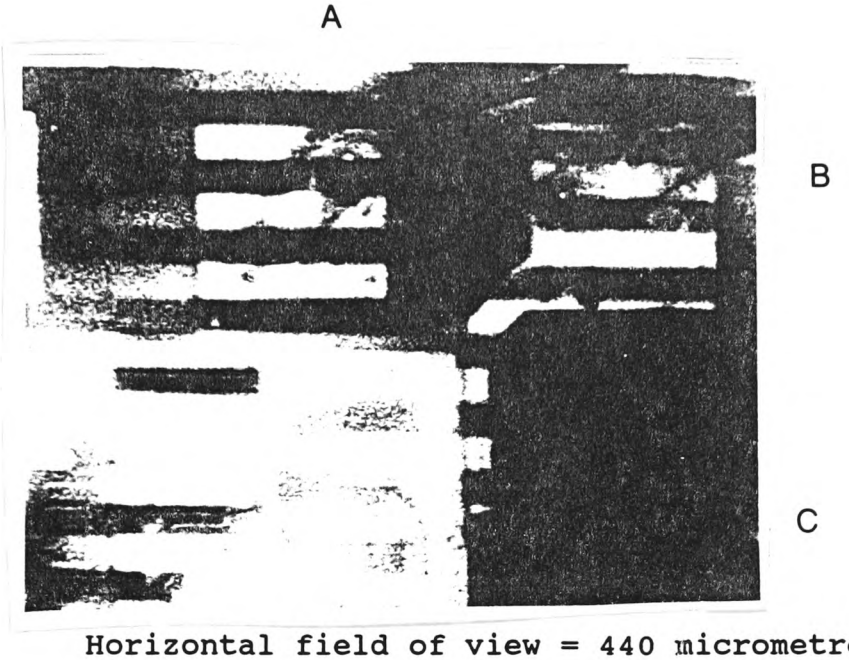

Horizontal field of view = 440 micrometres.

Dynamic voltage contrast image, the applied signal's frequency being 22.7 Hz.

Figure 7.3

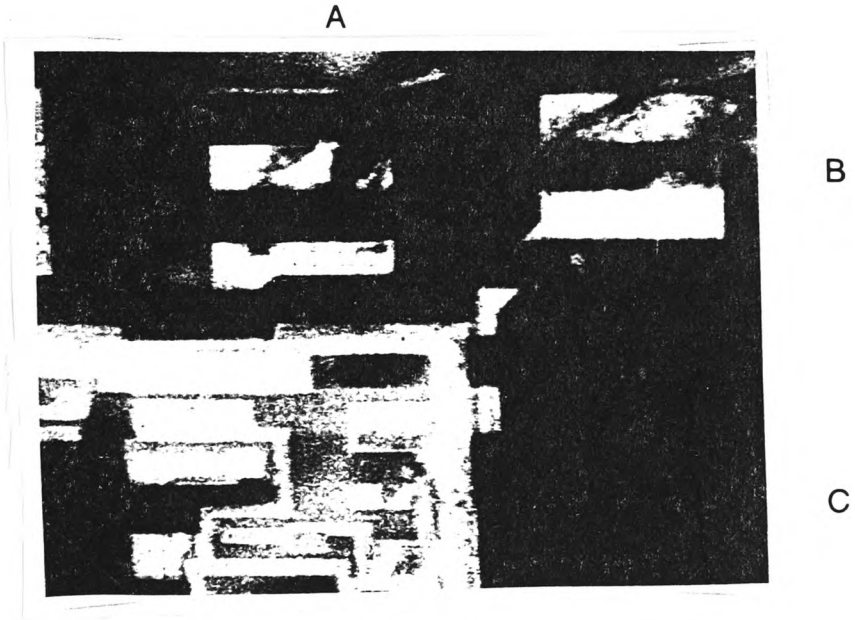

Horizontal field of view = 440 micrometres.

As figure 7.4, but with the applied signal frequency increased to 13.9 Hz, giving an increased number of stripes whose widths have decreased.

aperture off the optical axis, so that no electrons reach the specimen. The blanking plates are kept at this voltage for a selected period, then discharged, so the primary beam moves back to the optical axis and SE emission occurs. The blanking plates remain at ground potential for a relatively short time, typically 10 to 25% of the input signal period. After this, the beam is once more deflected off the optical axis until the next signal period begins. The process is repeated with the detector integrating over all the periods of emission producing a SE image. By varying the length of the delay between the drive unit trigger and point at which the electron beam is pulsed on, the device may be imaged at any time during the input signal period.

Again based on previous work, the following procedure was used to set the VMEC for quantitative voltage measurement. With the equipment operating in a stroboscopic mode, the offset and photomultiplier bias were increased to compensate for the reduction of signal arising from the fact that the primary beam no longer continually irradiates the specimen. Then, an S-curve was collected from the region of the device at which voltage measurements were to be made. The extraction electrode, offset level, and photomultiplier bias were altered until an S-curve with the steepest slope was obtained. At this point, the detector was considered to be at its optimum setting for waveform measurement. Care had to be taken when altering the extraction electrode voltage. As this defocused the primary electron beam, refocusing was required. This problem became more acute for the smaller geometries of nodes from which the waveforms were to be

collected.

Figures 7.6 and 7.7 are examples of stroboscopic voltage contrast images. Figure 7.6 was recorded with a delay between the trigger pulse and plate discharge of 50 nanoseconds. The electron beam then irradiated the specimen for 20 nanoseconds. The beam was then pulsed off the optical axis for the remainder of the signal period. This cycle was repeated until the image had been recorded.

For figure 7.7, the delay time was increased to 120 nanoseconds, after which the beam was pulsed on for 20 nanoseconds and then off again. These two figures show the signals carried by the device's input and output pins to be 180 degrees out of phase with each other, confirming the devices ability to function as an inverter.

With the SEM and the Lintech system working in the stroboscopic mode, waveforms were collected from the above device. Figure 7.8 was obtained from the input bond pad and figure 7.9 from the output pad. The two signals are superimposed on each other in figure 7.10. It can be seen that the two nodes are 180 degrees out of phase with each other. The signal amplitudes were measured and found to be 4.4 volts for the input and 4.2 volts for the output. These values were lower than expected, probably because they were collected from the top of the wire bond (the rougher surface of the wire giving an enhanced angular distribution to emitted SEs). The measurements were later repeated, and voltage readings of 4.9 for the input and 4.7 for

Figure 7.5

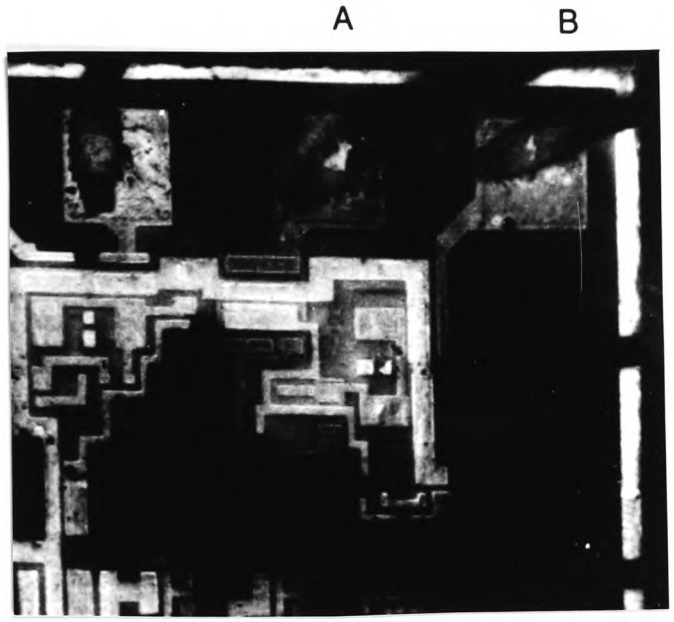

Horizontal field of view = 750 micrometres.

Still a dynamic voltage contrast image, but with the applied signal having a frequency of 550 kHz. The light and dark stripes are not resolved, but an intermediate level of contrast is seen.

Figure 7.6.

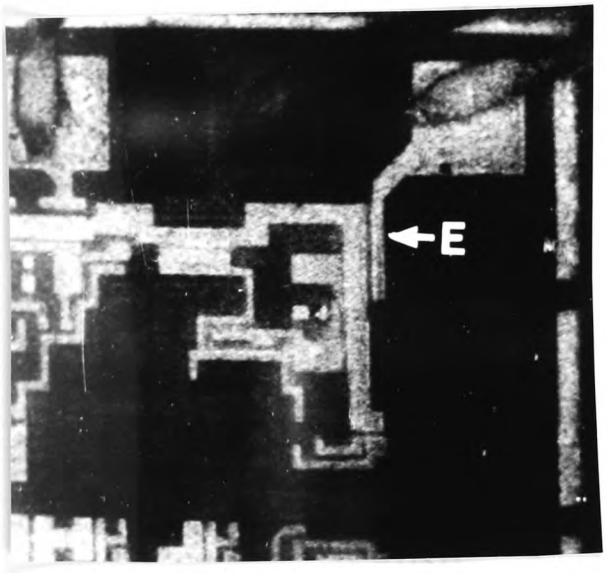

Figure 7.7.

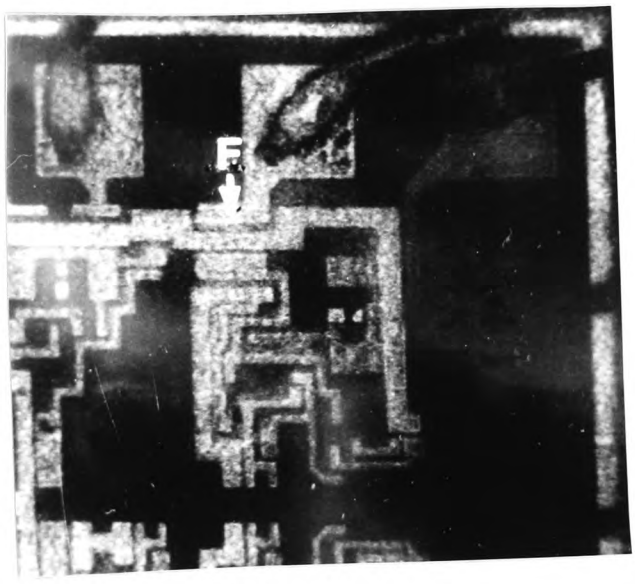

Horizontal field of view = 750 micrometres.

The images above are produced using the stroboscopic technique. The applied signal frequency is 550 kHz. The time delay between the two images is 70 nanoseconds.

Figure 7.8

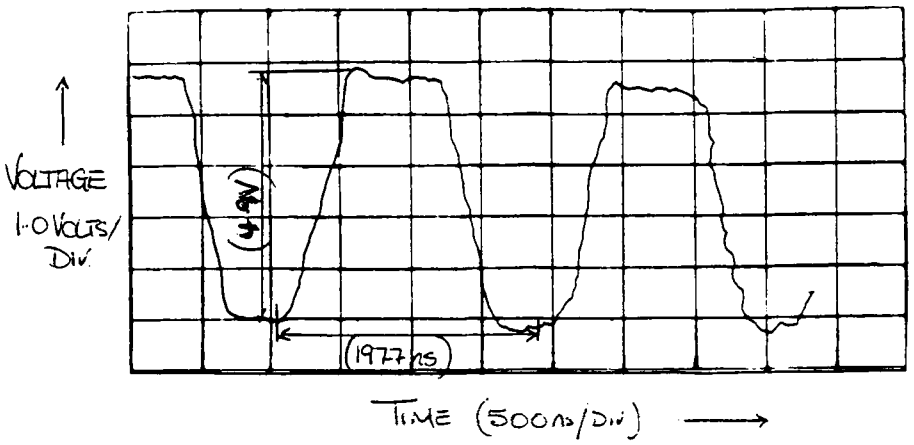

Figure 7.9

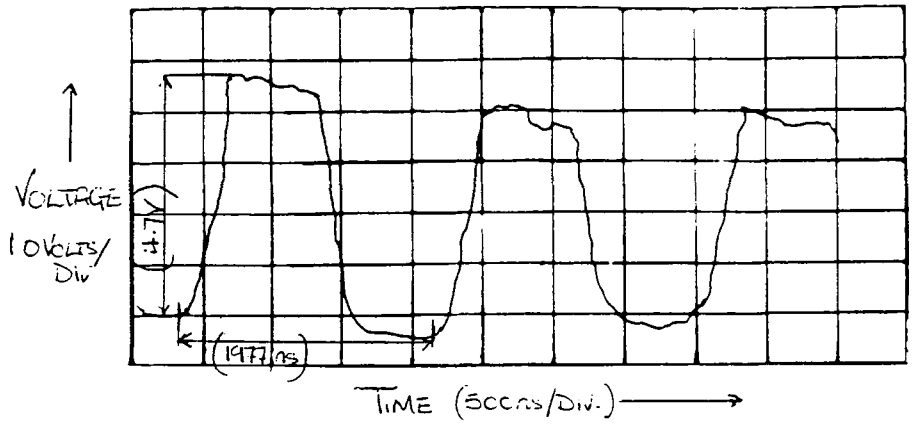

Figure 7.10

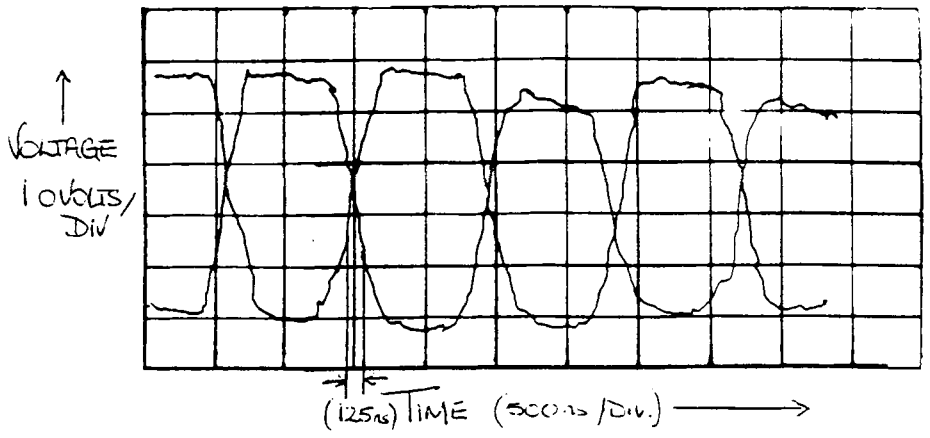

the output pads were obtained. The voltage readings were made with an accuracy of +/- 0.25 volts.

From waveforms collected from the input and output bond pads, the propagation delay for an input signal at 550kHz was found to be 75 +/- 5 nanoseconds.

(7.2) ELECTRON BEAM TESTING OF A 32-bit MICROPROCESSOR (TRANSPUTER) DEVICE.

The device was mounted in a ceramic package with 84 metal pins in a grid array. The metallic lid was carefully removed with a scalpel blade, with care being taken so as not to damage either the device or the aluminium bond wires. The device was known to be covered with a passivation layer of silicon dioxide. This was carefully removed with hydrofluoric acid buffered with ammonium fluoride. The device was then mounted within the SEM in a purpose-built holder (figure 7.11), which contained a 5 MHz clock generator and necessary interface circuitry as described in appendix 3. The device holder also allowed the transputer's internal clock to be accessed, and this was used to connect the device to the Lintech system, providing the signal to trigger the beam blanking unit.

All electrical connections to the device and its holder were made via the feedthrough system in the chamber wall. A programme had been written in Occam, the primary programming language of the transputer, which would exercise the device during testing. This code was loaded into the transputer from an IBM PC using an IMS B002 development interface board. This communication system

Figure 7.11

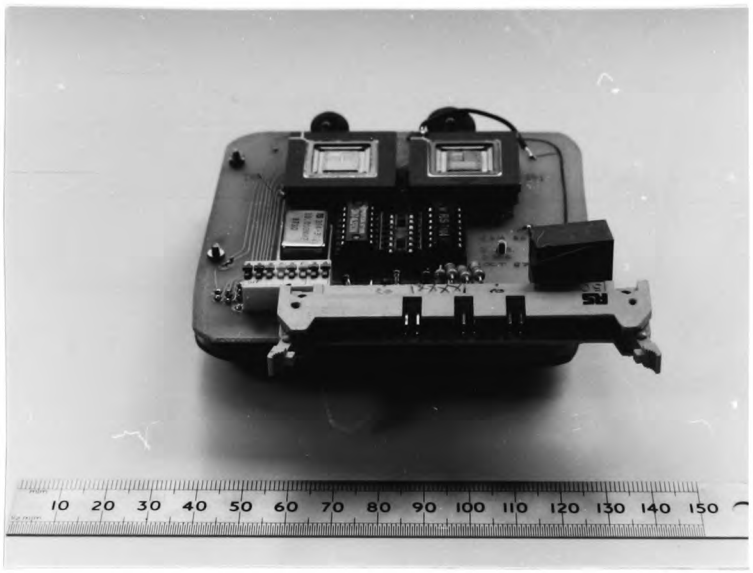

Purpose built holder for EBT on transputer devices, showing two devices; one a failure and the other a 'Golden' or reference device.

allowed the device to output a reference signal to the same PC.

The device was exercised prior to EBT to ensure that the sample preparation had not damaged it, and that the interface system was working satisfactorily. This communication system was then used to continually monitor the transputer during testing, to check if irradiation by the low energy electron beam disrupted the performance of the device. This was found not to be a problem, but if the transputer was operated for long periods within the SEM's vacuum chamber, the device became very warm.

The SEM's optics were set with a beam energy of 1 keV and a current of 3 nanoamps. The value of acceleration voltage was selected because the metal line width was down to 1.5 micrometers and (as shown in figure 6.4), the beam diameter is dependent on this energy. Also, at higher potentials, there was concern about penetration of the beam, as well as the generation of aluminium K line x-rays [Ranasinghe, D. 1987]. The high beam current was selected to compensate for the very short beam pulse width required for the stroboscopic imaging and measurement of a device which is functioning at 15MHz.

Initially, a real time voltage contrast image was obtained. This showed combinations of static and dynamic voltage contrast, and figure 7.12 is a typical example. The width of the observed stripes indicating the phase and timing relationship of adjacent metal conductor tracks. Using these imaging modes, the device was completely scanned and reference made continuously to a 'floor' plan of the circuitry (appendix 4), so as to become familiar

Figure 7.12

Dynamic voltage contrast image of a a selected area of the T414 transputer. Variation of stripe width is due to the different frequencies of signal carried by various lines.

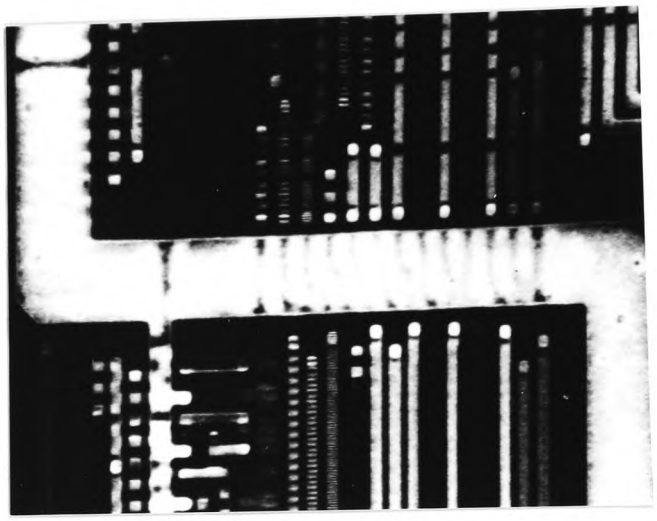

Horizontal field of view = 97 micrometres.

with the layout.

The 'on-chip' clock generator was then investigated using the stroboscopic mode. The blanking drive was triggered directly from the device, and an electron beam pulse width of 15 nanoseconds was used. As before, by changing the delay time between the trigger to the blank drives, and the beam pulse "on", the clock circuit could be observed during any part of its 15MHz clock cycle, with a time resolution of +/-2 nanoseconds.

The stroboscopic images of the on chip clock generator circuit are shown in figures 7.13 and 7.14. The time separation between the two images is 14 nanoseconds.

There are four clock generators, 90 degrees out of phase with one another. These provide the main bus signals, which synchronise all device functions. With the stroboscopic system, it was shown that the actual phase relationship could be displayed. This is achieved with the Lintech system, by introducing a second delay between the trigger pulse, the beam pulse, and the frame ramp generator which provides the scan of the electron beam in the SEM's monitor. The result is a stroboscopic image with a linear variation of time from the top of the monitor display to the bottom. This can be seen in figure 7.15, which shows four aluminium conductor tracks, each carrying the output signal from one of the four phase clock generators. When the track is at ground, it appears bright and when the track is at +5 volts, it appears dark. It can be seen that the signal does not have a 50% duty cycle between positive and ground bias.

Figure 7.13

Stroboscopic voltage contrast image of part of the T414's internal clock generator circuit. The device is operating at a frequency of 15 MHz.

Horizontal field of view = 95 micrometres.

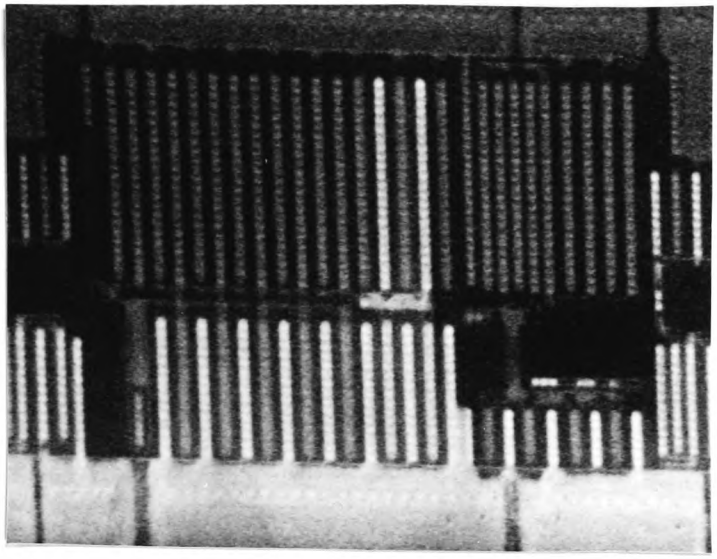

Figure 7.14

This second stroboscopic image was taken after a time delay of 14 ns, and shows the same field of view as figure 7.13, but the applied signal has a phase differance of 180 degrees.

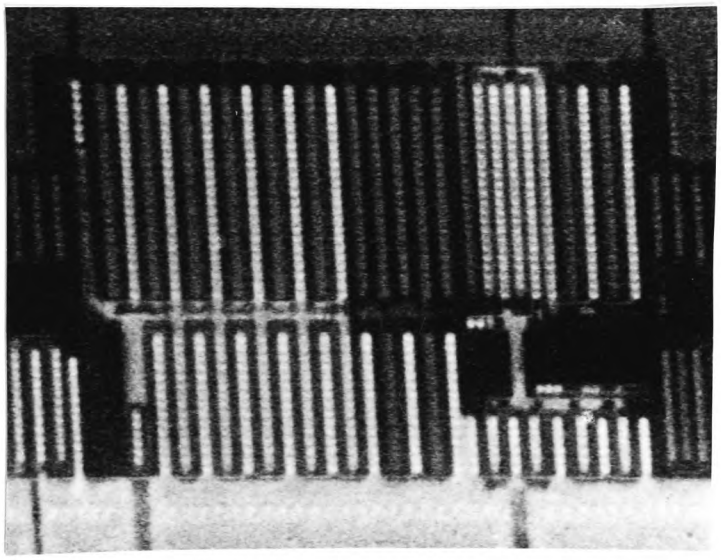

Figure 7.15

Below is a logic state map of part of the T414's four phase 'bus' circuit. The image shows light and dark stripes, similar in appearance to the dynamic voltage contrast image. However, the time resolution has been increased. Each dark stripe corresponds approximately to 22 ns.

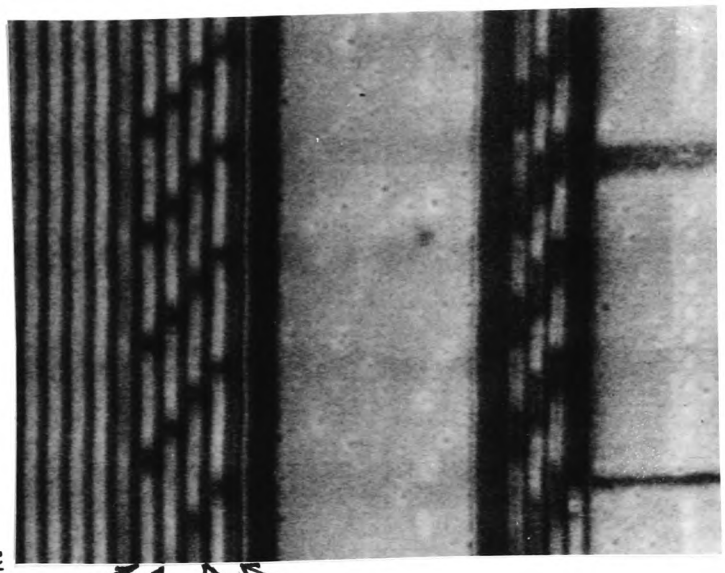

Horizontal field of view = 71 micrometres.

Figures 7.16 a,b and c

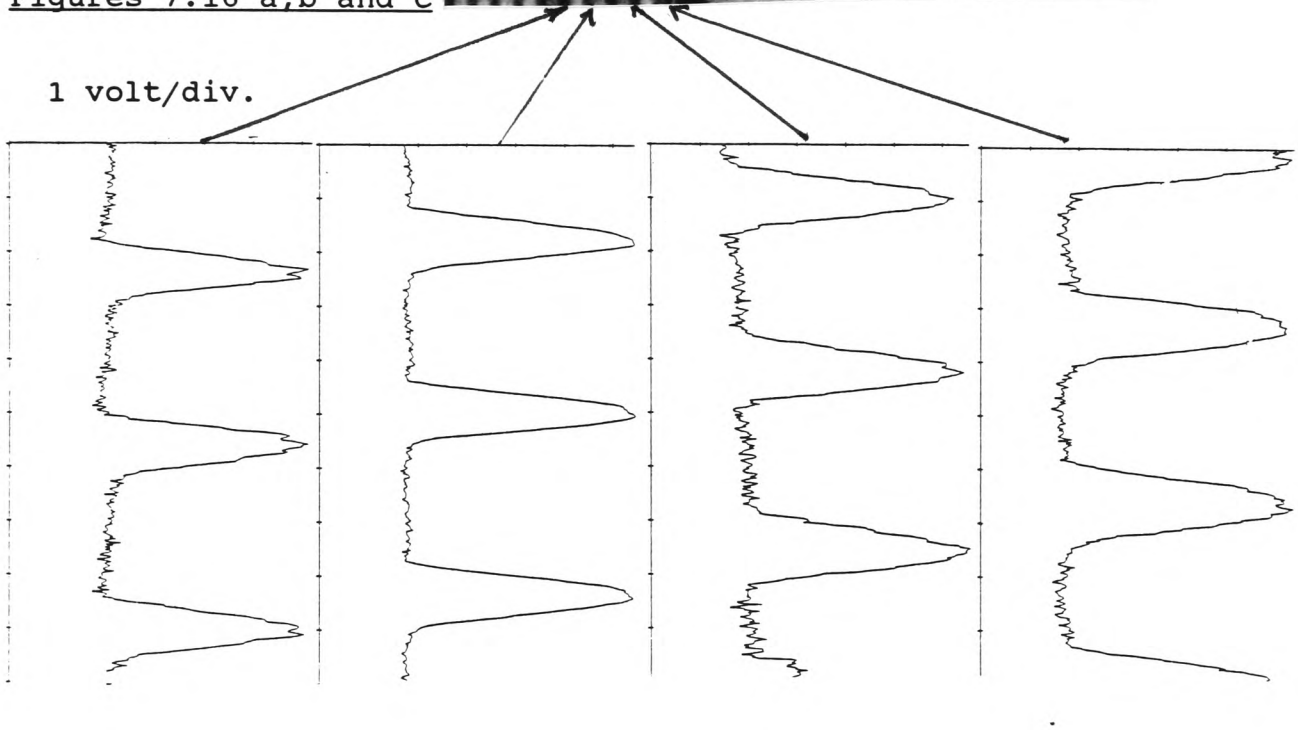

Each of the above waveforms was collected from one of the four main 'bus' lines. The peaks on each waveform can be seen to correspond to the narrow dark stripes (observed in figure 7.15), when the device is positively biased. Each line is 90 degrees out of phase.

This was confirmed by collection of a waveform from each of the 1.5 micrometre tracks. These are shown in figures 7.16 a to d, and demonstrate the ability of the EBT system to extract such information from the internal circuitry of the device.

The EBT system was then used to measure the parameter of gate propagation delay. In the case of the transputer, this has important implications with regard to the correct functioning of the central processing unit (CPU) interrupt lines. When data is being transferred via one of the transputer's links, it is necessary that the CPU be interrupted before data can be transferred from another transputer in an array of devices. If the propagation delay in the interrupt is too long, then the CPU may well be out of phase when the data arrive.

The delay time was determined by the collection of two waveforms, one from the input to a CMOS inverter, and the second at the output. The two waveforms are superimposed on one another in figure 7.17.

The waveforms show the rising edge of the input and the falling edge of the output. These were expanded in time by a factor of 10 in figure 7.18, and the delay measured at the 1.5volt switching point. This value was selected because it is typical of the switching voltage for a CMOS inverter [Sze 1983]. The delay time was found to be 2 +/- 0.5 nanoseconds, which is below the value of 3 nanoseconds which is the maximum time allowed for this device function.

The exercise demonstrated how the EBT system could very

Figure 7.17

The two wave forms below were collected at input and output lines of a signal inverter circuit on the T414. They can be seen to be 180 degrees out of phase with each other.

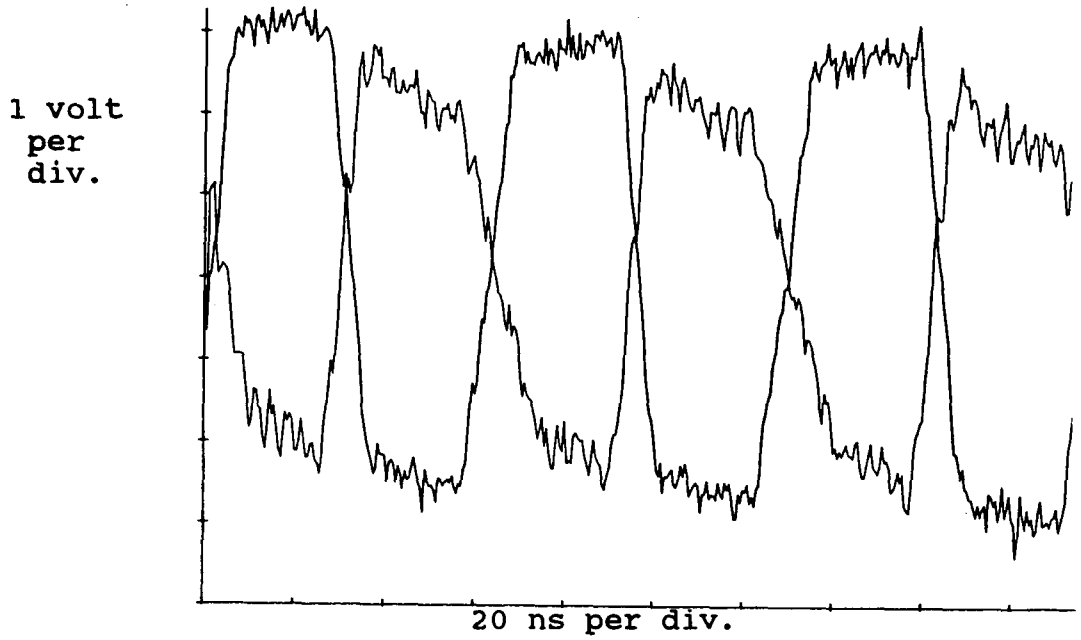

Figure 7.18

Part of the waveforms shown in figure 7.17, the time axis expanded by a factor of 10. The propagation delay of the signal travelling through the inverter circuit was determined as the time difference between the input and output signals at +1.5 volts.

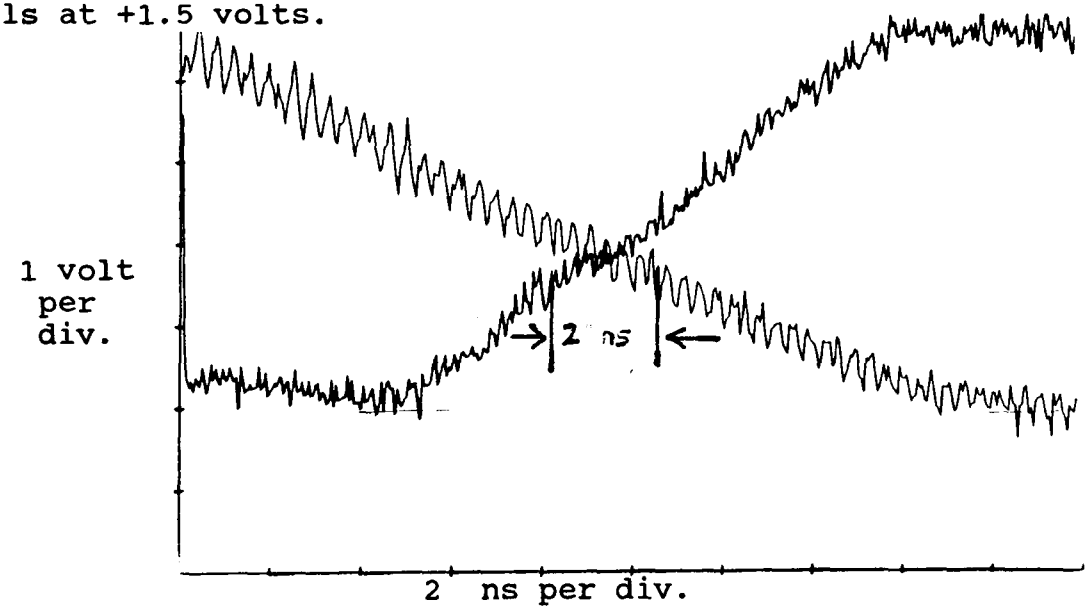

rapidly determine this parameter, which is a time consuming and haphazard procedure using conventional metallic needle probes.

The final application of EBT was to collect a waveform from a polysilicon conductor, which was buried under a layer of boron phosphate silicate glass (BPSG). Measurement is possible because of capacitive coupling between the top of the BPSG and the buried polysilicon conductor. The results are shown in figure 7.19. The waveform (B) from the buried conductor has a much reduced signal amplitude and an increased peak width, compared to (A) which was collected from the aluminium track on the surface of the device, where it connects to this specific buried track. Despite the error introduced by such reductions in signal level, the usefulness of the procedure must be recognised in that there is no other non destructive method of making such a measurement.

(7.3) ELECTRON BEAM TESTING OF A 64K STATIC RANDOM MEMORY (SRAM) DEVICE.

This product had just undergone a design update, and when final functional testing had been carried out, it was found that the data output (Q) and the low power select pins (E) were out of specification. The product was therefore required to be subjected to a failure analysis exercise. As it was suspected that the problems were at circuit level, EBT offered an attractive option for such investigations, and allowed the extraction of information concerning the chemical or physical processes which may have contributed to the failure [Fantini 1984].

Figure 7.19

These waveforms were collected from a metal line which connects to a buried polysilicon interconnector, which is capacitively coupled to the dielectric material immediately above. It can been seen that it is possible to sense the voltage change of the buried interconnector.

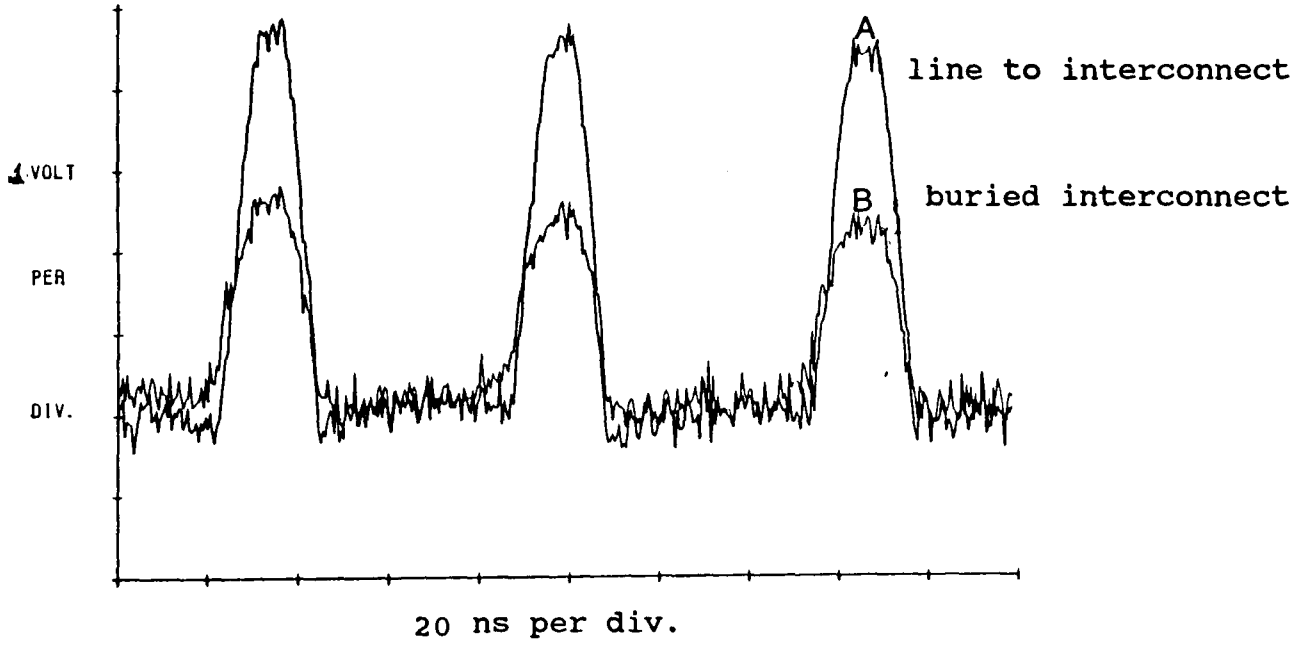

A device holder was designed and constructed, in which two of the devices were mounted close to one another in 22 pin dual-in-line sockets. This was done because sub-specification devices were produced only after the design update. Therefore, the failure analysis strategy involved the use of one of the pre-design update devices as a reference or 'golden ' device.

The metal lids were removed from the two devices, which were then mounted into their respective holders within the SEM chamber. All electrical connections were made using the feedthrough system. Pins Vss (ground) and Vcc (+5V) were connected to a standard dc voltage supply. With the exception of pins Q and E, all other pins were kept permanently at ground (low) or +5V (high), as required.

The SEM was operated with a beam energy of 0.8kV and a current of 1 nanoamp.

The 'golden' device was viewed first, using a low frequency (20 Hz), and a voltage amplitude of 5volts. A square wave was applied, first to Q and then E. The resultant images were of poor quality, as in figure 7.20, due to the silicon nitride passivation layer which completely covered the devices. It was decided to remove this layer, so the devices were returned to the failure analysis laboratory at INMOS, where the passivation was removed using a plasma etching technique. The devices were retested after etching, to ensure that no further damage had been caused during the processes. Voltage contrast images were then obtained using the conventional SE detector,

Figure 7.20.

This is a voltage contrast image of a selected area of the 64k SRAM device. Contrast is poor due to the presence of a dielectric passivation layer. Note also that the metallisation beneath this layer is only visible when it is not positively biased.

E

Horizontal field of view = 740 micrometres.

showing static voltage contrast for nodes tied at ground and +5 volts. The 20 Hz signal was applied to Q and E, the internal circuitry associated with each of these pins was clearly visible, because of the alternating light and dark stripes (dynamic voltage contrast), which appear superimposed on such components.

Once sufficient information about the layout of the device had been gathered, the VMEC detector was inserted into the SEM and the frequency of the applied square wave was increased to a more realistic value of 0.6 MHz.

The work was then concentrated on the failure of pin E. From the earlier functional test data, it had been concluded that the problem was likely to be in the 'buffer' circuitry. Stroboscopic images of the buffer circuit were captured, digitised, and stored in the PC. A stroboscopic image of the buffer with the input signal to the buffer high, figure 7.21, was overlaid onto the image captured with the input low, and is shown in figure 7.22. Registration of the two images was achieved by selecting a regular shaped feature which was common to both images, and then by continuously manipulating the device with the X,Y and rotation movement controls of the SEM stage, whilst continually subtracting the live image. When the selected reference feature completely disappeared, the images were considered to be completely aligned. The timing difference between the two images is 800 nanoseconds. The subtracted image is shown in figure 7.23. If features have the same contrast in the two original images, they will completely cancel. If, however, they are different, then contrast appears in the

Figure 7.21.

The same area of the device as shown in figure 7.20, but the passivation layer has been removed. Voltage dependent contrast can be seen. This area is part of the 'buffer' circuitry which had a signal of 0.6 MHz applied to it.

Horizontal field of view = 370 micrometres.

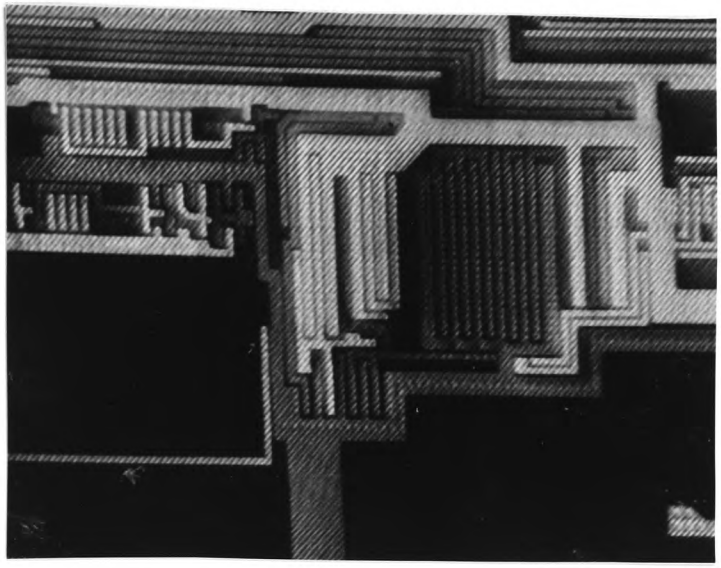

Figure 7.22

This is the same area of the device as above, but the applied signal is 180 degrees out of phase.

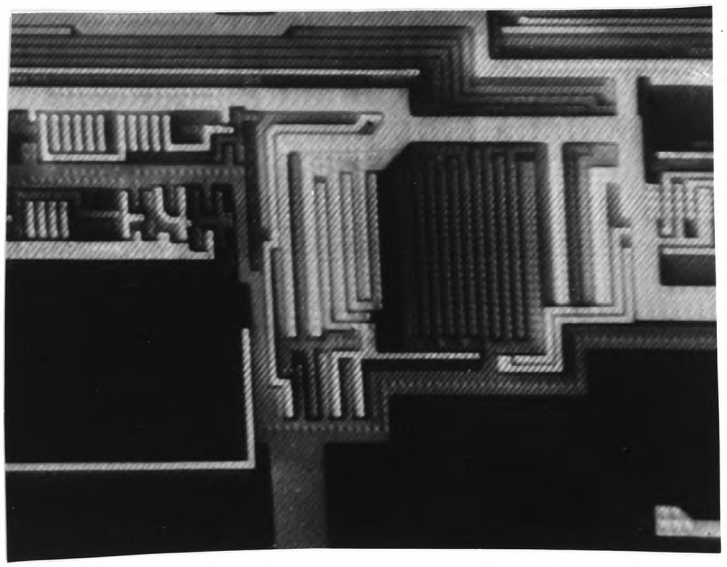

Figure 7.23

This is the resultant subtracted image, obtained by overlaying the two previous images. Only those nodes with contrast difference between the two are seen.

Horizontal field of view = 180 micrometres.

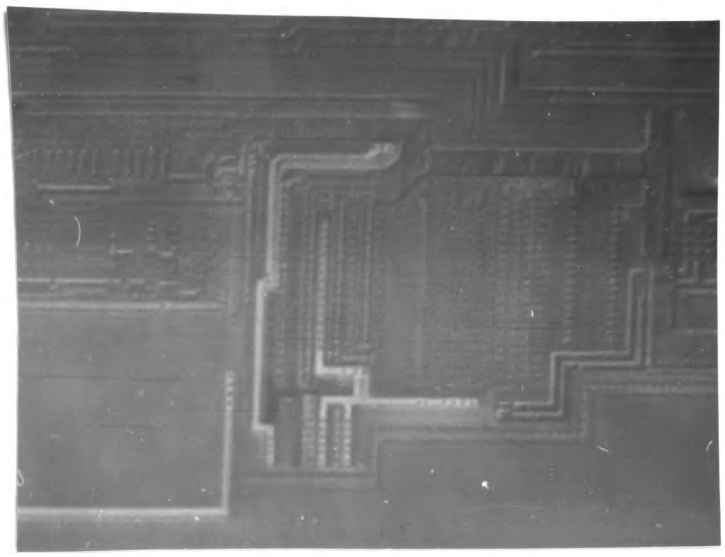

Figure 7.24

Schematic diagram of those nodes which should have shown contrast in figure 7.23.

The arrow indicates the node which was not observed and was suspected of being the failure.

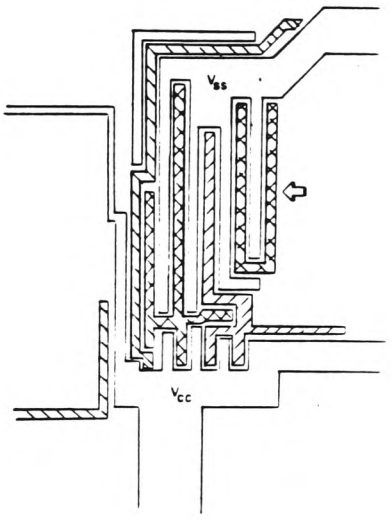

subtracted image. Figure 7.24, shows from previous knowledge how the subtracted image should appear. Of interest is the 'U'-shaped feature which should have appeared in the subtracted image (i.e showed opposing contrast when the input signal is high or low). Waveforms were collected from the input to the buffer and from the 'U'-shaped feature, and are shown in figure 7.25. From this information, it was concluded that the feature was held permanently to ground potential.

Subsequent investigation at INMOS revealed that the output of the buffer was not connected (as it should have been) to the drain of an N-channel transistor, and so was held permanently to Vss, the ground rail.

The second problem was with the data output pin (Q). When the low frequency signal used for tracing the circuitry associated with the output pin was followed on the functionally failed device, it was noted that the data output bond pad showed very little contrast change compared to the rest of the circuit. The 0.6MHz signal was then applied to Q. A stroboscopic image was collected when Q was meant to be high and again with a time delay of 800 nanoseconds, when it is low. Then the equivalent circuitry of the 'golden' device was imaged, at the high and low phases. These images were then subtracted from their counter-parts for the faulty device. For the data output high, the images showed complete cancellation. However, for the low phase, the bond pad was still visible as shown in figure 7.26. A waveform was then extracted from the output pad, and is shown as figure 7.27. The signals showed that the pad was tied high, not being

Figure 7.25

The waveforms below were collected from the node indicated in figure 7.24 by the arrow, and from the input to the buffer. It can be seen that the suspected failed element is permanently at ground potential.

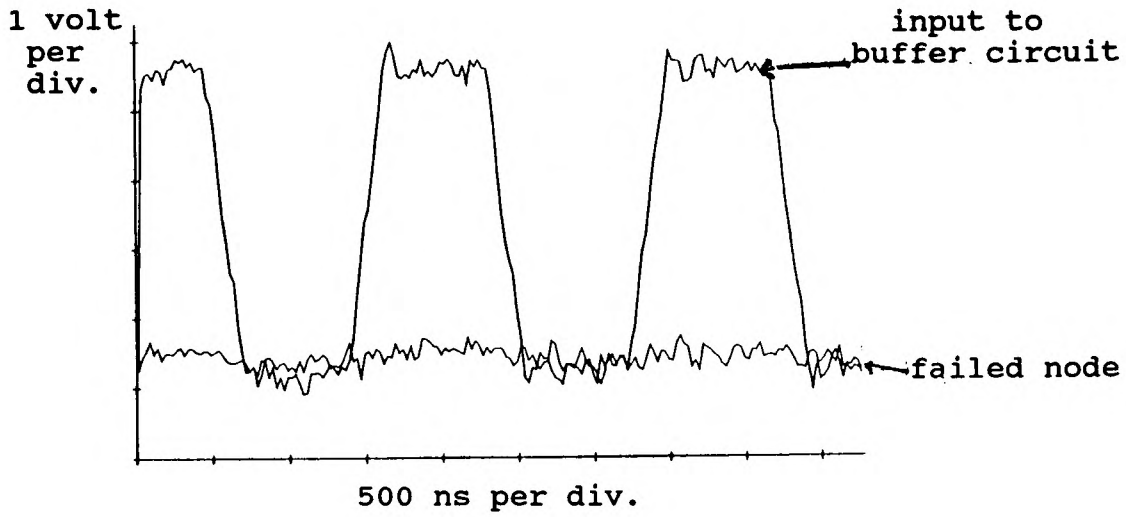

Figure 7.26

This image is formed by subtracting the two stroboscopic images of the output pad of the 64k SRAM which had failed functional testing. The pad signal should have completely cancelled out, but can still be seen.

Horizontal field of view = 740 micrometres.

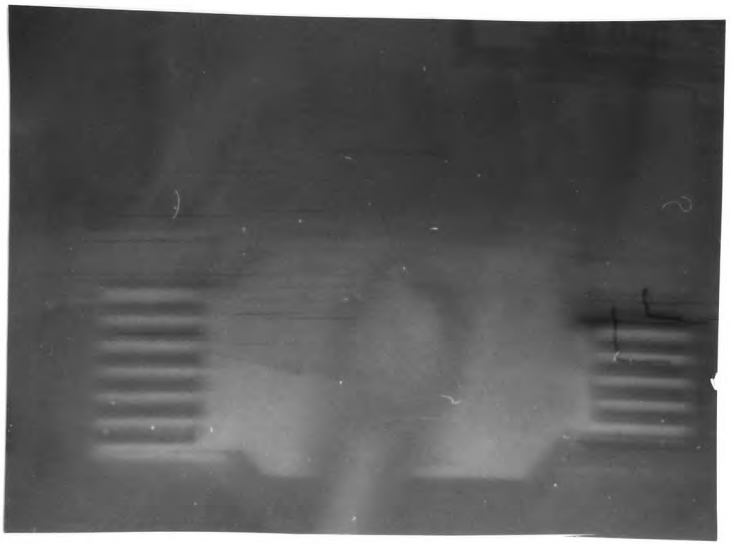

Figure 7.27

The waveforms below were collected from the input to the 'output' pad and the pad itself. It can be seen that the pad is held permanently high.

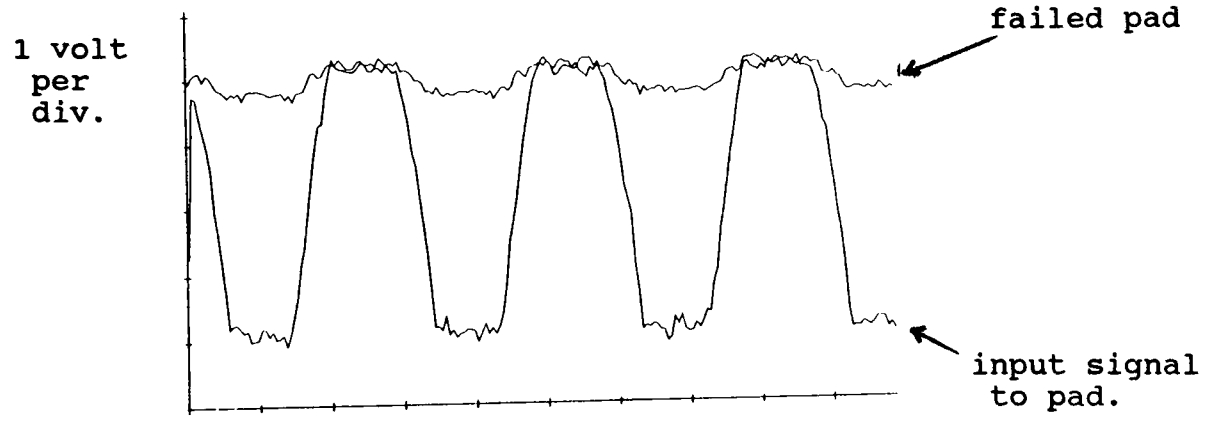

able to fall below 4.5volts.

Subsequent examination by the failure analysis department at INMOS revealed that the gate oxide beneath the polysilicon gate electrode was missing. As a result, the bond pad was tied to the adjacent Vcc power rail.

It was concluded that both these failures were due to error at the design stage.

CHAPTER 8.

CONCLUSIONS.

The conclusions of the project can be grouped into three categories:

Firstly, those relating to low voltage operation of the SEM in general, and those specific to the JSM 840.

Secondly those results derived from work on quantitative voltage measurements using the conventional Everhart-Thornley SE detector and the VMEC.

Finally those conclusions which are concerned with the application of EBT techniques in the analysis of MOS technology VLSI devices.

(8.1) LOW VOLTAGE OPERATION OF THE SEM.

For voltage contrast work using the SEM, acceleration voltages of around 1kV were found to be most suitable. Using such low beam energies, the SE yield is maximised. This is important, as voltage information can only be detected using the SE imaging system. It is also an advantage to use lower beam energies to minimise the deposition of energy at any significant depth within the specimen. The types of characteristic x-rays and their intensities are also limited, which is important if changes to the specimen's electrical characteristics are to be avoided.

There are, however, disadvantages to low voltage operation, particularly if the SEM's electron gun uses a tungsten thermionic emitter as an electron source. At these energies, the spatial resolution is considerably reduced, as the diameter of the primary electron probe is increased due to lens aberrations of which chromatic aberration is likely to be the most prominent.

For the JSM 840, the beam diameters used for electron beam testing were of the order of 1 to 1.5 micrometres. At such diameters, a workable compromise was reached between spatial resolution and the beam current impinging the specimen.

(8.2) QUANTITATIVE VOLTAGE MEASUREMENT.

It has been demonstrated that the study of voltage distributions within micro-electronic circuits is possible using the conventional SE imaging system of the SEM. This was particularly successful with devices which had a voltage difference of 5 volts. However, as will be described below, this type of detector is not sensitive to voltage differences of less than 1 volt. The voltage dependent contrast can only be used to give qualitative information, and the technique is at its most successful when the applied bias is positive with respect to ground potential. The reason for this was shown by measuring the SE detector output as a function specimen bias between -20 and +20 volts. When the specimen was biased from +1 to -20 volts, there was very little change in the detector output, and therefore in image contrast. A large difference was recorded for bias changes between +1 and +20 volts. However, unfortunately,

the detector output did not fall linearly with the specimen bias. When the bias exceeded +10 volts, the rate change to the detector output began to diminish, thus limiting the range of voltages over which the technique may be used, even for qualitative work.

The decrease of detector output as the specimen became positively charged was due to a retarding field immediately above the emitting surface. This increased in strength as the specimen became more positively biased.

To achieve quantitative voltage measurements, the VMEC was used. This detector's output allows an analysis of the SE energy profile, in the form of an 'S'-shaped curve, which is the integral of the energy profile. Using this detector, it has been possible to make voltage measurements from 0 to +15 volts. The work concentrated specifically on voltage measurement over the range 0 to 5 volts, which is typical of the majority of ICs.

The 'S'curves move along the filter electrode axis, in response to changing specimen bias. The curves also contain information concerning changes to the SE yield, which could be measured by differentiating the 'S'-curve data and measuring the area under the energy profile. Using this measurement scheme, it is possible to determine the effect on the SE emission profile of the retardation barrier and of any electrostatic fields generated from nodes adjacent to the SE emission point. These effects can give voltage measurement errors, as demonstrated in this study.

By using an extraction field between the emitting surface and the VMEC, the measurement error can be reduced. However, care is

required when selecting the strength of the field, as this affects the ability of the detector to sense SEs. It was found that an extraction electrode voltage of approximately 3 kV gave the maximum detector efficiency.

Concerning the voltage measurement error, this was found to be due to a number of factors including the width of the emitting node, the level of positive bias applied to it, the electro-static fields adjacent to it, and material differences.

As the line width decreased, it was found that the voltage measurement error increased accordingly. There are two reasons for this. The first is that as the node width begins to approach the diameter of the primary beam, so SEs are generated at the edge of the node; these having altered angular distributions. The second reason concerns the positive bias applied to the node. As the node dimensions decrease for a given level of positive bias, so the intensity of the associated retardation barrier increases, altering the SE energy profile.

Positive bias applied to nodes adjacent to the emission point also increases measurement error, once again by increasing the angular distribution, and so reducing the numbers of SE detected. In general, it was found that as the number of SEs detected was reduced, so the voltage measurement error increased logarithmically.

The final source of measurement error was found to be associated with differences between the materials under examination. The SE emission profile for any given irradiation

beam energy is a function of the target material, with both the yield and the energy profile changing. However, for EBT of VLSI devices, much of the analysis is likely to involve the measurement of voltage carried by aluminium conductor tracks. It may be that in the future, voltages may be required to be measured from both aluminium and 'short ranged' silicon conductors. Therefore the approximate 0.5 volt difference in baseline will need to be fully taken into consideration in such studies.

(8.3) APPLICATION OF ELECTRON BEAM TESTING.

It was found that the SEM could be operated with acceleration voltages of 0.8 and 1.0 kV, and beam currents of between 1 and 3 nanoamps, for electron beam test work. Using these parameters, spatial resolution was sufficient to resolve 0.5 micrometre features.

Using the conventional SE detector, it was possible to observe a voltage dependent contrast, when positive voltages were applied. The fact that this contrast was superimposed on the surface topographic contrast was useful, enabling the location of specific features with respect to one another.

By applying a low frequency square wave signal to the sample, a light and dark striped pattern was observed. The widths of the stripes and their numbers were dependent on the frequency of the applied signal, and upon the scan frequency of the primary electron beam. This observed 'dynamic' voltage contrast was found to be ideal for signal tracing. Applying the signal to a specific

input/output pin, the contrast was observed only on the circuitry connected to this pin. However the bandwidth of this type of signal was very narrow, limited to only a few tens of Hertz.

To observe the change of voltage contrast at higher frequencies, the stroboscopic technique was required, with the electron beam being repetitively deflected on and off the specimen. Such switching was synchronised to signals which were either applied to the specimen or generated by it. With this stroboscopic technique, voltage contrast changes at frequencies up to 15 MHz were observable. However, it was found to be necessary to use image processing, such as recursive filtering, to reduce the level of noise contained in the images. The noise component increased with frequency, due to the width of the primary beam irradiation pulse being reduced.

The logic state mapping technique was found to be ideal for displaying on the SEM monitor the phase relationship between different features on a specimen, such as the the main 'bus' signal on the microprocessor.

Other image processing techniques, such as image subtraction, were found to be very important, particularly as the number of nodes which were suspected of being part of a device's failure increased. Performance of the examination in conjunction with a reference device allowed the analysis time to be significantly reduced.

All of the devices tested had internal voltage 'swings' from ground to 5 volts positive. Quantitative voltage measurements

were made on all three devices, using the VMEC, which had been optimised via earlier characterisation work.

Considering the results obtained from the T414 Transputer device, voltage measurements were made on each of the four 'bus' lines; these having widths of approximately 1.5 micrometres and separation distances of 1 micrometre. At a frequency of 15 MHz, the mean voltage error was found to be only 300 millivolts.

It was possible to observe a voltage dependent contrast superimposed on the dielectric material immediately above buried polysilicon short ranging interconnectors within the transputer device. This was feasible because the top surface of the dielectric was capacitively coupled to the buried conductor. However, due to the capacitance of the dielectric material, the amplitude of the voltage change was found to be only 2.8 volts, and the rise and fall times of the signal increased in comparison to those of waveforms obtained from the aluminium track which is connected to the buried conductor.

(8.4) GENERAL CONCLUSIONS

The project has shown that EBT is possible using various features of the SEM. These techniques offer significant advantages for the study of VLSI devices. These comprise:

(1) the ability to observe the voltage distribution over relatively large areas of a device, whilst the application of a low frequency signal to specific pins will make the circuitry connected to them immediately identifiable.

(2) The observation of devices at their working frequency, including comparison of a failed device with a good one.

(3) Quantitative measurements of both voltage and timing, using an electron beam, having an energy which has been careful selected to avoid charge injection, loading the sample and limiting the types of x-ray generated.

The beam is a non-physical contacting probe, which can be accurately aligned to nodes as small as 1.5 micrometres. However, the detector must be able to suppress the two types of local field effects. Failure to do this results in measurement error. Finally, because buried conductors are capacitively coupled to the surface of any overlying insulating material, semi-quantitative voltage-time measurements are also possible for such circuit elements.

REFERENCES

Bishop, H.E. Methods of surface analysis techniques and applications.
Editor. Wallis Pub. Cambridge University Press (1989).

Chung, M.S. and Everhart, T.E. Simple calculation of energy distribution of low-energy secondary electrons emitted from metals under electron bombardment.
Journal of Applied Physics. Vol.45 No.2 (1974) pp707-710.

Davidson, S.M. SEM microcharacterisation of semiconductors.
Editors. Holt and Joy Pub. Academic Press (1989).

Dekker, A.J. Solid State Physics.
Pub. Macmillan & Co. Ltd. (1962).

Dinnis, A.R. Static and dynamic measurments using an electron probe.
J.Phys. E:Sci. Instrum. 21 (1988) pp522-533.

Dinnis, A.R. Detectors for quantitative voltage contrast on submicron devices.
Microelectronics Eng.7 (1987) pp139-146.

Einspruch, N.G. ed. VLSI Handbook.
Pub. Academic Press. Inc. 1985.

Everhart, T.E. Contrast formation in the scanning electron microscope.
Phd. Thesis University of Cambridge (1958).

Everhart, T.E. and Hoff, P.H. Determination of kilovolt electron energy dissipation vs penetration distance in solid materials.
J. of Applied Physics. 42,13. (1971) pp5837-5846.

Everhart, T.E. and Thornley, R.F.M. Wide-band detector for micro-microampere low-energy electron currents.
J.Sci.Instrum.37 (1960) pp246-250.

Fatini, F. Reliability problems with VLSI.
Microelectron. Reliab. 24, (1984) pp275-296.

Fleming, J.P and Ward, E.W. A technique for accurate measurement and display of applied potential distributions using the scanning electron microscope.
Scanning Electron Microscopy IITRI (1970) P467-472.

Fujioka, H. and Ura, R. Waveform measurement at GHz.
App. Phys. Lett. 39 (1) July (1981) pp81-87.

Goldstein, J.I. et.al. Scanning Electron Microscopy and X-Ray Microanalysis.
Pub. Plenum Press. New York (1981).

Gopinath, A. Estimate of minimum measurable voltage in the SEM.
J.Phys. E: Sci.Instrum. 10 (1977) pp911-913.

Gopinathan,K.G. and Gopinath, A. A sampling scanning microscope.
J.Phys. E: Sci.Instrum. 11 (1978) pp229-233.

Jansen, G.H. et.al. Energy broadening in electron beams: A comparison of existing theories and Monte Carlo simulation.
J.Vac. Sci. Technol, B3 (11) (1985) pp453-470.

Joy, D.C. A model for calculating secondary and backscattered electron yields.
J. of Microscopy Vol.147:Pt1 (1987) pp51-64.

Joy, D.C. An introduction to Monte Carlo simulations.
Inst.Phys. Conf. Ser. No.93:Vol.1. (1988) p23-32.

Khursheed A, The computer aided design of electron detectors of the scanning electron microscope.
Ph.d Thesis. University of Edinburgh (1983).

Lintech Instruments Limited technical brochure (1982).

MacDonald, N.C. Potential mapping using Auger electron spectroscopy.
Scanning Electron Microscopy, IITRI, Chicago (1970) pp481-485.

McKay, K.G. Secondary electron emission.
Advanced Electronics 1 (1948) pp65-130.

McMullian, D. Early days of SEM in Cambridge.
J. of Microscopy Vol.139:Pt2. (1985) pp129-138

Menzel, E. and Buchanan, R. Some recent developments in low voltage E-beam testing of ic's.
J.of Microscopy, Vol.140:Pt3 (1985) pp331-349.

Menzel, E. and Kubalek, E. Fundamentals of electron beam testing of integrated ciruits.
Scanning Vol.5 (1983) pp103-122.

Miyoshi, M. et.al. Effects of electron beam testing on the short channel metal oxide semiconductor characteristics.
Scanning Electron Microscopy IV (1982) pp1507-1514.

Mulvey, T. The SEM and microcircuits.
Microscopy and Microanalysis. July. issue No.6 (1988) pp13-17.

Oatley, C.W. and Everhart, T.E. The examination of p-n junctions with the scanning electron microscope.
J. Electronics 2, (1957) pp568-571.

Nakamae, K et.al. Local field effects on voltage contrast in the scanning electron microscope.
J.Phys.D:Appl. Phys.,14 (1981) p1939-60.

Napchan, E. Applications of Monte Carlo simulations in the SEM study of heterojunctions.
Inst. Phys. Conf. Ser. No.87: section 11 (1987). p733-738.

Plows, G.S. and Nixon, W.C. Stroboscopic Scanning Electron Microscopy.
J.Phys. E:Sci.Instrum. Series 2. 1. (1968) pp595-600.

Ranasinghe, D.W. et.al. Electron beam irradiation effects on MOS-transistors and its significance to E-beam testing.
Microelectronic Engineering 7 (1987) pp397-403.

Reiners, W. et.al On the primary electron energy dependence of radiation damage in passivated NMOS transistors.
Inst.Phys.Conf.Ser.76 section 12 I.O.P (1985)p p507-512.

Richards, B.P. and Trigg, A.D.
The GEC. Journal of Research. Vol. 3. No.3 (1985) pp167-180.

Russell, J.D. et.al. Electron beam irradiatiion effects in MOS transistors.
Inst. Conf. Ser. No.100: Section 9 (1989) pp697-702.

Smith, K.C.A. The Scanning Electron Microscope and its field of applications.
Ph.d Thesis. University of Cambridge (1956).

Sze, S.M. VLSI Technology.
Pub.McGraw-Hill (1983).

Wallis, J.M. ed. Methods of surface analysis, techniques and applications.
Pub. Cambridge Univ. Press (1990).

Wells, O.C. and Bremer, C.G. Voltage measurement in the Scanning Electron Microscope.
J.Phys.E:Sci.Instrum. Series2.1. (1968) pp902-906.

Wolfgang, E. et.al. Electron-beam testing of VLSI circuits.
IEEE Journal of Solid State Circuits. Sc14. No.2 (1979) pp471-481

Erratum

Stewart, A.D.G. The origins and development of scanning electron microscopy.
J.of Microscopy Vol.139:Pt2 (1985) pp 121-127

Inst. Phys. Conf. Ser. No 100: Section 9
Paper presented at Microsc. Semicond. Mater. Conf., Oxford, 10–13 April 1989

Electron beam testing for the failure analysis of VLSI devices

D R Jones and M Woodward

Gwent College of Higher Education, Allt-yr-yn Avenue, Newport, Gwent, NP9 5XA, U.K.

ABSTRACT: Electron beam testing (EBT) uses the phenomenon of voltage contrast to observe the potentials on VLSI device nodes and the fact that modern scanning electron microscopes (SEM) can operate at low primary beam energies (0.2 to 1 KeV), producing non-capacitive and non-destructive probing. This paper shows how the techniques of dynamic voltage contrast, voltage coding and stroboscopic voltage contrast, are used to extract voltage level and timing data from any part of a VLSI device. This data can then be used for the failure analysis or design verification of such devices.

1. INTRODUCTION

Advances in VLSI device technology have resulted in continual increases in circuit integration and component density. This has resulted from the continuing reductions of internal geometries, now at 1.25 to 1.5 micron line widths in volume production. As a consequence of these advances problems have arisen in the functional testing of such devices , the conventional automatic test equipment (ATE) being restricted to the testing of the peripheral test circuiting or bond pads only. EBT with its advantages of non-capacitive, non-destructive probing and accurate alignment of the electron beam probe is able to perform the internal testing of VLSI devices (Wolfgang et al 1979). Using the full range of EBT techniques the VLSI device can be completely characterised for voltage level and timing data (Menzel and Buchanan 1985). Unlike ATE probing, EBT probing allows the extraction of data from passivated devices and buried multilevel conductors using capacitive coupling voltage contrast (CCVC). (Menzel and Kubalek 1981).

However, fully quantitative voltage contrast data is only available from unpassivated or depassivated devices, due to signal attenuation caused by charge storage effects in the dielectric material. Timing data is only marginally affected by passivation or interlevel dielectric and complete timing diagrams may be produced (Görlich et al 1986).

There are two effects which assist the EBT of passivated devices: the conductivity induced by the electron beam in the insulator when using high primary beam energies of 2 to 4 KeV (Sugiyama et al 1988) and the capacitance coupling voltage contrast (CCVC) obtained when using low primary beam energies of 0.5 to 1 KeV. (Görlich et al 1986).
In this page we compare results from depassivated and passivated devices to show how EBT can be used as an effective failure analysis tool.

2. SYSTEM DESCRIPTION

The system consists of a scanning electron microscope with the addition of some external equipment. This equipment includes the EBT electronics rack and monitors, a system to exercise the device under test (DUT), and a P.C. with software to perform image differencing, plus a plotter to produce hard copy waveforms. Figure 1 illustrates the complete system.

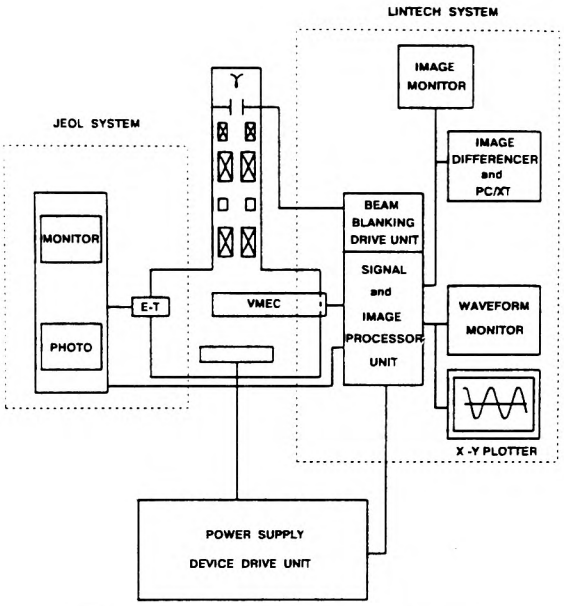

FIGURE 1 : EBT Test System

Packaged devices are opened, and placed in a zero insertion force socket on a test board in the SEM. The devices can be exercised from a signal generator and power supply if simple tests are to be made, from a device tester or P.C. with appropriate software if advanced tests are to be carried out. Two dual-in-line (DIL) packages or pin-grid-array (PGA) packages can be inserted side by side for direct comparison of a "good" (or "golden") device with the ATE functional failed device.

Electrical test signals are transmitted to the I.C. devices through screened, cables via an interface plate. These provide a continuous, shielded signal path into the SEM vacuum chamber. With short lead lengths, signals up to 30 MHz can be used and monitored, although the EBT system will process signals at up to 250 MHz. Future modifications should allow signal rates up to 100 MHz to be used. The SEM primary beam energy is used in the range 0.6 to 1.0 KeV depending on application. Voltage resolution is typically ± 50mV with ± 200ps timing resolution.

3. IMAGING MODES

3.1 Static Voltage Contrast

In static voltage contrast, the state of the device circuit elements can be deduced from the voltage contrast mechanism i.e. a more positive line will appear dark and a more negative line bright. This method can be used to locate problems with power bus lines.

3.2 Dynamic Voltage Contrast

Dynamic Voltage contrast, or voltage coding, is an interference effect which occurs when the frame scan or line frequency of the display monitor beats with the clock frequency of the device. Depending on how close a multiple of the clock frequency is the frame scan rate of the monitor, horizontal or vertical stripes appear, wandering across the screen display. If the frame scan rate is synchronised to the clock frequency the stripes can be held in a steady state and measurements of frequency made, if the monitor frame scan frequency is accurately known. The frequency of this "barber's pole" or "candy stripe" effect is limited to less than 50kHz due

to the bandwidth of the secondary electron detection chain (Wolcott and Sziklas 1987). This technique can be used to trace the path of an applied signal through the device.

3.3 Stroboscopic Voltage Contrast

Fast timing measurements, greater than 50kHz require stroboscopic voltage contrast. The electron beam is blanked in synchronisation with the clock frequency of the DUT. Stroboscopic images are captured at typically 10ns internal sample width and may be stored on video tape, in the frame store of the P.C., or as a series of photographs. This technique can be used to identify floating lines or stuck bits.

3.4 Waveform Mode

The SEM electron probe can be positioned on a single circuit line or node and the voltage in that line measured quantitatively as a function of time using stroboscopic voltage contrast on a depassivated device.

3.5 Logic Mapping

A modification of stroboscopic voltage contrast is called logic mapping. In this mode active states in the circuitry appear as a series of alternating light and dark bands representing the high and low states of the signal (as dynamic voltage contrast at low frequencies). This technique can be used to compare the phase relationships of adjacent conductor lines.

3.6 Comparison of Passivated and Depassivated Devices

Figure 2 compares the images obtained from a fully passivated device with that from a depassivated device and the resulting waveforms obtained. As shown the image quality is reduced for the passivated device, but is good enough to qualitatively observe the line. The quantitative voltage waveform compared for the two lines with the same applied signal shows a reduced voltage level, due to attenuation by the dielectric material, but the timing data is only marginally affected.

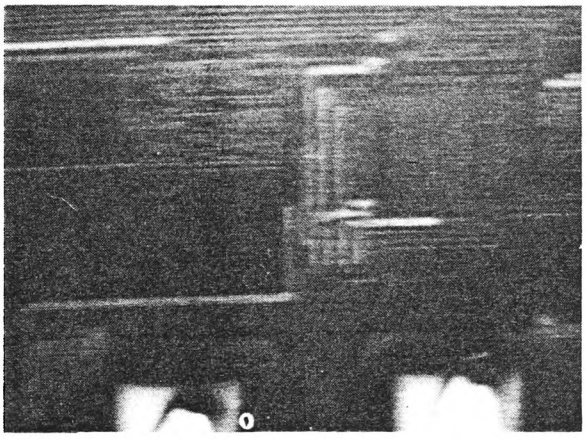

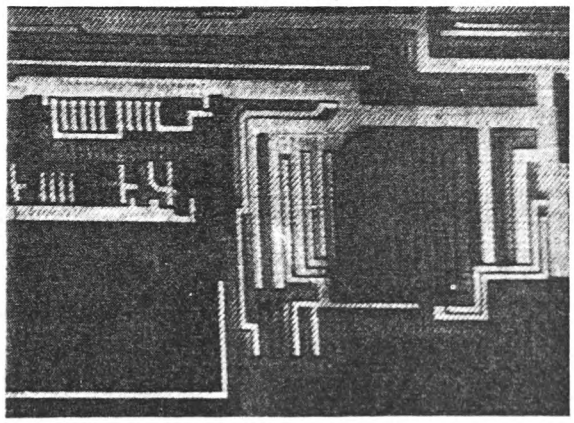

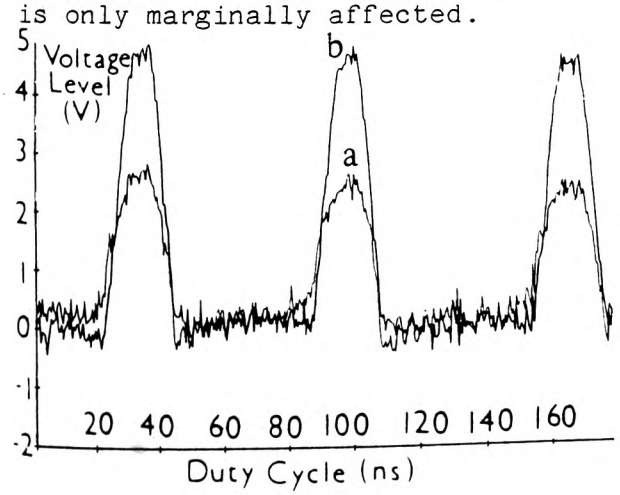

FIGURE 2 : Comparison of a) Passivated b) Depassivated Devices

4. FAILURE ANALYSIS OF VLSI DEVICES

4.1 Detection of Stuck Output

Figure 3 is an image difference micrograph of golden device compared to a functional failure device at the output stage of a 64KSRAM I.C. Images of the golden and functional failure device were captured and stored in the frame store of the P.C. for each half cycle of the complete duty cycle. The area to be investigated was located by data from the ATE prober. As shown by figure 3 there is a difference in the signal voltage contrast between the devices on one half of the cycle. This indicates that the output circuitry is stuck "high". Examination of the waveforms from the output lines in figure 4 confirm that output does not go "low". Further investigation and deprocessing revealed that the line was tied at the V_{DD} supply rail level due to missing gate oxide under the polycide gate of the output transistors.

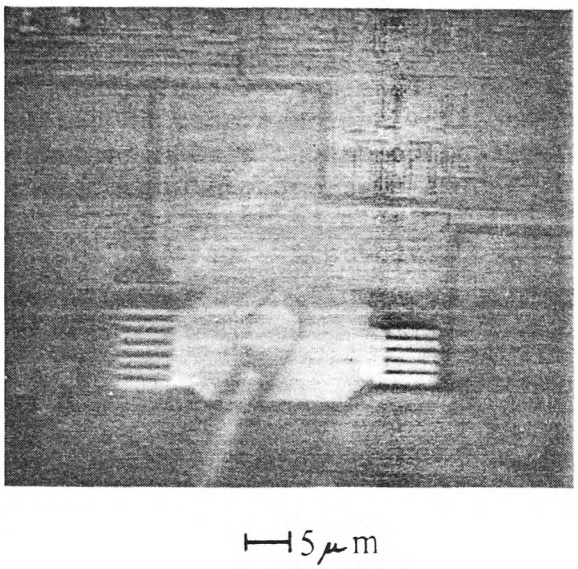

FIGURE 3 : Difference Image of Stuck Output

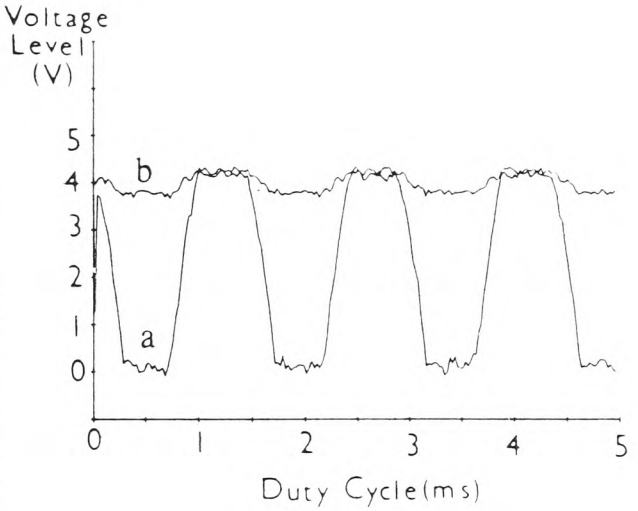

FIGURE 4 : Voltage Waveforms
a) Golden Device
b) Failed Device

4.2 Detection of Missing Interconnection

The image difference micrograph of figure 5 shows the chip select buffer circuitry of a VLSI device for a golden and functional failure DUT. Comparison of the micrograph and the waveform plots of figure 5 shows that the functional failure DUT does not go high and that in this standby mode the buffer line was floating. Upon investigation it was found that a design error had occurred and that the output of the buffer was not connected to the drain of an N-channel transistor. A fix for this design error was instigated for the next revision of the device.

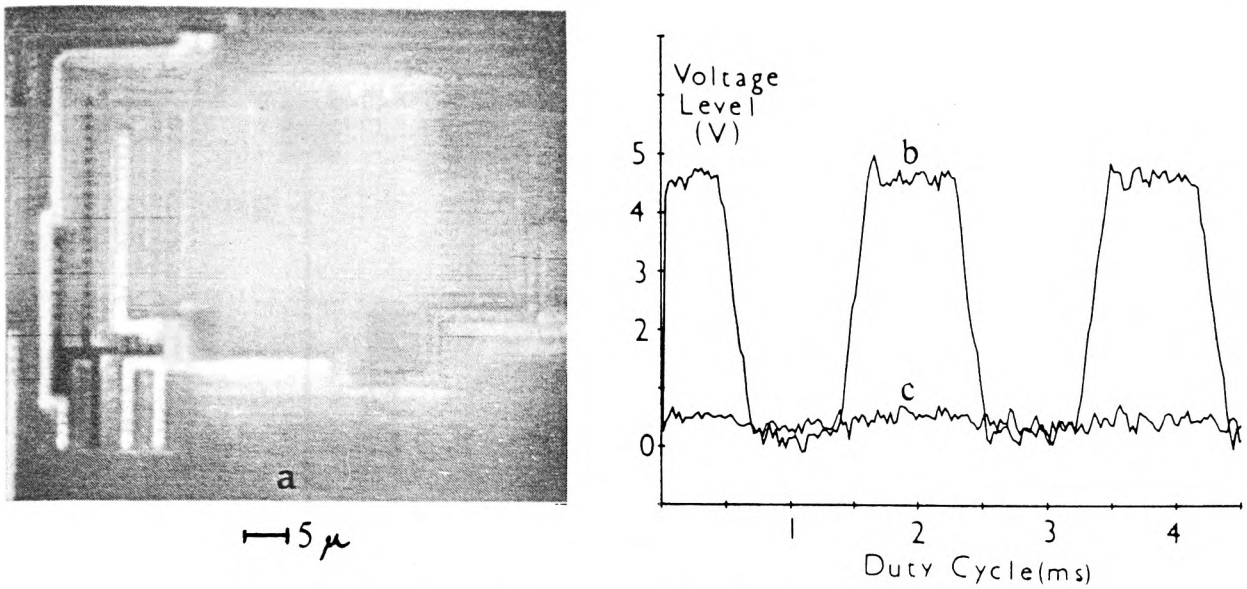

FIGURE 5 : a) Difference Image of Buffer Circuitary;
b) Voltage Waveform of Golden Device;
c) Voltage Waveform of Failed Device

5. CONCLUSION

Conventional ATE probing provides good general functional test data on VLSI devices. However to pinpoint the exact cause of failure it is necessary to probe the circuitry around the failed pin bondpad. Microprobing using fine metal probes is possible, but introduces the risk of damage to the fine line geometries and capacitance loading. EBT provides a means to probe conductor lines without damage or capacitive loading and is the only method of probing through a passivation or interlevel dielectric layer. We have demonstrated that EBT is a powerful tool for fault detection and design verification of VLSI devices.

6. ACKNOWLEDGEMENTS

We would like to thank all the people who have helped in this project. Particular thanks to David Seal, Mark Chapman and Howard Kent of INMOS plc Newport and to Gwent College for their continual support.

7. REFERENCES

Görlich S, Herrmann K D, Reiners W and Kubalek E 1986 Scanning Electron Microscopy vol III 447-464
Menzel E and Buchanan R 1985 Journal of Microscopy vol 140 pt 3 331
Menzel E and Kubalek E 1981 Scanning Electron Microscopy vol I 305-322
Sugiyama N, 1 Keda S and Uchikawa Y 1988 Scanning vol 10 3-8
Wolcott J S and Sziklas E B 1987 Microscopy of Semiconducting Materials 1987 eds A G Cullis and P D Augustus (IoP Publishing, Bristol) Inst. Phys. Conf. Ser. No 87; Oxford 6-8 April 1987
Wolfgang E, Linder R, Farjeks P and Feurbaum H 1979 IEEEJ Solid-State Circuits vol Sc-14

APPENDIX 1.

FLOOR PLAN OF THE CALIBRATION SAMPLE SUPPLIED BY BRITISH TELECOM.

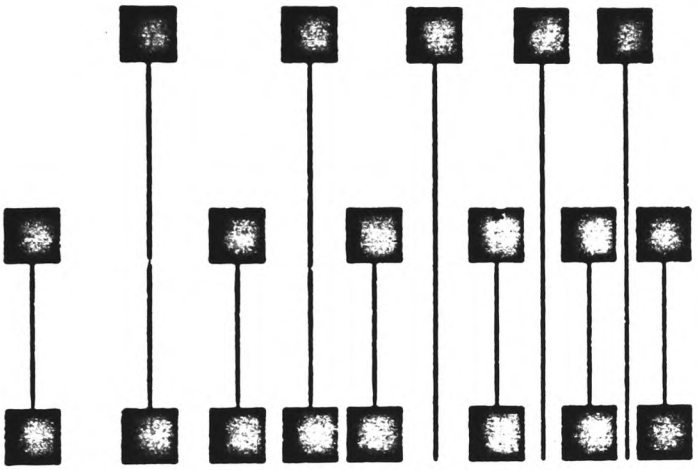

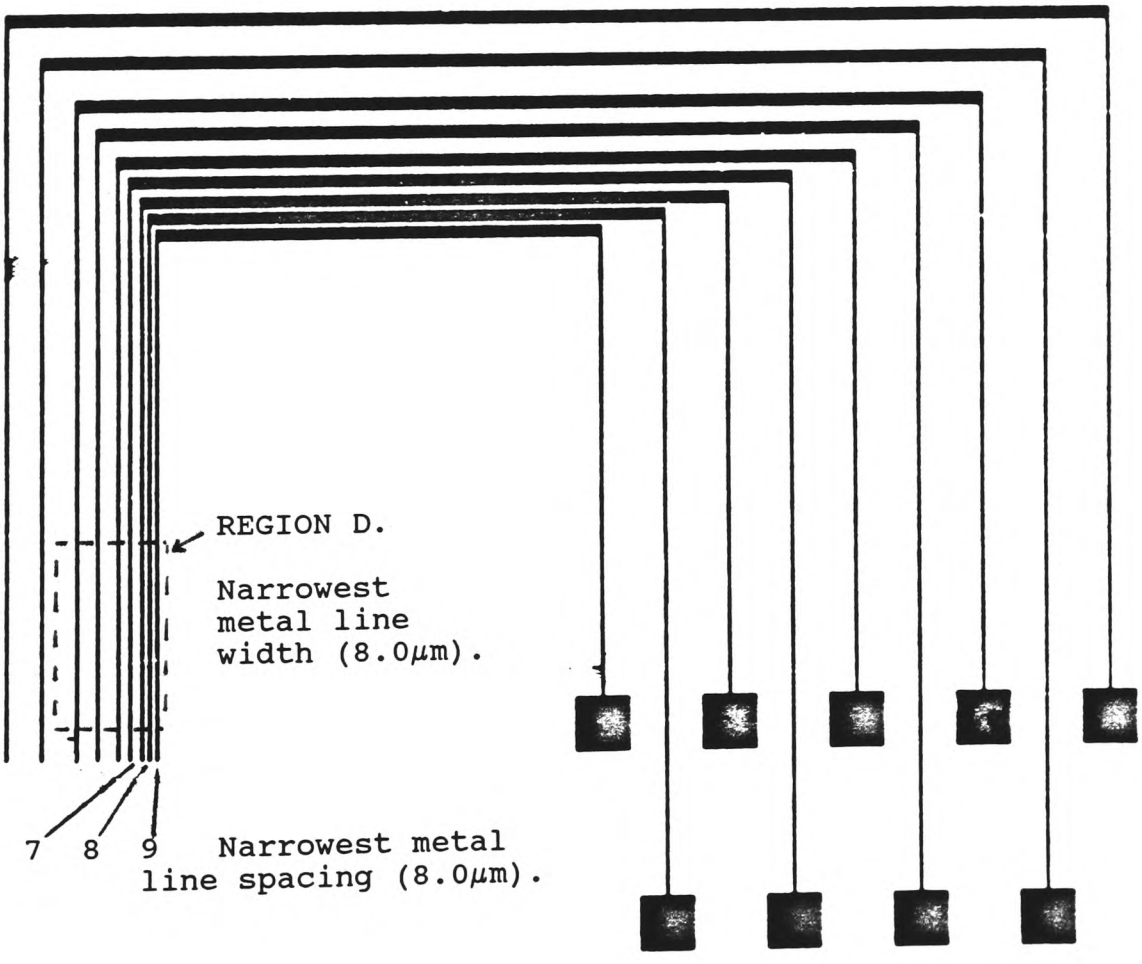

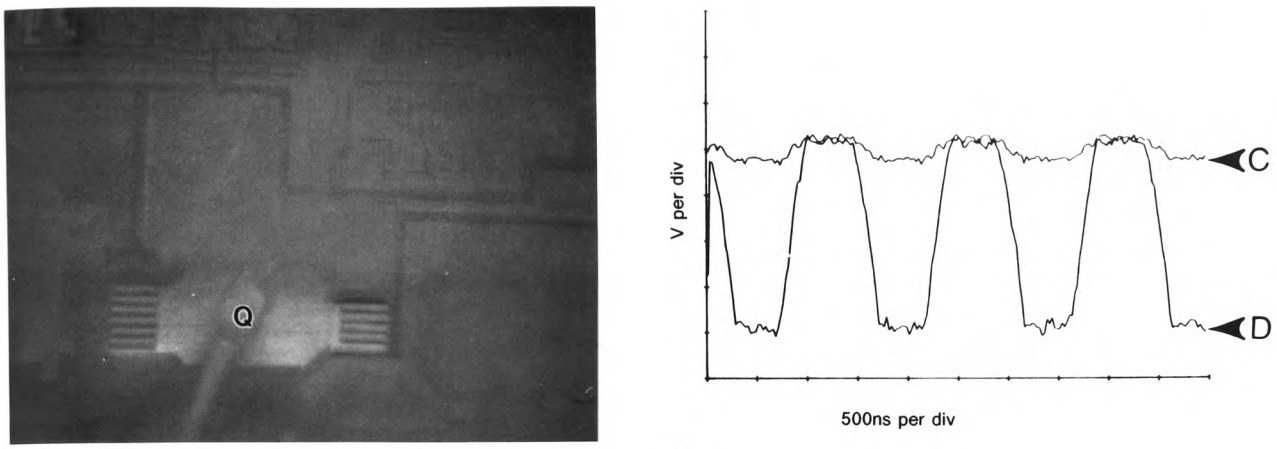

FIG. 4 (a) Subtracted image of data output bond pad low of the "golden" devices from that of the pad low of the failed device. (b) Waveform extracted, 'C' from the data output bond pad of the failed device. 'D' from the golden device.

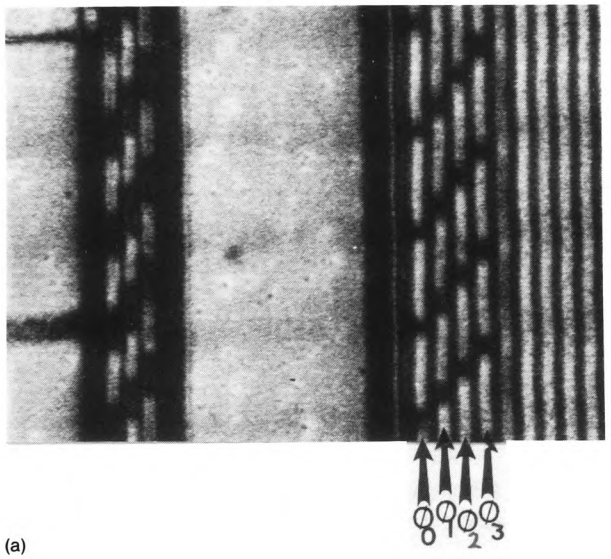

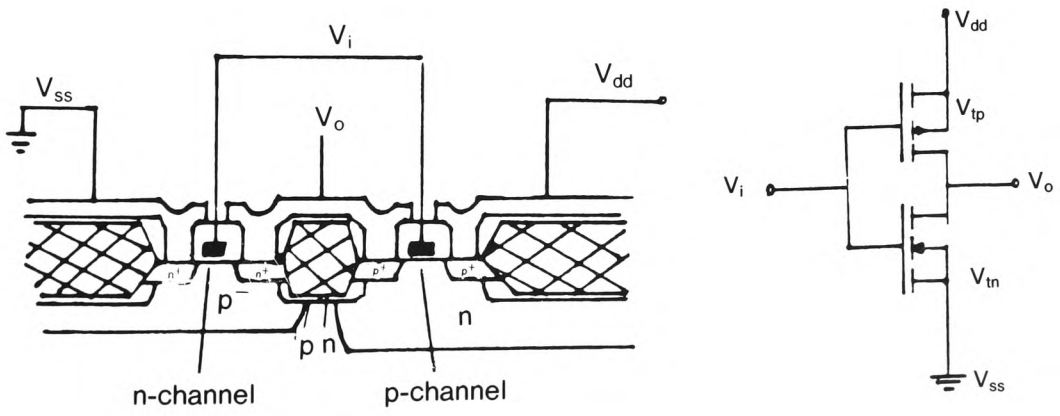

FIG. 5 a and b. Panels c and d on next page.

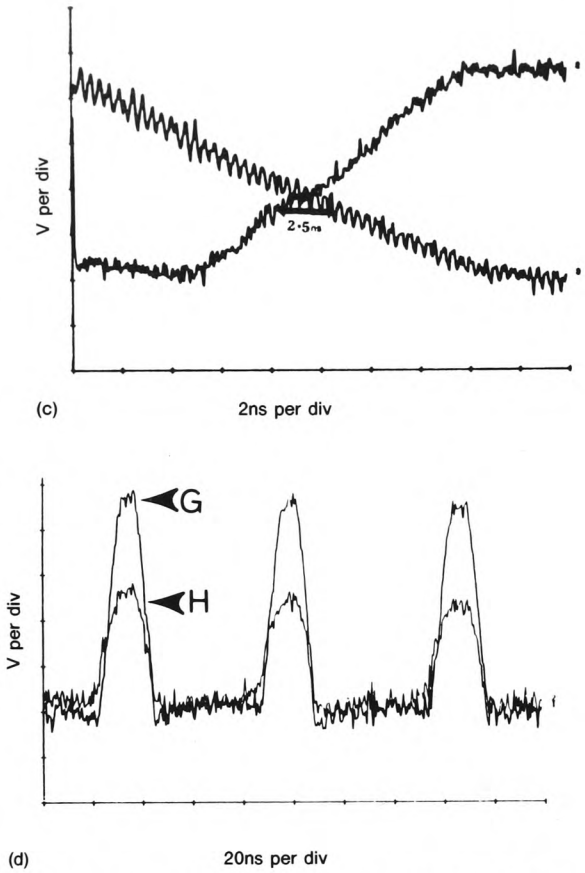

FIG. 5 (a) Logic map of the four-phase clock. This shows the phase relationship between the "on-chip" 15 MHz generators of a transputer device. (b) Schematic of a typical CMOS inverter circuit. (c) Determination of propagation delay, waveform 'E' the rising edge of the input, 'F' the falling edge of the output. (d) Waveform 'G' from the input to a buried conductor, 'H' from the buried conductor.

"The Transputer Family"), only nine connections were required into the chamber. One of these connections carried a trigger pulse from the high frequency "on-chip" clock. This was used to synchronize the blanking plates of the EB tester to the DUT. The test program was designed to exercise the processor of the DUT, and also to continually output information to the PC so that its performance during testing was continually monitored.

The signal propagation delay was determined by extracting waveforms from the input and output of an inverter (Fig. 5a). The schematic for a typical CMOS inverter is shown in Figure 5b. This delay being an important parameter for any CMOS device. If the delay is too long then timing errors will occur; for example, in the central processing unit (CPU). A good CMOS device would have a propagation delay of 2–3 ns. A value of 2.5 ns was measured.

The timing information required was of the phase relationship between the four phase clock generators. Figure 5c showed that the generators were functioning correctly.

In addition to the above, a waveform was extracted from a buried polysilicon line (Fig. 5d). This line was covered by 1 μm of dielectric material. Although there is a loss of voltage amplitude and a timing error, the extracted data may still be of use.

Summary

This work was intended to demonstrate that a conventional SEM with additional equipment, is able to perform many EB testing techniques. The techniques are used here to extract voltage and timing information from the internal nodes/lines of active VLSI devices. Also the ability to extract such data from buried conductors demonstrates that these techniques may be used for the analysis of multilevel devices.

Finally, it can be concluded that EB testing has an important role in the failure analysis and design verification of semiconductor devices.

Acknowledgments

This paper is based on a presentation made at the annual meeting SCANNING 89/EM WEST. I wish to thank Prof. David G. Howitt, University of California Davis, for my invitation and financial support. Mr. Edward David of the British Council for the travel grant. Special thanks to David Seal, Mark Chapman, and Shane MacCarvill of INMOS plc Newport. Thanks also to the following at Gwent College: Mel Harris, O.B.E., Clive Day, Mike Meredith, Tony Roberts, Ted Tate and Alex Wilson.

References

Fantini F: Reliability problems with VLSI. *Microelectron Reliab* 24, 275-296 (1984)

Görlich S, Herrmann KD, Reiners W, Kubalek E: Capacitive coupling voltage contrast. *Scanning Electron Microscopy* II, Chicago (1986) 447-464

Lukianoff GV: History of scanning electron beam testing development. *Microelec Eng* 7, 115-127 (1987)

Menzal E, Kubalek E: Fundamentals of electron beam testing of integrated circuits. *Scanning* 5, 103-122 (1983)

Newbury DE, Joy DC, Echlin P, Flori CE, Goldstein JI: *Advanced Scanning Electron Microscopy and X-ray Microanalysis*. Plenum Publ. Corp., New York (1986)

Reiners W, Görlich S, Kubalek E: On the primary electron energy dependence of radiation damage in passivated NMOS transistors. *Inst Phys Conf Ser* 76 section 12, 507-512 (1985)

APPENDIX 2.

ASYST PROGRAMME USED FOR ANALYSIS OF 'S'-CURVES.

```
def.vuport clear.function.keys clear.control.keys line.edit forget.all
   real scalar int.data
   integer scalar min.dat integer scalar max.dat
   graphics.display
   vuport top.bit
   .015 .25 vuport.orig
   .97 .74 vuport.size
   def.vuport
   18 0 24 79 window {bot}
   1 1 16 78 window {top}
   graphics.buffer []video
   real dim[ 199 ] array x-data
   real dim[ 199 ] array y-data
   real dim[ 199 ] array diff.dat
   dim[ 4 ] array []line.positions

       : read.basic.file
       {top} screen.clear
       20 5 goto.xy
       " a:\" ."    File name for opening " "input "cat defer> basic.open
                        \ 0 = dummy number
       0 begin basic.read dup 0 <> while 0 do catenate loop repeat drop
       basic.close
       []size sub[ 2 , swap ] dup   \ discard the dummy
       []size sub[ 1 , swap , 2 ] y-data :=
       []size sub[ 2 , swap , 2 ] x-data :=
       ;

      : read.in.data top.bit vuport.clear {top}
      screen.clear
      read.basic.file
    {top} screen.clear cursor.off {bot}
    ;

     : plot.
      top.bit vuport.clear " +" symbol
      x-data y-data xy.auto.plot cursor.off ;

   : differentiate top.bit vuport.clear
     x-data differentiate.data abs dup diff.dat :=
     y-data swap xy.auto.plot ;

   : print.screen screen.print bell bell ." Screen dump complete " ;

: data.integrate

    []line.positions [ 1 ] []line.positions [ 3 ] > if
    y-data []line.positions [ 1 ] [>] true.indices []min max.dat :=
    y-data []line.positions [ 3 ] [>] true.indices []min min.dat :=
    else
    y-data []line.positions [ 3 ] [>] true.indices []min max.dat :=
    y-data []line.positions [ 1 ] [>] true.indices []min min.dat :=
    then
    x-data differentiate.data abs sub[ min.dat , max.dat min.dat - ]
    []sum int.data :=
```

```
    {top} 50 0 goto.xy
    ." Integrated Data = " int.data . {bot}

;

: Set.Integration.Limits

    0 []line.positions :=
    {bot} 0 0 goto.xy
    ." Move Cursors to Select Integration Limits"
    top.bit
    world.coords
    normal.coords .6 .975 readout>position
    world.coords
    []line.positions readout>array
    array.readout
    interpret.keys
;

: ret.as
    def.vuport
    normal.display
    clear.function.keys
    clear.control.keys
    forget.all
    quit
;

: go

    f1 function.key.does read.in.data
    f2 function.key.does plot.
    f3 function.key.does differentiate
    f4 function.key.does set.integration.limits
    f5 function.key.does data.integrate
    f6 function.key.does print.screen
    f10 function.key.does ret.as


   graphics.display
   {bot}
    5 1 goto.xy " F1 = Read Data" "type
    5 2 goto.xy " F2 = Data Plot" "TYPE
    5 3 goto.xy " F3 = Differentiated Data Plot" "type
    5 4 goto.xy " F4 = Set Integration Limits" "type
    45 1 goto.xy " F5 = Integrate Data" "type
    45 2 goto.xy " F6 = Print Screen" "type
    45 3 goto.xy " F10 = Exit Program" "type
    text.cursor.off interpret.keys

;

{bot} screen.clear 8 3 goto.xy  " Type Go to start" "type
```

APPENDIX 3.

INTERFACE BOARD FOR THE T414 TRANSPUTER.

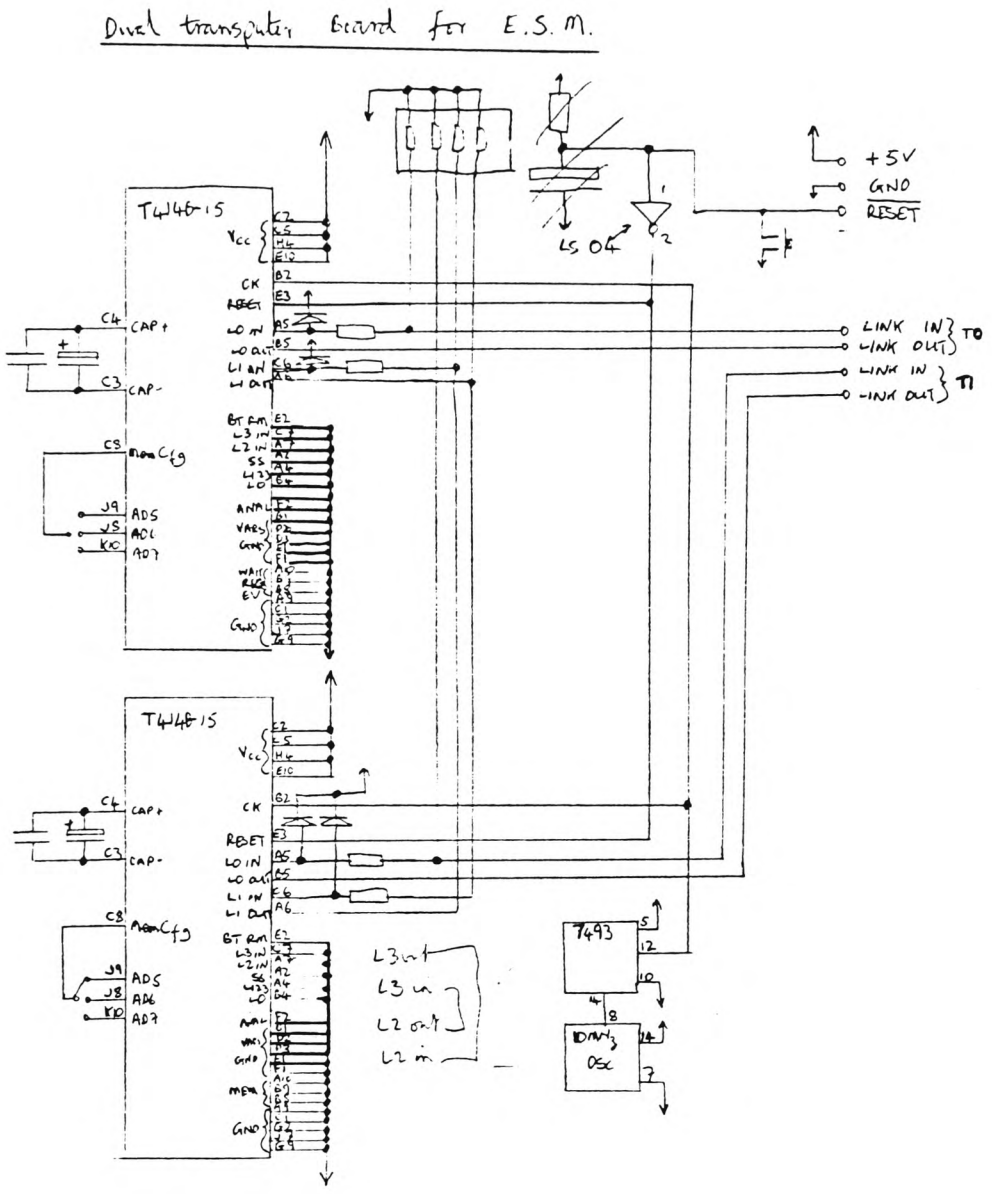

NOTES
- NO EXTERNAL RAM FITTED - PROGRAMS MUST USE INT ONLY.
- LINK SPEEDS ARE 10 Mbps.
- CONNECTIONS CHARACTERISED FOR T414B-15. FOR -20 PARTS, OR T800, CHANGE CHAR CONNS.

APPENDIX 4.

IDENTIFICATION OF PIN CONECTIONS TO THE T414 TRANSPUTER.

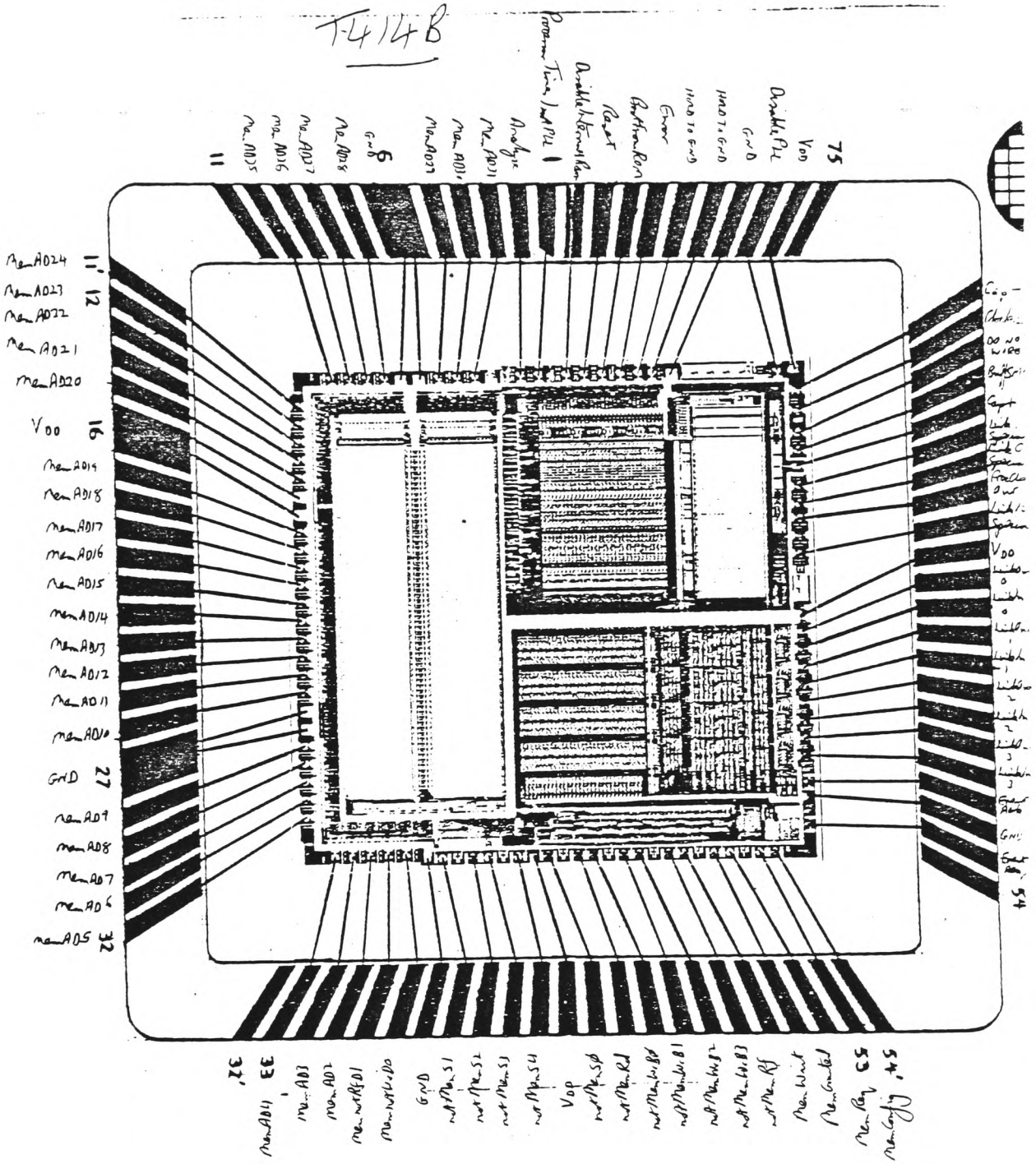

SCANNING Vol. 11, 199-204 (1989)

Received April 15, 1989

The Application of Low-Voltage Scanning Electron Microscopy for the Analysis of VLSI Devices

M. WOODWARD, D.R. JONES

Gwent College of Higher Education, Allt-yr-yn Avenue, Newport, Gwent, Wales

Introduction

The semiconductor industry in recent years has become more and more reliant upon the application of electron microscopy. The scanning electron microscope (SEM) is used to perform many tasks, ranging from routine inspection of device geometries to the more specialist techniques such as charge collection modes (Newbury *et al.* 1986).

As semiconductor technology has advanced, so more and more SEM techniques have been researched and developed. One such technique is electron beam testing (EBT). Although techniques of EB testing have been used for many years (Lukianoff 1987), it has only been of late that the semiconductor industry has become more generally aware of the techniques and their advantages. This interest in EB testing has been a direct result of advances in design and fabrication technology. As a consequence, metal line widths on volume production devices of 1.5 to 2.0 μm are not uncommon today. Linked to this is an increase in component density within devices. These advances have led to problems of functionally testing such devices. The conventional automatic test equipment (ATE) relies on the relatively large bond pads or peripheral circuitry to input/output test signals via metallic probes. The EB tester replaces the metallic probe, for the extraction of voltage and timing data, with a low-energy electron beam (0.5–2.0 keV). The advantages of these techniques are:

1. No physical damage is introduced
2. The E-beam does not capacitively load
3. Data may be extracted from conductors which are buried beneath dielectric materials
4. Accurate alignment of the E-beam using the deflection coils of the EB testers scan coils.
5. The display of electrical potential distribution over large areas of the device under test (DUT)

Applying an electrical bias to a specimen within the SEM will have a direct effect on the emitted secondary electron (SE) energy distribution spectrum (Menzel and Kubalek 1983). The phenomenon is termed *voltage contrast*. This contrast will appear superimposed on the usual topographic/materials information of the SE image. The emission of SE from the more positive biased areas results in a decrease in detector output and hence appears relatively darker. The more negative areas appear brighter because their SE emission will produce a higher detector output. Quantitative measurement of surface potential requires the determination of the shift of SE energy distribution spectrum, which is caused by the applied bias.

Instrumentation and EB Testing Techniques

The EB test system has been developed around a JEOL JSM840 SEM, to which an "add-on" Lintech Instruments EB tester is interfaced. To this equipment a Brian Reece Scientific Instruments video subtraction unit has been attached (Fig. 1).

The tungsten filament gun and associated electron optics of the JSM840 give it a capability of operating at low acceleration voltages between 0.2 and 1.0 keV, which is necessary to minimize electron beam irradiation damage, particularly to the more sensitive CMOS devices (Reiners *et al.* 1985). For the detection of qualitative voltage contrast information the conventional Everhart-Thornley SE detector is used, but for the

Address for reprints:

M. Woodward
Gwent College of Higher Education
Allt-yr-yn Avenue
Newport, Gwent, Wales NP9 5XA, UK

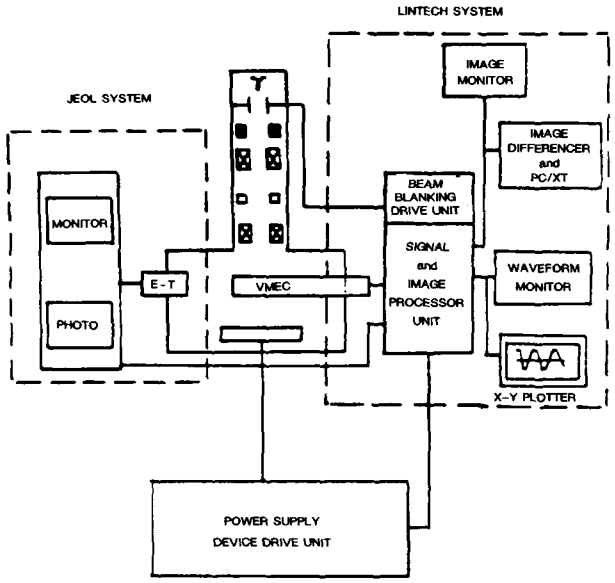

FIG. 1 Schematic of the EB test system.

detection of both qualitative and quantitative information, particularly the latter for waveform extraction, the voltage measurement electron collector (VMEC) is used. The VMEC is a planar type detector/spectrometer (Fig. 2). It is constructed so as to house a scintillator, and in addition, a series of annular grids:

1. The suppressor grid to reduce the likelihood of "stray" backscatter electrons being detected.

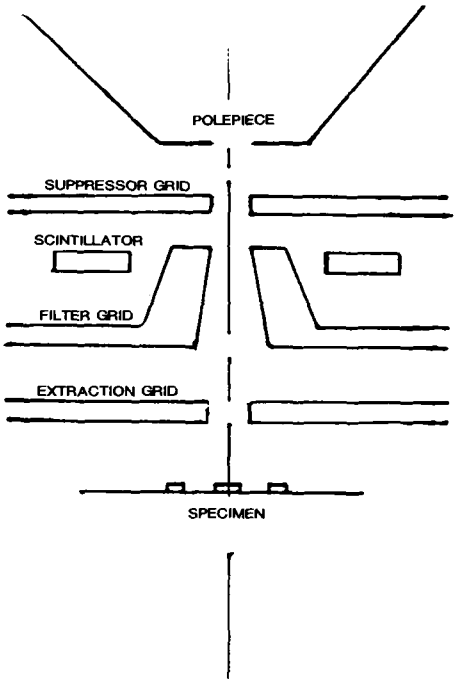

FIG. 2 The construction of the VMEC.

2. The extraction grid to which a high positive potential up to 5 keV may be applied. This generates an electrical field between the detector and the devices under test (DUT), to eliminate localized surface retarding fields and "crosstalk" between adjacent nodes/lines. Each of these effects may reduce the voltage resolution of the detector.
3. The filter grid analyses the energy of incoming SE, by the application of a retarding field. A feedback loop system is used in conjunction with retarding field to maintain a constant detector output with respect to changing surface potential. The changes of retarding field voltage are used to determine the surface potential.

To produce the necessary stroboscopic effect, blanking plates are positioned between the gun and the first condenser lens. These rapidly switch the primary electron beam on and off by deflecting the beam off the optical axis. This is achieved by applying a square wave which is synchronized to the DUT. Given that the DUT signal's cycle is equal to a value Tx, a suitable primary beam pulse width will be between 10 and 25% of TX. An image processor is incorporated into the test system which performs signal averaging/recursive filtering of the inherently noisy images. Using the above system, measurements of up to 250 MHz are possible. Results are either in the form of an image displayed on a monitor which may be photographed, or stored on video tape or digitized and stored on disk. Waveforms are displayed on a monitor, stored on disk or a hard copy produced using an X-Y plotter.

The following EB testing techniques are possible with this system.

1. Static voltage contrast, which displays the static potential of various nodes/lines with respect to each other.
2. Dynamic voltage contrast displays a characteristic alternating light and dark striping sometimes termed the "barber's pole" effect. The stripes are observed because of the relationship between the E-beam scan frequency and the node/line signal. This effect can be observed for signal frequencies up to 1 MHz. Applications of this technique include signal tracing to establish the "active" and "passive" nodes/lines, the phase of "active" nodes/lines, and also to determine the frequency of internally generated signals up to 1 MHz.
3. Stroboscopic voltage contrast to display a static image of a dynamic system. Such images are produced of nodes/lines in the frequency range 0.05–250 MHz.
4. Logic mapping achieved by varying the delay between the trigger signal and the E-beam pulse. This is then synchronized to the frame ramp generator of the SEM. The result is a stroboscopic image

which displays the nodes/lines at various phases simultaneously.
5. Waveform extraction from internal nodes/lines with voltage resolution of ±50 mV is possible, with subnanosecond timing resolution.

Procedure and Results

EB testing was used for the analysis of the following very large-scale integrated (VLSI) devices, E-beam energy 0.8 keV and current 1 nA.

1. 64K Static random access memory (SRAM) product (CMOS 2.0 μm design rules)
2. 32-bit microprocessor transputer product (CMOS 1.5 μm design rules)

The 64K SRAM had failed functional testing using ATE. Two pins were found not to perform to specification. These were the data output (Q) and the low power standby select pin (CE). More data were required to determine failure "mode"; that is, the cause of improper functioning. This work being an integral part of the failure analysis methodology, the conclusions derived from this would be used to establish the failure "mechanism," that is the chemical/physical process which led to the failure (Fantini 1984).

The metal lid was removed from the 22-pin dual-in-line (DIL) ceramic package, exposing the device. Similar preparation of a 64K SRAM "passed" functional automatic testing equipment (ATE) device was also carried out. This would be used as a reference or "golden" device. The devices were mounted side by side on a small printed circuit board (pcb) sample holder and placed within the vacuum chamber. Electrical connections were made via a feedthrough interface in the wall of the vacuum chamber using screened lease, the total length of which were kept to a minimum to minimize input/output signal deterioration. Pins Vss and Vcc were connected to the power supply, 0 volts and 5 volts, respectively. All remaining pins were tied low to 0 or high to 5 volts, except Q and CE, to which a low frequency (200 Hz) 5-volt square wave was applied. A dynamic contrast image, obtained using the conventional Everhart-Thornley SE detector, was used to trace the circuitry which related to the CE. The phase relationship of the circuit's active nodes/lines was observed. The VMEC was then inserted between the devices under test (DUT) and the polepiece. A high frequency (0.6 MHz) was applied. The poor quality image obtained (Fig. 3a) is caused by the presence of silicon nitride passivation over the device's surface. Testing is possible with the passivation "in situ," by the technique of capacitively coupled voltage contrast (Gorlich *et al.* 1986). It was decided to remove this layer by the plasma etching technique. The device was then re-examined, stroboscopic images (Fig. 3b, c) were obtained. This area of the device is known to be the "buffer" circuitry and it was suspected from ATE data that the failure was within this region. Stroboscopic image of the input to the buffer was captured, digitised, and stored in the PC's memory. A delay was then introduced of 0.8 μs between the trigger and the E-beam pulse. The image then formed was that of the input to the buffer high. The input to the buffer low was then subtracted from this image (Fig 3d). The subtracted image shows nodes/lines which differ in contrast from each of the original images. From previous knowledge of the buffer circuitry, it was expected that the subtracted image should have appeared as in Figure 3e. The 'U'-shaped feature had completely subtracted, indicating a similar level of contrast at the input to the buffer low and high. Extracting a waveform from this U-shaped feature (Fig. 3f) showed that it was permanently held to ground. Further investigation and deprocessing revealed that the output of the buffer was not connected to the drain of an N-channel transistor. It was tied permanently to the ground rail V_{ss}.

The second failure associated with the Q was investigated. As previously, all pins were tied high or low and the low frequency square wave applied to the data output circuitry, signal tracing was performed with the VMEC still in the SEM. The characteristic voltage contrast was not observed on the data output bond pad, but was observed on the rest of the data output circuitry. The higher frequency signal was then applied and stroboscopic images obtained. The image subtraction technique was used as previously, but with images collected and stored from the data output bond pad from the "golden"device. The images of the data output bond pad at the high phase of the cycle completely subtracted, while those of the low phase did not (Fig. 4a). A waveform extracted (Fig. 4b) showed that the bond pads' voltage did not fall below 4.5 volts.

Further investigation and deprocessing revealed that the gate oxide beneath the polycide gate electrode was missing. As a result, the bond pad was tied to the adjacent V_{cc} power rail (5 V).

The other device investigated was a 32-bit microprocessor "transputer" device. EB testing being used to characterize propagation delay and extract timing data from the high frequency (15 MHz) "on chip" clocks.

This device was packaged in a ceramic 84-pin-grid array (PGA). The metal lid was removed and then the silicon dioxide passivation was performed using a "light" P-etch. The 84-pin device was placed in a zero force insertion (ZIF) holder. Again the system arranged so that a "golden" device could be mounted simultaneously. This pcb also contained some interface circuitry and many decoupling capacitors. The board, once mounted within the SEM, was interfaced to a PC and a power supply. This enabled a test program to be loaded to the DUT. Because of the unique operation of the transputer device (INMOS product information

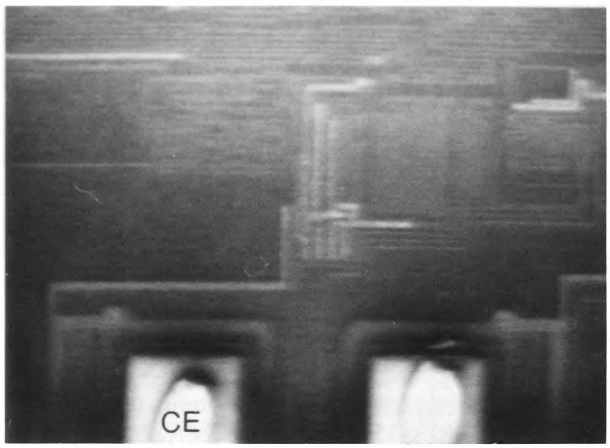

(a)

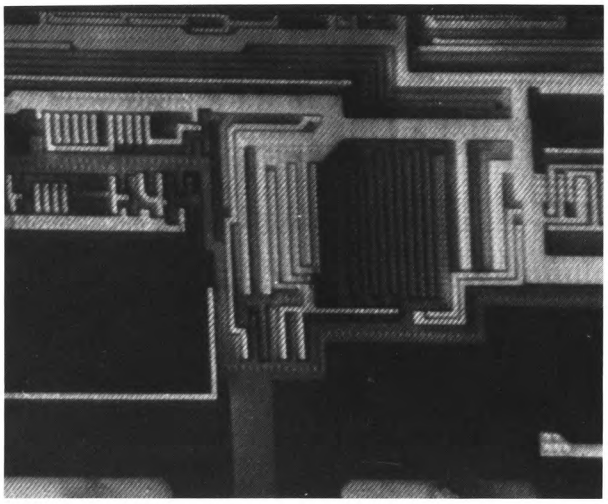

(b)

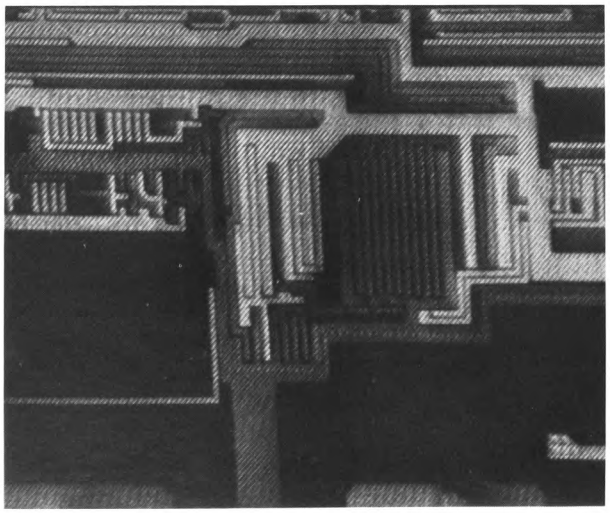

(c)

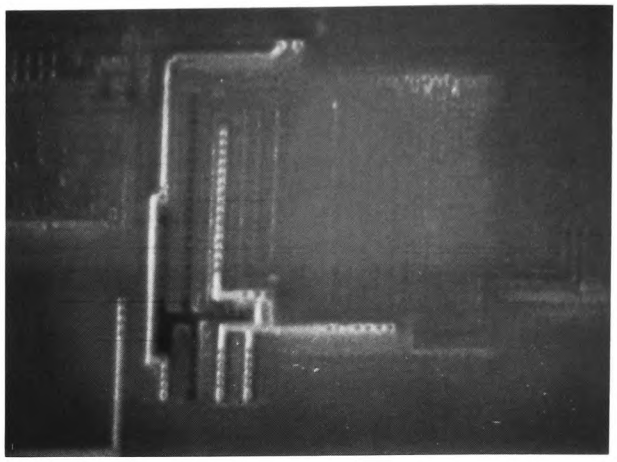

(d)

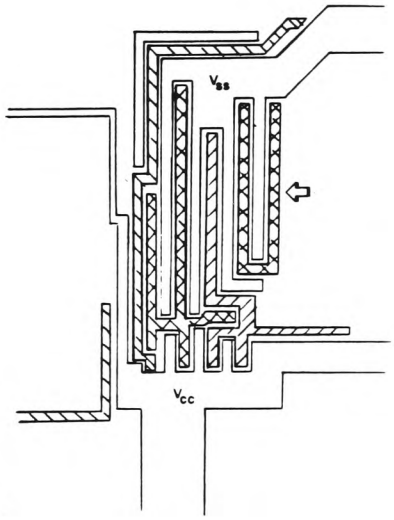

(e)

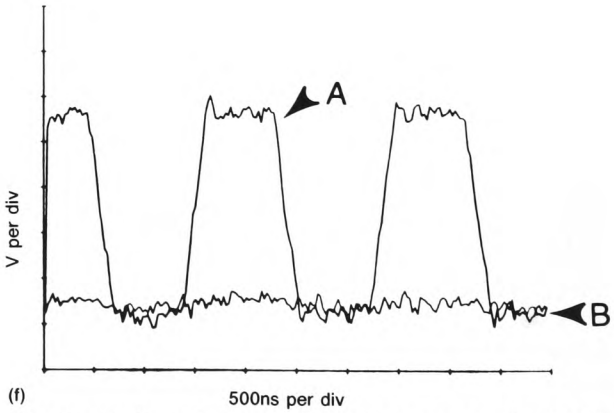

(f)

FIG. 3 (a) Capacitively coupled voltage contrast showing the "active" circuitry of pin "CE," which is buried beneath 1 μm of silicon nitride. (Horizontal field of view=740 μm.) (b) and (c) Stroboscopic voltage contrast images of "CE" buffer circuit. Where (b) input to buffer low T=0 and (c) input to buffer high T=800 ns. (d) Subtracted image (b) and (c). (e) Schematic, metal layout of buffer, hatching indicates nodes expected to be observed in (d). Arrow indicates 'U'-shaped feature not active. (f) Extracted waveforms 'A' input to buffer, 'B' feature held permanently to ground.